ISTANBUL TECHNICAL UNIVERSITY ★ GRADUATE SCHOOL OF SCIENCE ENGINEERING AND TECHNOLOGY

INVESTIGATION OF OPTICAL AND WETTABILITY PROPERTIES OF POLYMER COATINGS

M.Sc. THESIS

Elbruz Murat BABA

Department of Nano Science and Nano Engineering

Nano Science and Nano Engineering Programme

MAY 2015

ISTANBUL TECHNICAL UNIVERSITY ★ GRADUATE SCHOOL OF SCIENCE ENGINEERING AND TECHNOLOGY

INVESTIGATION OF OPTICAL AND WETTABILITY PROPERTIES OF POLYMER COATINGS

M.Sc. THESIS

Elbruz Murat BABA
513121005

Department of Nano Science and Nano Engineering

Nano Science and Nano Engineering Programme

Thesis Advisor: Prof. Dr. Esra Ozkan ZAYIM
Co-Advisor: Assist. Prof. Dr. Elif Ozen CANSOY

MAY 2015

İSTANBUL TEKNİK ÜNİVERSİTESİ ★ FEN BİLİMLERİ ENSTİTÜSÜ

POLİMER KAPLAMALARIN OPTİK VE ISLANABİLİRLİK ÖZELLİKLERİNİN ARAŞTIRILMASI

YÜKSEK LİSANS TEZİ

Elbruz Murat BABA
513121005

Nano Bilim ve Nano Mühendislik Anabilim Dalı

Nano Bilim ve Nano Mühendisliği Programı

Tez Danışmanı: Prof. Dr. Esra Özkan ZAYİM
Eş Danışmanı: Yrd. Doç. Dr. C. Elif Özen CANSOY

MAYIS 2015

Elbruz Murat BABA, a **M.Sc.** student of ITU **Institute of Nano Science and Nano Engineering** student ID **513121005**, successfully defended the **thesis** entitled "**INVESTIGATION OF OPTICAL AND WETTABILITY PROPERTIES OF POLYMER COATINGS**", which he prepared after fulfilling the requirements specified in the associated legislations, before the jury whose signatures are below.

Thesis Advisor :	**Prof. Dr. Esra Ozkan ZAYIM** Istanbul Technical University	.....
Co-advisor :	**Assist. Prof. Dr. Elif Ozen CANSOY** Piri Reis University	.....
Jury Members:	**Assist. Prof. Dr. Mehmet Şeref Sönmez** Istanbul Technical University	.....
	Assoc. Prof. Dr. Sevim İşçi Turutoğlu Istanbul University	.....
	Assist. Prof. Dr. Safettin Yıldırım Istanbul Technical University	.....

Date of Submission : 4 May 2015
Date of Defense : 29 May 2015

To my family and dearest friends,

FOREWORD

I would like to express my greatest gratitude, to my supervisor of studies, Assoc. Prof. Dr. Esra Ozkan Zayim, whose expertise, patience and understanding helped my work in this thesis.

I would also express my greatest gratitude to my co-supervisor, Assist. Prof. Dr. C. Elif Cansoy, without her help, expertise and constant support, this work would be impossible for a marine engineer.

I would like to try to express my gratitude, however it is impossible, to my family; expecially to my mother Zühal Kurt and to my father Süleyman Zeyyat Baba whose support were vital and far beyond the desire for every son.

I would like to thank Selin Ayça Karnap for her omnipotent patience and selfless help.

I would like to thank to all my friends and colleagues whose support, kind patience and compassion were felt very close.

May 2015

Elbruz Murat BABA
(Naval Architect and Marine Engineer)

TABLE OF CONTENTS

Page

ABBREVIATIONS

HDPE	**:** High Density Polyethylene
LDPE	: Low Density Polyethylene
PP	**:** Polypropylene
PVOH	: Polyvinyl alcohol
N66	: Nylon 6,6
N6	: Nylon 6
PMMA	**:** Poly(methyl methacrylate)
PVAc	: Polyvinyl acetate
PPPE	: Polypropylene polyethylene copolymer
PS	: Polystyrene
γ_S	: surface tension
γ_{SL}	: Interfecial tension between solid-liquid
γ_{SV}	: Interfecial tension between solid-vapour
γ_{LV}	: Interfecial tension between liquid-vapour
γ_{LW}	: liftsitz cander waals interaction component
γ_{AB}	: acid base interation component
θ_e	: Equilibrium contact angle
θ_a	: Advancing contact angle
θ_e	: Receding contact angle
CAH	: Contact Angle Hysteresis
r_W	**:** Wenzel Roughness Factor
θ_e^r	**:** Equilibrium Contact Angle Of Real Surface
θ_e^s	**:** Equilibrium Contact Angle Of Flat Surface
f_s	**:** Fraction Of Solid Surface Area Wet By The Liquid
SFE	**:** Surface Free Energy
W_a	**:** Work Of Adhesion
W_c	**:** Work Of Cohesion
d	**:** Dispersion
p	**:** Polar
I	: Induction
h	**:** Hydrogen-Bonding
n	**:** Refractive Index
k	**:** Extinction Coefficient
E_g	**:** Energy Gap
hv	**:** Photon Energy
α	**:** Absorption Coefficient
C_{Tauc}	**:** Tauc Constant
w	**:** Rotational Frequency
c	**:** Speed Of Light In Vacuum
ε	**:** Dielectric Constant
r	: Reflectance Fresnel Coefficient
S	**:** Poynting Vector

LIST OF TABLES

Page

LIST OF FIGURES

Page

INVESTIGATION OF OPTICAL AND WETTABILITY PROPERTIES OF POLYMER COATINGS

SUMMARY

Controlling wettability is an important property and highly desired by industry due to its wide range of advantages, such as; anti-bacterial, anti-ice and self-cleaning. Obtaining such advantages through engineering surface coatings presents highly challenging environment because, for example, one need to design highly porous surface for a chemically hydrophobic polymer coating to obtain anti-icing or self cleaning properties but porosity decreases light propagation and made the material opaque. Real struggle, and the most desired by industry, is finding the Goldilock Zone for such coatings, if not the perfect one.

Controlling liquid behaviour is an ancient dream for us sapiens. We crafted cups to hold, canals to channel even built dams to harness the power within. Over the years, despite getting better at capturing the liquid, we were unable to prevent its harmful or undesirable effects after a certain point. It has been recently emphasized that nature is in fact very successful about avoiding its harmful effects with presenting liquid repellent properties. Water striders, a bug which have the ability to stand on water using its superhydrophobic legs, and water lilies (lotus) with self cleaning properties can be given as natural examples due to their unique water repellent properties. Learning the ways of nature about how to deal hazardous environment or how to enhance our inventions is the best key for success in engineering.

Water repellent surfaces attracts many attention from industry with not only their self cleaning properties but also anti-fouling, drag reduction and many properties that were mentioned above. Two heading of water repellent surfaces can be mentioned as focussed in this thesis; hydrophobic surfaces and superhydrophobic surfaces where surfaces that have water contact angles larger than 90° called hydrophobic and larger than 150° called superhydrophobic. Main reason for the focus on these topics is their potential on marine enhancement properties. Drag reduction would be reduce carbon emissions in tremendous amounts when considered that the global shipping sector is responsible for approximately %2 of global greenhouse gas emissions which can be comparable for even countries. Anti-ice property could make working conditions on ships over cold climates better and increase the life expectancy of ships. Direct effect of water repellent properties will most likely be on hull applications as presenting anti-fouling properties and substituting present poisonous coatings with non-poisonous superhydrophobic coatings.

The aim of this study is to create a knowledge basis of further studies and marine applications based on water repellent surfaces. High density polyethylene (HDPE), low density polyethylene (LDPE), polypropylene (PP), polyproplyne-polyethylene copolymer (PPPE), polyvinyl alcohol (PVOH), nylon 6 (N6), nylon 6,6 (N66), polystyrene (PS), poly(methyl methacrylate) (PMMA) and polyvinyl acetate (PVAc) coatings were tested for surface and optical properties. Surface free energy studies were conducted and correlations were presented. Great deal of data were obtained in order to understand polymer surface behaviours as well as how to enhance the properties.

Last study was performed using dispersed SiO2 nanoparticles in order to create surface roughness. Polystyrene was chosen for this study for its adequate properties such as, high contact angle value, relatively low surface energy and easy to work under room conditions as well as high transmittance. As a result of this study, superhydrophobic SiO2 nanoparticle dispersed polystyrene coatings were obtained. Extensive correlations were derived between surface and optical properties with respect to the nanoparticle content.

POLİMER KAPLAMALARIN OPTİK VE ISLANABİLİRLİK ÖZELLİKLERİNİN ARAŞTIRILMASI

ÖZET

Yüzey ıslanabilirliğinin kontrolü, sağladığı sayısız avantaj sebebiyle endüstri tarafından gittikçe artan bir ilginin odak merkezi konumundadır. Özellikle sunduğu kendini temizleme, buzlanma önleyici, anti bakteriyel, sürüklenme azaltıcı ve denizel kirlenme önleyici gibi sayısız özelliğinden dolayı endüstriyel uygulama alanları oldukça geniştir. Fakat her ne kadar elde edilebilecek özellikler çok büyük avantajları barındırsa da bu yüzeylerin üretilmesi kendi zorluklarını da beraberinde getirmektedir. Örneğin; kendini temizleyen su tutmayan süperhidrofobik yüzeylerin yapılması için yüzeyin enerjisinin düşük olması ve pürüzlülük barındırması gerekir fakat pürüzlülük ışık geçişinin azalmasına sebep olmaktadır. Eğer bu ve benzeri yüzeyler üretilecekse birden fazla parameter birlikte düşünülerek, geniş yelpazede malzeme kullanımı göz önünde bulundurulmalı ve yüzey davranışları üzerine hakimiyet yüksek olmalıdır.

İnsanlık tarihin ilk zamanlarından beri sıvıların, özellikle de suyun, kontolü ve zararlarının önlenebilmesi için çalıştı. İçinde tutabilmek için kupalar, enerji üretebilmek için barajlar, üzerinde durabilmek için gemiler ve bir çok makine için borular tasarlandı. Birçoğunda tasarımlar doğadan alınırken birçoğunda da doğaya karşı düşünülebilen her türlü şekilde karşı koymaya çalışılmıştır. Geçtiğimiz yıllarla beraber sıvıyı belirli alanlarda kontrol edebilme becerimiz her ne kadar artsa da sıvıların zararlı ve istenmeyen etkilerine karşı koyma konusunda çok da başarılı olunamamıştır. Yakın zamanlarda anlaşılmıştır ki, doğa bu zararlı etkilerden uzak durma veya kontrol etme konusunda, insanlığın tüm çabalarına rağmen, teknolojik ilerlememizi gölgede bırakacak nitelikte oldukça etkili ve çeşitli yöntemler geliştirmiştir. Örneğin, bir böcek türü olan Aquarius remigis, sahip olduğu süperhidrofobik bacaklar sayesinde havayı paketler halinde hapsederek su üzerinde rahatlıkla durabiliyor ve bunu o kadar etkili yapıyor ki her bir bacağının suda ortaya koyduğu kaldırma kuvveti bacağın kendi ağırlığının 300 katına kadar ulaşabiliyor. En bilinen ve kendini temizleme etkisine (lotus effect) ismini veren nilüfer çiçekleri, kendilerini temizleyebilen yüzeyleri sayesinde kirleticilerden kolaylıkla kurtulabiliyorlar. Doğanın su ile baş etme çeşitliliği, insanlığın henüz karşılaşmadığı problemlerine dahi çözümler barındırdığı göz önünde tutulduğunda, bu konudaki endüstriyel ilerlememizin anahtarı konumundadır.

Su itici yüzeylerin iki önemli alt başlığı bu tezin odak noktası olarak gösterilebilir; hidrofobik ve süperhidrofobik yüzeyler. Yüzey su temas açıları 90°'den fazla olan yüzeyler hidrofobik yüzey, 150°'den fazla olanlar ise süperhidrofobik yüzey olarak adlandırılırlar. Bu çalışmada bu alanlara odaklanılmasının asıl sebebi denizcilik alanında sahip oldukları yüksek potansiyeldir. Süperhidrofobik yüzeyler yüksek su

itici özellikleri sayesinde deniz taşıtlarının su ile temasını barındırdıkları hava paketleri sayesinde minimuma indirerek önemli avantajlar sunabilir, örneğin; yüksek sürtünme direnci düşüşü sağlayabilir, gemi izini (wake) azaltarak gemilerin uzak mesafelerden tespitini zorlaştırarak askeriyede yüksek avantaj sağlayabilir, sahip olduğu antibakteriyel özellik gemilerin yüzeylerinde mikroskopik canlıların tutunmasını ve birikmesini önleyerek şimdilik kaçınılmaz olan performans düşüşünü engelleyebilir, buz oluşumunu önlemesi sayesinde soğuk bölgelerde faliyet gösteren deniz yapıları ve taşıtlarının performanslarını ve güverte güvenliğini oldukça yüksek oranda arttırabilir ve gemilerin boru sistemlerinde ve hatta ballast tanklarının içerisinde kullanılarak birçok problemin önüne geçilebilir. Ayrıca mevcut zehirli gövde kaplamalarının yerini alabilme potansiyeli denizlerin de kirletilmesini önlemek açısından oldukça önemlidir. Uluslararası denizcilik düzenlemelerinin bu konuda aldığı kararlar da düşünüldüğünde bunun ekonomik sonuçları da göz önünde bulundurulmalıdır. Özellikle sürtünme direnci üzerinden gemilerin karbon ayak izlerini azaltması en büyük etkisi olacaktır. Dünyadaki gemi taşımacılığının tüm dünya karbon emisyonu miktarının yaklaşık %2'sinden sorumlu olduğu düşünüldüğünde bu orandaki herhangi bir azalmanın dünyaya etkisi bir ülke ile kıyaslanabilecek ölçüde büyük olacaktır. Buna ek olarak, gemilerde yaratacağı performans artışı ve maliyet düşüşleri taşımacılık maliyetini de azaltacağı için gemi taşımacılığına yönelimi ve hatta kapasitesini arttıracaktır. Karbon ayak izi açısından, birim yük için mevcut en verimli taşımacılık gemi taşımacılığı olduğu düşünüldüğünde dolaylı olarak da dünyadaki karbon izinin azalmasını sağlayacaktır.

Süperhidrofobik yüzeylerin üretimi şimdiye kadar farklı malzeme ve metodlarla ulaşılmış olsa da interdisipliner çalışma ile bu yüzeylerin gerçek çıktılarının üretimi her zaman problemli olmuştur. Yüzey davranışı üzerine hakimiyet her ne kadar oldukça önemli olsa da, üretim sırasında aynı zamanda bu yüzeylerin pratik uygulamaları için de hakimiyet sahibi olunmalıdır. Gemilerin gövde tamirleri için mevcut optimum üsreler düşünüldüğünde çok daha hızlı sökülecek bir kaplama kendi avantajlarını ortadan kaldıracaktır. Diğer taraftan bakılırsa, sadece deniz araçlarının çetin koşullarına hakim olanursa ihtiyaç duyulan çözüm konusunda ufuk sınırlı kalabilir ve sadece mevcut durum tekrarlanır. Bu çalışmanın sonucunda ulaşılması amaçlanan nokta, belirtilen iki alanı birleştirecek bir ortak zemin yaratmak ve ilerideki çalışmalar için ortak bir hakimiyet oluşturmaktır.

Bu çalışmanın ana hedefi gemicilik alanındaki uygulamaları ve sonraki çalışmalar için bilgi zemini oluşturmaktır. Buradan yola çıkarak yapılacak çalışmalar ile yukarıda bahsedilen gelişmelere ulaşmak oldukça mümkündür. Bu çalışmada, yüksek moleküler ağırlıklı polietilen (HDPE), düşük moleküler ağırlıklı polietilen (LDPE), polipropilen (PP), polipropilen-polyetilen kopolimer (PPPE), polivinil alkol(PVOH), naylon 6 (N6), naylon 6,6 (N66), polistiren (PS), polimetilmetakrilat (PMMA) ve polivinilasetat (PVAc) polimer yüzeyler sahip oldukları yüzey davranışları, optik karakteristikler ve ıslanabilirlik özellikleri üzerine incelenmiştir. Polimer çeşidi geniş

tutularak optik ve ıslanaiblirlik özellikleri arasındaki geçişlerin hangi parametrelerle mümkün olduğu gösterilmeye çalışılmıştır. Yüzey enerji hesaplamaları yapılmış ve sahip oldukları karakteristik özellikleri arasında bağıntılar kurularak ayrıntılı karakterizasyon verileri sunulmuştur.

Son çalışmada nanoboyutlu SiO_2 parçacık dispersiyonu yüzey pürüzlülüğü yaratmak için kullanılmıştır. Çalışma için polistiren polimeri seçilmiş olup sahip olduğu yüksek su tema açısı, oda şartlarında kolay çalışabilirliği, yüksek optik geçirgenliği ve görece düşük yüzey enerjisi gibi özellikleri bu çalışmada seçilmesi için etkili olmuştur. Nanoparçacıklar politirene içerisinde tanıtılmadan önce sonic homojenizatör ile polistirenin çözüldüğü çözücüde dağıtılmış ardından polimerle beraber tekrar homojenizatör ile işleme sokulmuştur. Örnekler spin kaplama tekniği ile hazırlanmıştır. Elde edilen kaplamalar hidrofobikten süperhidrofobiğe kadar ulaşan geniş bir skala sunmuştur. Örneklerin incelenmesi için ayrıntılı temas açısı ölçümleri ile ıslanabilirliği incelenmiş optik karakterizasyonu ile de aralarında bağıntılar kurulmuştur.

Ulaşılan örneklerin oluşturduğu yelpaze aynı zamanda SiO_2 miktarının doygunluğunu göstermesi açısından da yardımcı olmuştur. Optik karakterizasyon sonuçları ile örneklerin temas açıları arasında korelasyon kurulduğunda, belirli bir noktadan sonra temas açısı açısından bir avantaj yaratmadığı gibi optik geçirgenliğinin de düştüğü görülmüştür.

Yapılan çalışmalar ile süperhidrofobik yüzeylere ulaşılmış ve sonraki çalışmalara zemin oluşturması amaçlanan interdisipliner hakimiyete ulaşılmıştır.

1. INTRODUCTION

Controlling wettability is a critical for industry due to its wide range of advantages, such as; anti-fouling, oil-water separation, anti-bacterial, anti-ice, self-cleaning and flow enhancement [1-10]. Challenging environment for obtaining such highly advantages surfaces is great especially impossible to obtain such surfaces without answering conflictive requests. For example; superhydrophobic coatings are great for surface protection in various ways and perfect for optical devices but superhydrophobicity can not be obtained with absence of roughness. Because of the surface roughness decreases light propagation engineering optimum property for such surfaces is hard but mandatory. In order to control the wetting behaviour of the surface, chemical structure and surface morphology need to be well understood and well manipulated.

Measuring contact angle values of surfaces is a great method to obtain parameters such as surface free energy, which is directly related with the water repellency of the surface, as these values carry thermodynamic characteristics of the solid surfaces. Several methods [11,12] are being used to quantify the surface characteristics of the solid surfaces as calculating surface free energies. In general, most preferred approaches are Van-Oss Good approach and Fowkes (later Owens/Wendt) geometric mean method.

In this thesis, two main studies were performed. First of all, 10 polymer coatings HDPE, LDPE, PP, PPPE, PVOH, N66, N6, PS, PMMA and PVAc thin films were synthesized and investigated for their optical and wetting behaviours. Later, in order to investigate surface behaviours of given polymer surfaces, surface energies of samples were calculated using water, formamide, ethylene glycol and methylene iodide as test liquids. CA decrease was found as a result of the increase in surface energies of polymers because of higher adhesion interactions between the liquid drop and the solid polymer surface. Then, optical absorption studies were performed and increase in the band gap was found as well as correlations between optical and surface

behaviours of surface coatings were demonstrated. The maximum band gap was achieved for PPPE and PMMA films and absorption of the films occurred in the wavlengths below 300 nm. Above this point coatings diplay excellent transparency, which is characteristic for wide band gap material [13,14]. This study created a strong foundation for further studies. Also, results and correlations between HDPE, LDPE, PP, PVOH and N66 polymer surfaces were published [15]. Second, superhydrophobic surfaces were synthesized using SiO_2 nanoparticles for its easy accessability and non-toxicity. PS is used as polymer coating for this study because of our previous study showed that PS demonstrates high water CA as having relatively low surface energy as well as great transparency. Wide range of PS coatings with dispersed SiO_2 nanoparticle content were prepared and characterizations performed extensively. Later, atomic force microscopy (AFM) measurements were performed on 5 μm^2 and 30 μm^2 surface areas. AFM results showed roughness increase as nanoparticle content increase as intended. Also, water contact angle measurements indicated that contact angle values were increased as surface roughness increase and superhydrophobic surfaces were obtained. On the other hand, some samples demonstrated CA increase despite their surface roughness decrease. He et al. reported that formation of nanoparticle aggregates is more important than Root-Mean-Square roughness (RMS) [16]. This report explains and supports our results where CA increase occurred while roughness value drop observed. This matter discussed in further sections. Last of all, transmittance and reflectance values were measured and refractive index (n) and extinction coefficient (k) values derived using NKD spectrophotometer software. Using obtained data, band gap values were calculated using Tauc method [17,18].

The aim of this thesis is to create knowledge basis for further studies. In order to advance in engineering on surface modification and control, foundations need to be well studied if not completely understood. Behaviour differencies between flat and rough coatings hold great value to understand and control surface properties. Obtaining superhydrophobic coatings via relatively easy and cheap method was the final goal which was achieved and characterizations were performed extensively.

2. SURFACE AND INTERFACE

2.1 Liquids

A liquid defined as a medium, which takes the shape of a container without necessarily filling it while fluid refers collectively to solids and liquids [19]. Difference between liquid and gas state are usually described with their density, mobility and immiscibility. Liquid state have higher cohesive force (intermolecular forces such as hydrogen bonding and Van der Waals forces) and liquid molecules have somewhat limited mobility. When compared with gases, liquid molecules have shorter mean free path than gas molecules. The distance between molecules in a liquid is so small it is roughly equal to the molecular diameter, and the effect of intermolecular forces is correspondingly so large that the properties of liquids depend on the forces acting between the molecules [19-22].

Liquids demonstrate higher resistance to compression due to the small space between their molecules when compared with solids. This also gives a possibility to separate liquid from solid by their response; while solids behave elastically, liquids behave inelastic under pressure.

2.2 Solids

Solids can be categorized into two types according to their wetting behaviour; solids which contain high energy and low energy. High energy solids have chemical bonds contain high energy that keeps them together, low energy solids have lesser energy in their bonds, essentially physical forces (van der Waals). Breaking the latter bonds are relatively easier. However, transition is possible between high and low energy surfaces and changeable dynamic surfaces have been reported during the years [13–15] which can be performed via photon-driven surface energy changes.

Mobility of the solid surface molecules are highly limited. Unlike other surfaces, like liquid surfaces, their position is fixed; neither their molecules can move to another

place nor spontaneously contract to minimize their surface area. This leads to a non-equilibrium surface for solids, contradict to liquid surface which immediately forms equilibrium surface due to its high mobile surface molecules. This does not mean surface tension is missing in solids; inward pull of the solid atoms and surface tension are exist. Problematic part is; procedure of the solid surface measurement is obscure and indirect measurements are preferable. The main reason is having much less surface mobility compared to the liquids [19-22].

Most solid materials, at certain temperatures, deform elastically and may recover to their original size. When applied force increased, specimen will break but the breaking force never equal to the cohesion forces between solid molecules. Weak points, defects and previously occurred cracks are the cause of breaking.

Solids are tend to be contaminated with substances and these contaminants form a thin layer at their surfaces without protection. Without protection, solid surface would be coated with a film or a greasy material in a short time. Surface contamination, even if the contaminated surface formation is monolayer, will affect the characterization processes considerably. Given the fact that the surface tension measurement is in a direct relation with solid surface, surface composition is highly important for surface tension measurements.

Overall, ideal surface is assumed flat and chemically homogenous. Other than the absolute zero (0 K), extreme uneven surfaces often present at solid surfaces. Higher temperature leads more defects. These uneven surface characteristics of solid surfaces create surface roughness due to the varying length scales [19-22].

On the other hand, chemically homogeneous surface can be obtained if the surface consists of the same chemical groups. Otherwise it is called chemically heterogeneous. Chemical structure of the top layers of solids determine the surface properties. It is important to consider chemical structure because the surface affects adhesion, adsorption, wettability, biocompatibility, printability, and lubrication behaviour of surface [22-26]

2.3 Surface/Interfacial Tension

The surface tension is the force which tend to minimize the area of the surface and direction of the surface tension is inwards from surface, perpendicularly (Figure 2.1). Responsible for phenomenon of surface tension is the process of cohesion which can be described as attractive forces between molecules of liquids. Surface tension is dimensionally equivalent to surface free energy, but they have conceptual differences and surface tension can be regarded as a two dimensional negative pressure due to its two-dimensional analogue of the bulk pressure unit (N/m^2). Also definition of surface free energy for solids is the work spent in the forming a unit area of the solid surface [19] which is same for the liquids. However this definition indicates that the surface free energy is not equal to the surface tension for solids though they are numerically equal.

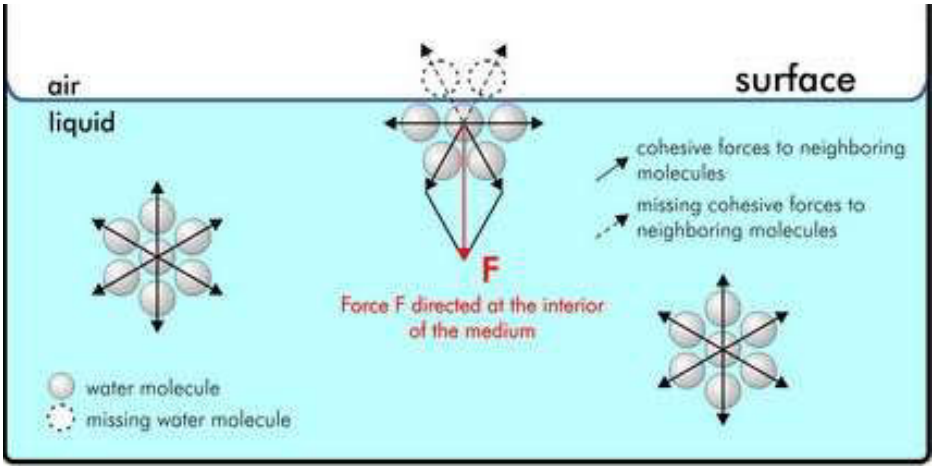

Figure 2.1 : Surface tension of a water.

In order to consider surface tension between two immiscible phases, we refer to as the interfacial tension. It is important to measure interfacial tensions (solid-vapour and solid-liquid) but direct measurement is difficult especially when a solid phase involvement present. Contact angle measurement [27-31] is the simplest way to determine the solid surface tension as an indirect approach. In liquids, cohesive forces are the cause of surface tension. Inside the bulk of the liquid, particles are surrounded with same particles and this results a net force of zero. On the other hand, at the surface, partially surrounded particles are being pulled inward as shown in Figure 2.1 [27].

This creates an internal pressure which is the reason of the surface tendency to minimize its area.

2.4 Factors Affecting Surface Tension

As mentioned above, surface tension is in a direct relation with the molecular interaction of the bulk, henceforth any factor that affects this interaction also affect surface tension.

When the temperature is increased, kinetic agitation and evaporation increases. As a result, inward pull may be expected to become less, thus weakening the molecular interactions, and the surface tension almost invariably decreases [19-22].

Non pure liquids have different surface tension, therefore adding chemicals to a liquid changes the surface tension characteristic of the liquid.

The presence of impurities on the surface of a substance directly affects the surface tension of the liquid. Surface impurities decreases contact angle value due to their interaction with the liquid.

2.5 Liquid Surface/Interfacial Tension Measurement Methods

There are several methods to measure liquid surface tension. Equipment based on the ring and Wilhelmy plate detachment methods are commonly used and these can easily be applied to pure liquids, solutions and interfacial tension between two liquids. Capillary rise, drop volume and maximum bubble pressure are also commonly used and many cutting-edge instruments have been developed for their application. The optical drop shape determination and video image digitization method compares the optically determined contour of a pendant or sessile drop image with theoretical contour, which can be predicted by the Young-Laplace equation [19-22]. There are also dynamic methods, such as oscillating plate and capillary wave methods which are used to determine changes in surface tension with systems that are not in equilibrium.

3. CONTACT ANGLE

When a liquid drop on solid surface is considered, the drop is at an equilibrium state balanced by three forces; interfacial tensions between solid and liquid (SL), between liquid and vapour (LV), and between solid and vapour (SV) which can be observed from Figure 3.1. The contact angle, θ, is the angle formed by a liquid drop at the three-phase boundary where a liquid, gas and solid intersect, and it is included between the tangent plane to the surface of the liquid and the tangent plane to the surface of the solid, at the point of intersection [32, 33].

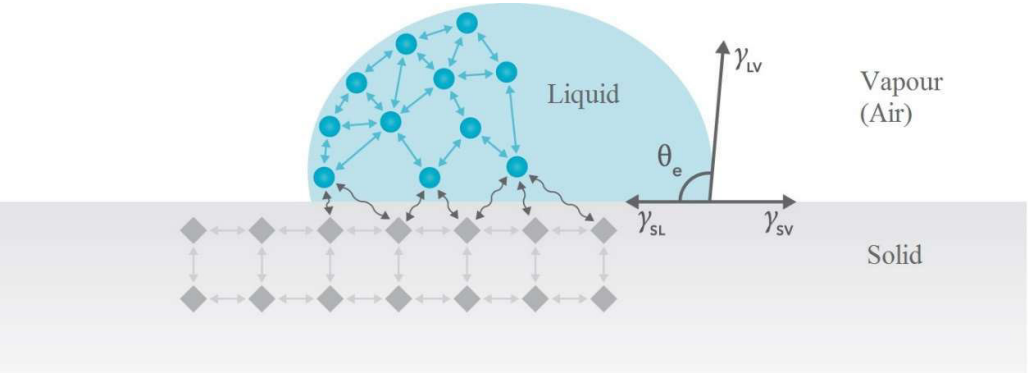

Figure 3.1 : Three-phase boundary where liquid, gas and solid intersect. γ_{SV} γ_{LV} γ_{SL} are interfacial tensions and θ_e is the contact angle.

First description of contact angle equilibrium was made by T. Young in 1805 [34]. The vectoral summation of three-phase contact angle;

$$\gamma_{SV} = \gamma_{SL} + \gamma_{LV} \cos\theta \qquad \textbf{(3.1)}$$

Where γ is the interfacial tension namely between solid-vapour (γ_{SV}), solid-liquid (γ_{SL}), liquid-vapour (γ_{LV}) and θ is the contact angle. From equation; if $\gamma_{SV} > \gamma_{SL} + \gamma_{LV}$ this corresponds to a high surface energy solid and θ is equals to 0 which means complete spreading of the liquid occurs. $\gamma_{LV}\sin\theta$ completes the vector forces of γ_{LV} and $-\gamma_{LV}\sin\theta$ balancing it which corresponds the stain force on surface..

Contact angle is a quantitative measure of wetting and every liquid, with low viscosity, can be used as for the drop unless the liquid is very volatile. Contact angle value indicates characteristics of solid-liquid interactions; if the θ value is high that indicates low solid-liquid interaction while low values mean high interaction. If the contact angle is lower than 90°, then the liquid is said to be wetting (or partially) the solid. If the contact angle is equal to 0°, this represents complete wetting.

If the water contact angle exceeds 90°, then the surface began to demonstrate hydrophobic properties. This happens when the energy of the solid surface falls behind the liquid molecules' attraction one another [19,22]. That means; if the force between molecules inside the liquid surpass the force between liquid surface and the solid, then contact angles which are exceed 90° can be observed.

If surface roughness and chemical heterogeneity exceed in a position that demonstrates water contact angle more than 150° and tilt angle less than 10°, the surface than called superhydrophobic. Superhydrophobic surfaces should also have lower contact angle hysteresis values.

3.1 Contact Angle Measurement

Contact angle measurement appear manageable, but there are few key parameters that must be considered in order to avoid thermodynamically wrong results and assumptions. These key parameters must be considered not only at measurement stage but also pre-measurement; ultra-clean substrate preparation, ultra-pure liquids for drop formation, drop evaporation (measurement needs to be fast in order to prevent evaporation), needle location inside the drop, and obtaining very sharp image. Less than perfect conditions would have an impact on to which leads to thermodynamically wrong results. Obviously perfect conditions are impossible but maintaining as perfect conditions as possible is mandatory.

There are two popular measurement techniques today; static contact angle measurement of a sessile drop via video recorder with high frame rate and dynamic contact angle measurement method using tensiometry.

3.1.1 Static contact angle measurement

Using video recorder with high frame rate is more popular and widely used in order to measure contact angle of a sessile drop than using goniometer-microscope. To apply this method, sample stage with precise controls and cold light source are also needed beside video camera as can be seen from Figure 3.2 :. This technique works with captured sharp image of the sessile drop resting on substrate. Tangent of the drop at the three-phase point is drawn at the captured drop frame which determines the contact angle. Using software analysis prevents subjective errors.

Figure 3.2 : Video recorder with high frame rate for contact angle measurement.

3.1.2 Dynamic contact angle measurement

Young equation (Eq. 3.1) assumes that the solid surface is ideal surface, suffers from absence of imperfections. However, ideal, absolute flat and chemically homogeneous surface does not exist. These imperfections inhibit one equilibrium contact angle of solid surfaces but create a range of contact angles [33-35]. Experimentally, only two types of contact angle measurement techniques are standardized [19,37];

1. **Advancing contact angle**, θa, is said to represent by the measured angle when a liquid drop is formed by injecting the liquid from a needle connected to a syringe onto a substrate surface (Figure 3.3). Liquid drop is allowed to advance on the fresh solid surface [19]. For each liquid-solid system there is a maximum value of advancing contact angle before three phase line is broken. The force

from needle and its material characteristic (such as water may climb onto some materials due to its wettability characteristics) while applying liquid may affect measurement, taking precaution is important. For example, coating the needle surface with paraffin wax or using Teflon or polypropylene needles can prevent climbing problems but also keeping the needle in the middle of the drop is needed in order to minimize the liquid applying force to drag three-phase line.

2. **Receding contact angle**, θr, can be measured when a previously formed sessile drop on the surface is contracted by applying a suction of the drop liquid through the needle (Figure 3.3) [19].

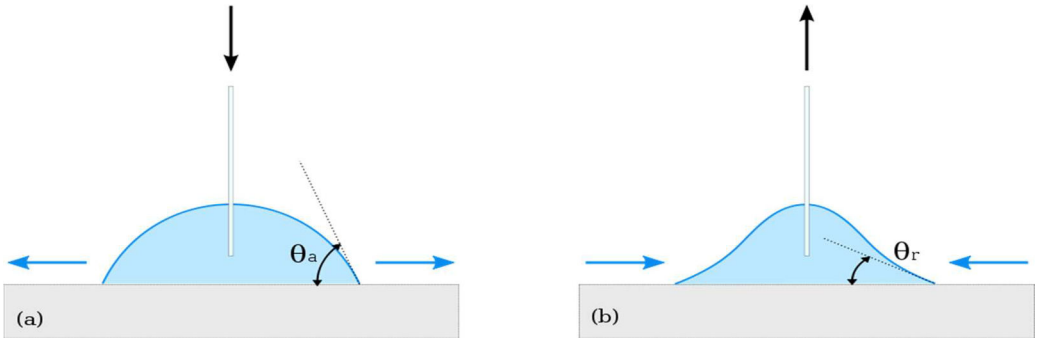

Figure 3.3 : Liquid injection and extraction inside the drop during (a) advancing (b) receding contact angle measurements.

Evaporation for liquids during contact angle measurement is undesirable, and it is unavoidable unless measurement is being done inside a closed chamber. On the other hand, evaporation can be used to obtain more reliable receding contact angle results, compared to needle-syringe sessile drop method. Evaporation enables minimum rate of withdrawal from the drop which minimizes the linear rate of retreat of the drop on the substrate [32]. Evaporation starts with decreasing contact angle and fixed contact radius began to shrink. Minimized withdrawal rate provides more reliable contact radius decrease which means more reliable contact angle values, compared to static needle-syringe drop method.

Precise advancing and receding contact angle measurements are extremely difficult as a result of their extreme sensitivity of surface chemical heterogeneity, the surface roughness and evaporation effect. Determination between ±2° is easy but it is merely impossible to reduce relative error of ±0.5°. The difference between θa and θr gives the contact angle hysteresis (CAH).

3.1.3 Contact angle hysteresis

There are some problems with this dynamic contact angle measurement method; first, extracting and receiving rate of liquid while measurement of receding and advancing contact angle is a problem, because linear rate of change of the liquid drop does not correspond at the liquid surface accordingly [30,32]. An appropriate rate is the order of 0.01 - 0.10 mm.min-1, which is very precise and slow, linear advance or retreat by using a motor-driven syringe. Second, there can be some deterioration caused by the needle which was used for introducing liquid. In order to prevent this, the needle should be positioned at the middle of the drop.

Overall there are several reasons for contact angle hysteresis;

I. Surface roughness,

II. Chemical heterogeneity,

III. Drop size effect,

IV. Molecular reorientation and deformation on solid surfaces,

V. Liquid absorption.

However surface roughness and chemical heterogeneity are the main and considered reasons for contact angle hysteresis.

3.1.3.1 Effect of surface roughness on contact angle hysteresis

Rough surface means actual surface area is greater than the plan surface area and this enhances liquid solid interaction. If the contact angle of a liquid drop on a flat surface is more than 90° then surface roughness increases this value even further. If the contact angle is lower than 90°, surface roughness decreases the contact angle value of the surface.

First Wenzel, in 1936, created a relation between contact angle and surface roughness by an assumption which indicates the drop liquids fills up the grooves on rough surface as can be seen in Equation 3.2. Wenzel introduced a roughness factor and his equation

combined with Young's equation enables us to right contact angle on a rough surface [37,19]:

$$\cos\theta_e^r = r_w \cos\theta_e^s = r_w\left(\frac{\gamma_{SL} - \gamma_{SL}}{\gamma_{LV}}\right) \quad \textbf{(3.2)}$$

Where, rw, is the ratio of real surface area and plan surface area, θ_e^r is the equilibrium contact angle of the real solid (rough surface) and θ_e^s is the equilibrium contact angle on a flat, smooth surface. In order to apply this equation surface roughness has to be at least in microscopic scale.

3.1.3.2 Effect of chemical heterogeneity on contact angle hysteresis

Contact angle hysteresis is a result on an atomically smooth surface if the surface demonstrates chemical heterogeneity. Heterogeneous surfaces possess different regions which demonstrate different contact angles. Due to the heterogeneity, hydrophobic regions will pin the motion of the contact line as the liquid advances thus increasing the contact angles [19, 35, 38]. While receding hydrophilic regions will hold back, therefore heterogeneity will increase contact angle hysteresis.

Cassie-Baxter tried to explain contact angle hysteresis for smooth surfaces possess varying heterogeneity with derivation of an equation in 1944 [39].

$$\cos\theta_e^r = f_1 \cos\theta_1 + f_2 \cos\theta_2 \quad \textbf{(3.3)}$$

Where f_1 and f_2 are the fractional area of the surface with contact angle of θ_1 and θ_2 [39]. When air pockets are represented on a rough surface and when the second component of the surface is assumed as air in which contact angle is equal to 180°;

$$\cos\theta_e^r = f_s \cos\theta_s - (1 - f_s) = f_s(\cos\theta_s + 1) - 1 \quad \textbf{(3.4)}$$

This equation found useful for heterogeneous surfaces, but cannot explained some problems which lead to CAH. This indicates that, in spite of the knowledge we gather around to understand the CAH, it is very complex to be able to fully understand for now.

4. SURFACE TENSION CALCULATIONS FROM STATIC CONTACT ANGLE

Contact angle carries the thermodynamic characteristics of the measured solid surfaces. Measuring contact angles of a series of liquids produces parameters (surface free energy (SFE), surface tension, critical surface tension etc.) which therefore quantifies the solid surface's wettability characteristics.

4.1 Fowkes (and Later Owens and Wendt's) Method

In 1964, Fowkes proposed that work of adhesion, Wa, and work of cohesion, Wc, can be separated into their dispersion (d), polar (p), induction (I), and hydrogen-bonding (h) components [40]. The dispersion component of the work of adhesion between a solid and a liquid could be expressed as;

$$W_a^d = \sqrt{((W_c^d)_S (W_c^d)_{LV}} = 2\sqrt{\gamma_S^d \gamma_{LV}^d} \quad \textbf{(4.1)}$$

And the interfacial tension for a solid-liquid system interacting by London dispersion forces alone can be given as;

$$\gamma_{SL} = \gamma_S^\circ + \gamma_{LV} - 2\sqrt{\gamma_{S^\circ}^d \gamma_{LV}^d} \quad \textbf{(4.2)}$$

Where $\gamma_{S^\circ}^d$ is dispersion component and γ_S° is surface tension from Fowkes method. Fowkes-Young equation was obtained by combining (4.2) and (2.1);

$$\gamma_{SL} \cos\theta = -\gamma_{LV} + 2\sqrt{\gamma_{S^\circ}^d \gamma_{LV}^d} - \gamma_{SV} \quad \textbf{(4.3)}$$

In 1969, Owen and Wendt proposed a new expression by dividing the surface tension into two new components, dispersive γ_i^d, and polar γ_i^p based on Fowkes equation [30].

$$W_a = 2\left(\sqrt{\gamma_{SV}^d \gamma_{LV}^d} + \sqrt{\gamma_{SV}^p \gamma_{LV}^p}\right) \quad \textbf{(4.4)}$$

Which based on these assumptions;

$$\gamma_i = \gamma_i^d + \gamma_i^p \quad \textbf{(4.5)}$$

$$\gamma_{SL} = \gamma_{SV} + \gamma_{LV} - 2(\sqrt{\gamma_{SV}^d \gamma_{LV}^d} + \sqrt{\gamma_{SV}^p \gamma_{LV}^p}) \quad \textbf{(4.6)}$$

By combining them with Young equation;

$$\gamma_{LV}(1 + \cos\theta_c)) = 2(\sqrt{\gamma_{SV}^d \gamma_{LV}^d} + \sqrt{\gamma_{SV}^p \gamma_{LV}^p}) \quad \textbf{(4.7)}$$

Owen and Wendt used only two liquids to solve this equation's unknown parameters γ_{SV}^d and γ_{SV}^p. $\gamma_{LV}^d = 21.8$ and $\gamma_{LV}^p = 51.0$ for water and $\gamma_{LV}^d = 49.55$ and γ_{LV}^p =1.3 mJm^{-1} for methylene iodide were used in order to calculate unknowns, using measured contact angle values on polymers. After that it would be easy to calculate total surface tension of the polymer from the ($\gamma_{SV} = \gamma_{SV}^d + \gamma_{SV}^p$) equation.

4.2 Van-Oss Good Approach

Based on the Lifshitz theory of attraction between macroscopic bodies, van Oss, Good and Chaudhury [41] developed a more advanced approach after 1985 to estimate the free energy of adhesion between two condensed phases [42]. Their suggestion was dividing solid surface components under two terms; first is Lifshitz-van der waals interactions, γ_{LW}, which containing dispersion, dipolar and induction interaction, and the second one is the acid-base interaction term, γ_{AB}, which containing electron donor-acceptor interactions, such as hydrogen bonding. It was thought that, Lifshitz calculations yield γ_{LW} which is the result of all the electromagnetic interactions taken together. Lifshitz-van der Waals also includes the interactions of pairs, triplets, quadruplets etc. of molecules within each phase, in all the actual configurations that are taken on when they interact.

Corresponding components of work of adhesions;

$$-W_a = \Delta G_{SL} = \Delta G_{SL}^{LW} + \Delta G_{SL}^{AB} \quad \textbf{(4.8)}$$

And the combining rule for LW components is given as;

$$\Delta G_{SL}^{LW} = \sqrt{\Delta G_S^{LW} \Delta G_L^{LW}} \quad \textbf{(4.9)}$$

This equation is in accordance with Fowkes approach and it has been experimentally demonstrated [42,43] that when only dispersion interaction forces are available between two phase materials, the interfacial tension, γ_{SL}^{LW} can be written as;

$$\gamma_{SL}^{LW} = \gamma_{SV}^{LW} + \gamma_L^{LW} - 2\sqrt{\gamma_S^{LW} \gamma_L^{LW}} \quad \textbf{(4.10)}$$

or

$$\gamma_{SL}^{LW} = (\sqrt{\gamma_S^{LW}} - \sqrt{\gamma_L^{LW}})^2 \quad \textbf{(4.11)}$$

This is referred as Good-Girifalko-Fowkes combining rule [44,45].

The free energy of interaction between materials (solid-liquid) in vacuum can be interpreted with surface tensions of these materials by the Dupré equation [46].

$$-\Delta G_{SL}^{LW} = \gamma_S^{LW} + \gamma_L^{LW} - \gamma_{SL}^{LW} \quad \textbf{(4.12)}$$

By combining them;

$$-\Delta G_{SL}^{LW} = 2\sqrt{\gamma_S^{LW} \gamma_L^{LW}} \quad \textbf{(4.13)}$$

Which suggest that energy of interaction is negative and interaction between two purely polar condensed phases always attractive.

However van Oss and Good adopted Small's combining rule because previous combining rule is not acceptable to acid-base interactions, it was very simple, which is not a geometric mean;

$$-\Delta G_{SL}^{AB} = 2(\sqrt{\gamma_s^+ \gamma_c^-} + \sqrt{\gamma_s^+ \gamma_L^+}) \quad \textbf{(4.14)}$$

Combining these equations with LW component the total interfacial free energy of adhesion can be obtained as;

$$-\Delta G_{SL} = 2(\sqrt{\gamma_S^{LW}\gamma_L^{LW}} + \sqrt{\gamma_s^+\gamma_L^-} + \sqrt{\gamma_s^-\gamma_L^+}) \quad \textbf{(4.15)}$$

Combining this equation with Young-Dupré equation, for negligible spreading pressure, general contact angle equation can be given as;

$$\gamma_{LV}(1+\cos\theta) = 2(\sqrt{\gamma_S^{LW}\gamma_L^{LW}} + \sqrt{\gamma_s^+\gamma_L^-} + \sqrt{\gamma_s^-\gamma_L^+}) \quad \textbf{(4.16)}$$

In order to obtain contact angle data, we need a set of values of $\gamma_L^{LW}, \gamma_L^- \; and \; \gamma_S^-$ for reference liquids. Van Oss and Good introduced an arbitrary relation for water. It was assumed that $\gamma_W^+ = \gamma_W^-$ for water, and γ^{AB} for water is known, $\gamma_W^+ = \gamma_W^- = 25.5 mjm^{-2}$ can be calculated from equation;

$$-\Delta G_{SL}^{AB} = 2(\sqrt{\gamma_s^+\gamma_L^-} + \sqrt{\gamma_s^-\gamma_L^+}) \quad \textbf{(4.17)}$$

Which can be rewritten for single phase;

$$\gamma_i^{AB} = 2\sqrt{\gamma_i^+\gamma_i^-} \quad \textbf{(4.18)}$$

since;

$$-\Delta G_i^{AB} = 2\gamma_i^{AB} \quad \textbf{(4.19)}$$

After finding reference values, polymer surface values γ_S^{LW}, $\gamma_s^+$and γ_s^- can be calculated either solving simultaneously using three different liquids or γ_S^{LW} can be determined by using a nonpolar liquid first, then two other polar liquids are used to determine γ_s^+ and γ_s^- (Table 4.1 [47,48]). Latter method sometimes produce negative square roots of γ_s^+ and γ_s^- and this attracts objections to this theory.

Table 4.1 : Test liquids surface tension values.

Liquid	γ_{LV}	γ_{LV}^d	γ_{LV}^p	γ_{LV}^{LW}	γ_{LV}^{AB}	γ_{LV}^+	γ_{LV}^-
Water	72.8	21.8±3	51.0	21.8	51.0	25.5	25.5
Ethylene glycol	48.0	-	-	29.0	19.0	1.92	47.0
Formamide	58.0	39.5±7	18.5	39.5	19.0	2.28	39.6
Methylene iodide	50.8	48.5±9	2.3	50.8	0	0	0

5. SPECTROSCOPY

The transmittance and reflectance values of the deposited films were measured by spectrophotometer analyses over the spectral range of 300-1000 nm.

5.1 Calculation of the Optical Constants and Band Gap

Tauc method was used in order to determine the band gap values using absorption coefficient [17,18]. Related data, refractive index (n) and extinction coefficient (k), was calculated using the theory of reflectivity of light. According to this theory, the reflectance of light from a film can be expressed in terms of Fresnel's coefficient. Reflectivity [17] can be given by;

$$R = {[(n-1)^2 + k^2\,]}\Big/{[(n+1)^2 + k^2\,]} \qquad \textbf{(5.1)}$$

The absorption coefficient (α);

$$\alpha = {4\pi k}/{\lambda} \qquad \textbf{(5.2)}$$

Where λ is the wavelength and k is the extinction coefficient. The extinction coefficient k and refractive index n were calculated using the transmittance and reflectance data, by the spectrophotometer software, ProOptix.

Empirical expressions for optical gap (Tauc gap) can be defined in terms of extrapolation of the extended states. Tauc model is widely used to determine optical gap in amorphous semiconductors where it is assumed square root distributions of conduction and valance band states, and disorder characteristics of amorphous semiconductors relaxes the momentum conservation, such that the momentum matrix element is independent of photon energy, hv, Tauc, Grigorocivi and Vancu defined an optical gap (E_{gTauc}) that is widely used among experimentalists reporting on the optical properties of films [17, 18]. Tauc relation [17] can be given as;

$$\sqrt{(\alpha(hv)hv)} = C_{Tauc}\,(hv - E_{g^{Tauc}}) \qquad \textbf{(5.2)}$$

Where α is the absorption coefficient, hv is the photon energy, C_{Tauc} is the Tauc constant in this extrapolation, and E_{gTauc} is the corresponding Tauc gap [17]. Necessary data for calculation was provided by software which was used for optical measurements. For the extrapolation method [17] by placing the calculated absorption coefficient in the Tauc formula $(\alpha hv)^{1/2}$ and $(\alpha hv)^2$ graphs were drawn. With the extrapolation of the linear parts of the graphs, band gaps of coatings are calculated and can be seen from Figure 9.5:-Figure 9.12: for flat coated polymers and Figure 9.21:-Figure 9.22: for superhydrophobic sample coating which has %70 SiO_2 nanoparticle content.

6. THIN FILM OPTICS

In order to obtain the magnitude of light beam that propagates one or more medium, boundary conditions apply to Maxwell Equation. These equations are so complicated that needs complex solutions. Therefore, we used assumptions. In this section, brief information about thin film optics is given.

6.1 Absorbing Mediums

Equation of propagating light in permeable medium can used in absorbing medium as well, if we use refractive index as complex number. The imaginary part is related to absorbance in medium. If we have a wave in a permeable medium that refractive index n, towards (λ, μ, ν) directions and rotational frequency ω, so the field vector,

$$E = E0expi\omega\left(t - \frac{n(\lambda x+\mu y+\nu z)}{c}\right) \quad \textbf{(6.1)}$$

where c is speed of light in vacuum.

In absorbing medium this equation evaluates,

$$E = E0expi\omega\left(t - \frac{\lambda(\lambda x + \mu y + \nu z)}{c} + \frac{i\beta(\lambda' x + \mu' y + \nu' z)}{c}\right) \quad \textbf{(6.2)}$$

where (λ', μ', ν') is the direction of maximum reduction (damping).

For a incident wave in normal direction,

$$E = E0expi\omega\left(t - \frac{(n - ik)(\lambda x + \mu y + \nu z)}{c}\right) \quad \textbf{(6.3)}$$

α and β from Eq. (6.2) are related to the direction of propagation and angle of incidence (θ).

$$\alpha^2 - \beta^2 = n^2 - k^2 \quad \textbf{(6.4)}$$

$$\alpha\beta cos\varphi = nk \quad \textbf{(6.5)}$$

$$sin\theta = \alpha sin\varphi \quad \textbf{(6.6)}$$

Equation 6.4, 6.5 and 6.6 give the relation between θ, φ, n and better detail than Snell Law.

6.2 Transmittance and Reflectance in Permeable Medium

For an isotropic medium, electromagnetic laws represent these equations,

$$div\ D = \varepsilon div\ E = 4\pi\rho \quad \textbf{(6.7)}$$

$$div\ B = \mu div\ H = 0 \quad \textbf{(6.8)}$$

$$curlE = -\frac{\mu}{c}\frac{\partial E}{\partial t} \quad \textbf{(6.9)}$$

$$curlH = \frac{4\pi\sigma E}{c} + \frac{\varepsilon}{c}\frac{\partial E}{\partial t} \quad \textbf{(6.10)}$$

Propagation of electromagnetic waves in uncharged medium represent with Maxwell equations.

$$\frac{\varepsilon\mu}{c^2}\frac{\partial^2 E}{\partial t^2} + \frac{4\pi\mu\sigma}{c^2}\frac{\partial E}{\partial t} = \nabla^2 E \quad \textbf{(6.11)}$$

$$\frac{\varepsilon\mu}{c^2}\frac{\partial^2 E}{\partial t^2} + \frac{4\pi\mu\sigma}{c^2}\frac{\partial H}{\partial t} = \nabla^2 H \quad \textbf{(6.12)}$$

For non-conducting medium (σ = 0);

$$\frac{\varepsilon\mu}{c^2}\frac{\partial^2 E}{\partial t^2} = \nabla^2 E \quad \textbf{(6.13)}$$

$$\frac{\varepsilon\mu}{c^2}\frac{\partial^2 E}{\partial t^2} = \nabla^2 H \quad \textbf{(6.14)}$$

Waves propagates at speed of $c/\sqrt{\mu\varepsilon}$. For almost every material, value of μ is nearly equals to unity at optical frequencies. Thus, the final speed turns into $c/\sqrt{\varepsilon}$, where ε is the dielectric constant and $n = \sqrt{\varepsilon}$ is obtained by using refractive index, n.. Finally, transmittance and reflectance obtained by applying boundary conditions to Maxwell equations. Coordinate system was given in Figure 6.1 :, where E_{0p}^{+} and E_{0s}^{+}, E_{0p}^{-} and E_{0s}^{-}, E_{1p}^{-} and E_{1s}^{-} are the components of incident, reflected and transmitted waves, respectively.

$$expi\left(\omega t - \frac{2\pi n_0 x sin\varphi_0}{\lambda} - \frac{2\pi n_0 z cos\varphi_0}{\lambda}\right) \quad \textbf{(6.15)}$$

$$expi\left(\omega t - \frac{2\pi n_0 x sin\varphi_0}{\lambda} + \frac{2\pi n_0 z cos\varphi_0}{\lambda}\right) \quad \textbf{(6.16)}$$

However, the equation evaluates for propagating wave,

$$expi\left(\omega t - \frac{2\pi n_1 x sin\varphi_0}{\lambda} - \frac{2\pi n_1 z cos\varphi_0}{\lambda}\right) \quad \textbf{(6.17)}$$

where λ is the wavelength in vacuum.

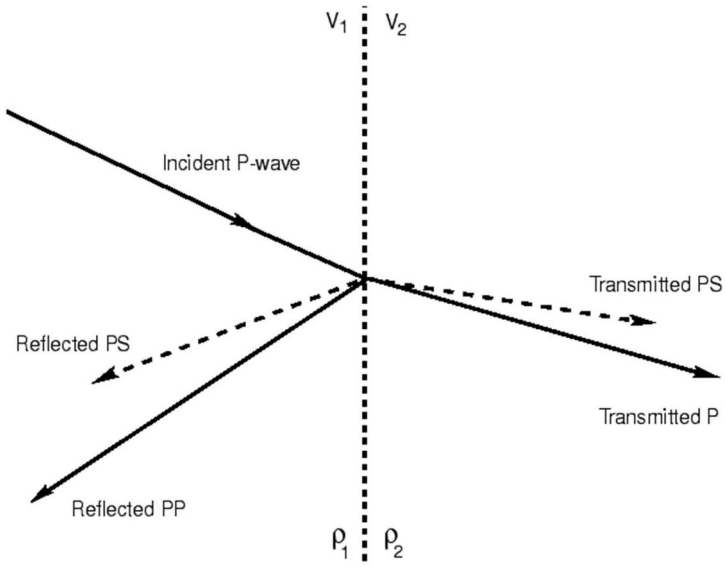

Figure 6.1 : Incident, transmitted and reflected wave.

$$E_{0x} = \left(E_{0p}^{+} + E_{0p}^{-}\right)cos\varphi 0 \quad \textbf{(6.18)}$$

$$E_{0y} = E_{0s}^{+} + E_{0s}^{-} \quad \textbf{(6.19)}$$

$$H_{0x} = n_0\left(-E_{0p}^{+} + E_{0p}^{-}\right)cos\varphi \quad \textbf{(6.20)}$$

$$H_{0y} = n_0\left(E_{0p}^{+} + E_{0p}^{-}\right) \quad \textbf{(6.21)}$$

and for first medium,

$$E_{1x} = E_{1p}^{+}cos\varphi_1 \quad \textbf{(6.22)}$$

$$E_{1y} = E_{1s}^{+} \quad \textbf{(6.23)}$$

$$H_{1x} = -n_1 E_{1s}^{+}cos\varphi_1 \quad \textbf{(6.24)}$$

$$H1y = n_1 E_{1p}^{+} \quad \textbf{(6.25)}$$

If we apply boundary conditions for transmitted and reflected wave,

$$\frac{E_{0p}^{-}}{E_{0p}^{+}} = \frac{n_0 cos\varphi_1 - n_1 cos\varphi_0}{n_0 cos\varphi_1 + n_1 cos\varphi_0} = r_{1p} \quad \textbf{(6.26)}$$

$$\frac{E_{1p}^{+}}{E_{0p}^{+}} = \frac{2n_0 cos\varphi_0}{n_0 cos\varphi_1 + n_1 cos\varphi_0} = t_{1p} \quad \textbf{(6.27)}$$

$$\frac{E_{0s}^{-}}{E_{0s}^{+}} = \frac{n_0 cos\varphi_0 - n_1 cos\varphi_1}{n_0 cos\varphi_0 + n_1 cos\varphi_1} = r_{1s} \quad \textbf{(6.28)}$$

$$\frac{E_{1s}^{+}}{E_{0s}^{+}} = \frac{2n_0 cos\varphi_0}{n_0 cos\varphi_0 + n_1 cos\varphi_1} = t_{1s} \quad \textbf{(6.29)}$$

Where r_{1p}, r_{1s} and t_{1p}, t_{1s} are the reflectance and transmittance coefficients of Fresnel, respectively. We need these coefficients to solve multilayer systems. From Eq. (6.26) to (6.29) we obtain,

$$t1p = 1 + r1p \quad \textbf{(6.30)}$$

$$t1s = 1 + r1s \quad \textbf{(6.30)}$$

and if $n_0 > n_1$, then t_{1p} and t_{1s} approach to 1.

Poynting vector represents with *S* and if we apply energy conservation and Poynting law,

$$|S| = \frac{c}{4\pi}[ExH] \tag{6.31}$$

$$|S| = \frac{c}{4\pi}n[E]2 \tag{6.32}$$

Therefore reflectance,

$$Rp = \frac{(E_{0p}^{-})^2}{(E_{0p}^{+})^2} = r_{1p}^2 \tag{6.33}$$

$$Rs = \frac{(E_{0s}^{-})^2}{(E_{0s}^{+})^2} = r_{1s}^2 \tag{6.34}$$

and transmittance,

$$Tp = \frac{n_1(E_{1p}^{+})^2}{n_0(E_{0p}^{+})^2} = \frac{n_1}{n_0}t_{1p}^2 \tag{6.35}$$

$$Ts = \frac{n_1(E_{1s}^{+})^2}{n_0(E_{0s}^{+})^2} = \frac{n_1}{n_0}t_{1s}^2 \tag{6.36}$$

For an incident normal wave, transmittance and reflectance values are,

$$Rp = Rs = \left(\frac{n_0 - n_1}{n_0 + n_1}\right)^2 \tag{6.37}$$

$$Tp = Ts = \frac{4n_0n_1}{(n_0 + n_1)^2} \tag{6.38}$$

If we apply Snell Law, we obtain Fresnel coefficients,

$$r1p = \frac{tan(\varphi_1 - \varphi_0)}{tan(\varphi_1 + \varphi_0)} \tag{6.39}$$

$$r1s = \frac{sin(\varphi_1 - \varphi_0)}{sin(\varphi_1 + \varphi_0)} \tag{6.40}$$

$$t1p = \frac{2sin\varphi_1 cos\varphi_0}{sin(\varphi_1 + \varphi_0)cos(\varphi_1 - \varphi_0)} \tag{6.41}$$

$$t1s = \frac{2sin\varphi_1 cos\varphi_0}{sin(\varphi_1 + \varphi_0)} \tag{6.42}$$

These equations are very popular for a layer but not so much for multilayers.

6.3 Reflection at Surface of Absorbing Medium

We can obtain propagation equations in absorbing medium by using complex refractive index as done in previous section. Thus, Eq. 6.26 to 6.29 evaluates,

$$Sin\varphi 1 = \frac{n_0 sin\varphi_0}{n_1 - ik_1} \tag{6.43}$$

So φ_1 becomes complex and does not represent refractive index unless $\varphi_0 = \varphi_1 = 0$. This is a special condition that we can easily find Fresnel refractive coefficients.

$$r_{1p} = r_{1s} = \frac{n_0 - n_1 + ik_1}{n_0 + n_1 - ik_1} \tag{6.44}$$

$$Rp = Rs = \frac{(n_0 - n_1)^2 + k_1^2}{(n_0 + n_1)^2 + k_1^2} \tag{6.45}$$

Except normal incident, reflection term becomes too complicated and needs assumption. Major part of absorbing materials, especially metals, show $n^2 + k^2 \gg 1$ in visible spectrum. With this assumption, equation 6.46 and 6.67 obtained;

$$Rp = \frac{(n^2 + k^2)cos^2\varphi_0 - 2ncos\varphi_0 + 1}{(n^2 + k^2)cos^2\varphi_0 + 2ncos\varphi_0 + 1} \tag{6.46}$$

$$Rs = \frac{(n^2 + k^2) - 2ncos\varphi_0 + cos^2\varphi_0}{(n^2 + k^2) + 2ncos\varphi_0 + cos^2\varphi_0} \tag{6.47}$$

The Fresnel transmittance coefficients are non-effective by the interaction between the amplitude of wave and propagation in absorbing medium. So complex Fresnel transmittance coefficients are,

$$r_{ip} = \sigma_{ip} e^{i\beta_{1p}} \tag{6.48}$$

$$r_{is} = \sigma_{is} e^{i\beta_{1s}} \tag{6.49}$$

where σ_{ip}, σ_{is} are the amplitude of reflected waves and β_{1p}, β_{1p} represent phase transformation at the surface. σ and β values represents as,

$$\frac{1+\sigma e^{i\beta}}{1-\sigma e^{i\beta}} = \frac{sin\varphi_0 tan\varphi_0}{[(n-ik)^2 - sin^2\varphi_0]^{1/2}} \quad \textbf{(6.50)}$$

6.4 Transmittance and Reflectance of Single Layer

We can use results that obtained in Section (6.3) to evaluate transmittance coefficients for non-absorbing single layer, which is limited by half infinitive non-absorbing mediums at both sides. Incident light beam separates into reflected and transmitted parts. We sum up both parts separately which is a useful method for single layer. Results are represents via Fresnel coefficients.

Fresnel coefficients from Eq. 6.26 to 6.29 will be represented as r_1, t_1 for propagation n_0 to n_1; r_1' and t_1' for propagation n_1 to n_0. Since, these coefficients are comply with both directions of polarization; it gives appropriate values to *r* and *t*. Thus, second index (p or s) will be ignored. From Fresnel reflectance coefficients, we can evaluate that r_1' equals to $-r_1'$. So, the amplitude of reflected consecutive rays are represented as r_1, $t_1 t_1' r_2$, $-t_1 t_1' r_1 r_2^2$, $t_1 t_1' r_1^2 r_2^3$, … and transmitted consecutive rays are represented as $t_1 t_2$, $-t_1 t_2 r_1 r_2$, $t_1 t_2 r_1^2 r_2^2$, … . δ_1 is the phase transition of transmitted rays,

$$\delta 1 = \frac{2\pi}{\lambda} n_1 d_1 cos\varphi_1 \quad \textbf{(6.51)}$$

so, the reflected amplitude,

$$R = r1 + t1t_1' r2 e^{-2i\,\delta_1} - t1t_1' r1 r_2^2 e^{-4i\,\delta_1} + \cdots \quad \textbf{(6.52)}$$

$$R = r1 + \frac{t_1 t_1' r_2 e^{-2i\,\delta_1}}{1 + t_1 t_1' r_2 e^{-2i\,\delta_1}} \quad \textbf{(6.53)}$$

This term is independent of time. For non-absorbing mediums, representing Fresnel transmittance coefficients is easier with r_1 and r_2 terms. From energy conservation and Eq. (6.26) and (6.29),

$$t_1 t_1' = -r_2^2 \quad \textbf{(6.54)}$$

so, Eq. (6.51) evaluates,

$$R = \frac{r_1 + r_2 e^{-2i\,\delta_1}}{1 + r_1 r_2 e^{-2i\,\delta_1}} \tag{6.55}$$

and the amplitude of transmitted rays

$$T = t1t2e^{-i\,\delta_1} - t1t2r1r2e^{-3i\,\delta_1} + t1t2r_1^2 r_2^2 e^{-5i\,\delta_1} - \cdots \tag{6.56}$$

$$T = \frac{t_1 t_2 e^{-i\,\delta_1}}{1 + r_1 r_2 e^{-2i\,\delta_1}} \tag{6.57}$$

Eq. (6.55) and (6.57) are general. For not normal incident, there are two possibilities due to polarization of incident light. For parallel coefficient, Eq. (6.22) and (6.23) are used; for perpendicular coefficient Eq. (6.24) and (6.25) are used.

If the layer is absorbing or is limited by absorbing mediums, we use complex values for n_0, n_1, and n_2. Thus, Fresnel coefficients become complex and calculating R and T values become complicated. The total energy of rays,

$$n_0 RR* = \frac{n_0(r_1^2 + 2r_1 r_2 cos2\delta_1 + r_2^2)}{(1 + 2r_1 r_2 cos2\delta_1 + r_1^2 r_2^2)} \tag{6.58}$$

$$n_2 TT* = \frac{n_2 t_1^2 t_2^2}{(1 + 2r_1 r_2 cos2\delta_1 + r_1^2 r_2^2)} \tag{6.59}$$

Then reflectance and transmittance evaluates,

$$R = \frac{r_1^2 + 2r_1 r_2 cos2\delta_1 + r_2^2}{1 + 2r_1 r_2 cos2\delta_1 + r_1^2 r_2^2} \tag{6.60}$$

$$T = \frac{n_2}{n_0} \frac{t_1^2 t_2^2}{1 + 2r_1 r_2 cos2\delta_1 + r_1^2 r_2^2} \tag{6.61}$$

From Eq. (6.26) to (6.29) Fresnel coefficients,

$$r_1 = \frac{n_0 - n_1}{n_0 + n_1} \text{ and } t_1 = \frac{2n_0}{n_0 + n_1} \tag{6.62}$$

$$r_2 = \frac{n_1 - n_2}{n_1 + n_2} \text{ and } t_2 = \frac{2n_2}{n_1 + n_2} \tag{6.63}$$

so, Eq. (6.56) and (6.57) becomes,

$$R = \frac{(n_0 - n_1)(n_1 + n_2)e^{i\,\delta_1} + (n_0 + n_1)(n_1 - n_2)e^{-i\,\delta_1}}{(n_0 + n_1)(n_1 + n_2)e^{i\,\delta_1} + (n_0 - n_1)(n_1 - n_2)e^{-i\,\delta_1}} \quad \textbf{(6.64)}$$

$$T = \frac{4n_0 n_1}{(n_0 + n_1)(n_1 + n_2)e^{i\,\delta_1} + (n_0 - n_1)(n_1 - n_2)e^{-i\,\delta_1}} \quad \textbf{(6.65)}$$

and finally refrectance and transmittance is given by,

$$\boldsymbol{R} = \frac{(n_0^2 + n_1^2)(n_1^2 + n_2^2) - 4n_0 n_1^2 n_2 + (n_0^2 - n_1^2)(n_1^2 - n_2^2)cos2\delta_1}{(n_0^2 + n_1^2)(n_1^2 + n_2^2) + 4n_0 n_1^2 n_2 + (n_0^2 - n_1^2)(n_1^2 - n_2^2)cos2\delta_1} \quad \textbf{(6.9)}$$

$$\boldsymbol{T} = \frac{8n_0 n_1^2 n_2}{(n_0^2 + n_1^2)(n_1^2 + n_2^2) + 4n_0 n_1^2 n_2 + (n_0^2 - n_1^2)(n_1^2 - n_2^2)cos2\delta_1} \quad \textbf{(6.9)}$$

These terms can be evaluated for non-absorbing mediums. If the film or the limiting mediums are absorbing, then we should change n_0, n_1 and n_2 values to $n = n\text{-}ik$.

In this section, we have tried to obtain optical constants of film by transmittance relation. We have measured transmittance due to wavelength and we have already known the refractive index of substrate and air, so we can calculate the refractive index, absorbing and damping coefficients of film.

7. MATERIALS AND METHODS

7.1 Polymers

7.1.1 Polyolefin

7.1.1.1 Polyethylene

Polyethylene [52] is the most common used plastic. It is a thermoplastic polymer consisting of long hydrocarbon chains and Its primary use is in packaging (plastic bag, plastic films, geomembranes, containers including bottles, etc.). Depending on the crystallinity and molecular weight, a melting point and glass transition may or may not be observable. Repeating unit of polyethylene can be seen in Figure 5.1 [53]

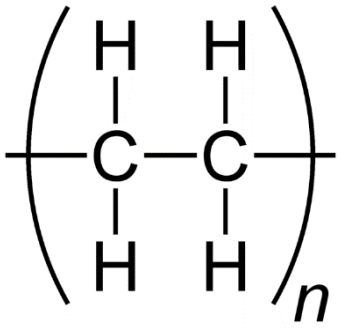

Figure 5.1 : Repeating unit of polyethylene.

For common commercial grades of medium- and high-density polyethylene the melting point is typically in the range 120 to 180 °C. The melting point for average, commercial, low- density polyethylene is typically 105 to 115 °C.

7.1.1.2 High density polyethylene

High-density polyethylene (HDPE) is a polyethylene thermoplastic made from petroleum. It is also called linear polyethylene, it is normally produced with molecular weights in the range of 200,000 to 500,000, but it can be made even higher. HDPE has stronger intermolecular forces and tensile strength than LDPE cause of its lesser branching. The density of HDPE can range from 0.93 to 0.97 g/cm3.The difference in

strength exceeds the difference in density, giving HDPE a higher specific strength. It is also harder and more opaque and can withstand somewhat higher temperatures.

7.1.1.3 Low density polyethylene

Low-density polyethylene (LDPE) is a thermoplastic made from the monomer ethylene. It was the first grade of polyethylene, produced by using a high pressure process via free radical polymerization.

LDPE is defined by a density range of 0.910–0.940 g/cm3. It can withstand temperatures of 80 °C continuously and 95 °C for a short time. Made in translucent or opaque variations, it is quite flexible, and tough but breakable.

LDPE has more branching (on about 2% of the carbon atoms) than HDPE, so its intermolecular forces (instantaneous-dipole induced-dipole attraction) are weaker, its tensile strength is lower, and its resilience is higher.

7.1.1.4 Polypropylene

Polypropylene (PP) is a type of thermoplastic polymer. It is manufactured from propylene gas, the chemical designation of polypropylene is *(C3H6)n* . This material can be used in a wide variety of applications; it serves both as a plastic and as a fibre, including packaging and labelling, textiles (e.g., ropes, thermal underwear and carpets), reusable containers of various types, laboratory equipment, loudspeakers, automotive components, and polymer banknotes. An addition polymer made from the monomer propylene, it is rugged and unusually resistant to many chemical solvents, bases and acids [51]. Repeating unit of polypropylene can be seen in Figure 5.2 [52].

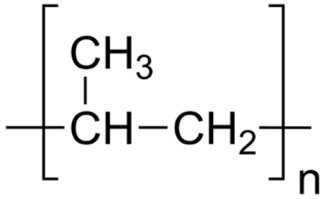

Figure 5.2 : Repeating unit of polypropylene.

Polypropylene has good resistance to fatigue. The melting point of polypropylene occurs at a range, so a melting point is determined by finding the highest temperature of a differential scanning calorimetry chart. Perfectly isotactic PP has a melting point

of 171 °C (340 °F). Commercial isotactic PP has a melting point that ranges from 160 to 166 °C (320 to 331 °F), depending on atactic material and crystallinity. There are three general types of polypropylene: homopolymer, random copolymer, and block copolymer.

7.1.1.5 Polypropylene polyethylene copolymer

Polypropylene-polyethylene copolymer (PPPE) is the copolymerized form of polypropylene and ethylene. Copolymerization of polypropylene results to be more flexible and tough; allows to be used as an engineering plastic. Randomly polymerized ethlyene monomer added to polypropylene homopolymer decreases the polymer crystallinity, lowers the melting point and makes the polymer more transparent [53].

7.1.2 Polystyrene

Polystyrene (PS) is a synthetic aromatic polymer made from the monomer styrene. Polystyrene can be solid or foamed. It is a rather poor barrier to oxygen and water vapour and has a relatively low melting point. Repeating unit of polystyrene can be seen in Figure 5.3 [54].

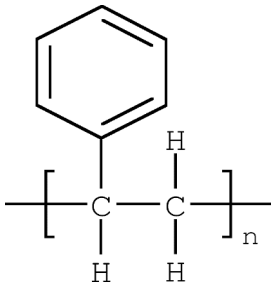

Figure 5.3 : Repeating unit of polystyrene.

As a thermoplastic polymer, polystyrene is in a solid (glassy) state at room temperature but flows if heated above about 100 °C, its glass transition temperature. It becomes rigid again when cooled.

Polystyrene is very slow to biodegrade and is therefore a focus of controversy. It is often abundant as a form of litter in the outdoor environment, particularly along shores and waterways, especially in its foam form.

7.1.3 Poly (methyl methacrylate)

Poly (methyl methacrylate) (PMMA) is a transparent thermoplastic. It has a density of 1.17–1.20 g/cm3. PMMA ignites at 460 °C (860 °F) and burns, forming carbon dioxide, water, carbon monoxide and low-molecular-weight compounds, including formaldehyde [52]. Repeating unit of poly(methyl methacrylate) can be seen in Figure 5.4 [56].

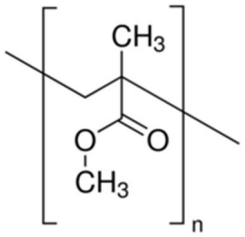

Figure 5.4 : Repeating unit of poly(methyl methacrylate).

PMMA swells and dissolves in many organic solvents; it also has poor resistance to many other chemicals on account of its easily hydrolyzed ester groups. Nevertheless, its environmental stability is superior to most other plastics such as polystyrene and polyethylene.

7.1.4 Polyamide

Polyamide is a macromolecule of repeating units linked by amide bonds. [57] Polyamides occur both naturally and artificially. Examples of naturally occurring polyamides are proteins, such as wool and silk.

Artificially made polyamides can be made through step-growth polymerization or solid-phase synthesis yielding materials such as nylons, aramids, and sodium poly (aspartate). Synthetic polyamides are commonly used in textiles, automotive applications, carpets and sportswear due to their high durability and strength. Repeating unit of polyamide can be seen in Figure 5.5 [58].

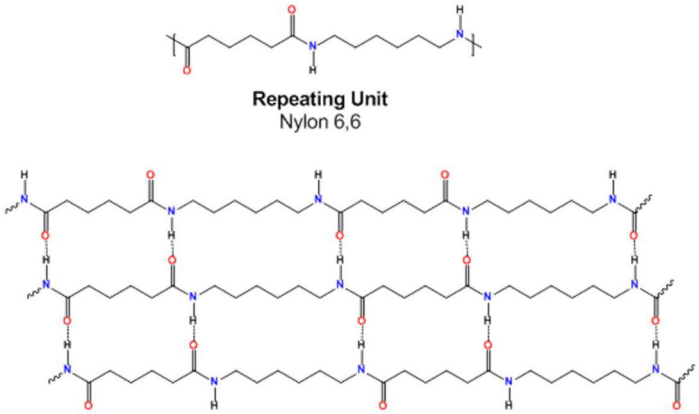

Figure 5.5 : Repeating unit of polyamide.

7.1.5 Polyvinyl alcohol

Polyvinyl alcohol (PVOH, PVA, or PVAl) is a water-soluble synthetic polymer. It is used in papermaking, textiles, and a variety of coatings. Polyvinyl alcohol has excellent film forming, emulsifying and adhesive properties. It is also resistant to oil, grease and solvents. It has high tensile strength and flexibility, as well as high oxygen and aroma barrier properties. However these properties are dependent on humidity, in other words, with higher humidity more water is absorbed. Repeating unit of polyvinyl alcohol can be observed in Figure 5.6 [59].

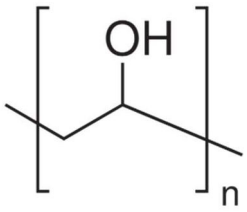

Figure 5.6 : Repeating unit of polyvinyl alcohol.

PVA has a melting point of 230 °C and 180–190 °C.

7.2 Thin Film Deposition

Thin films grow by the deposition of material atoms on any substrate. The thin film growth exhibits the following features:

I. Thin film growth of all materials starts with random nucleation process, which followed by nucleation and growth process (Figure 7.1).

II. The nucleation and growth stages are extremely dependent upon various deposition conditions; such as growth temperature, growth rate, and substrate surface chemistry.

III. External agencies, such as electron or ion bombardment, can modify nucleation.

IV. Film microstructure that is associated with structure defect, and film stress depend on the deposition condition of the nuclear stage.

V. Deposition conditions manage crystal phase and crystal orientation of the thin films. [60].

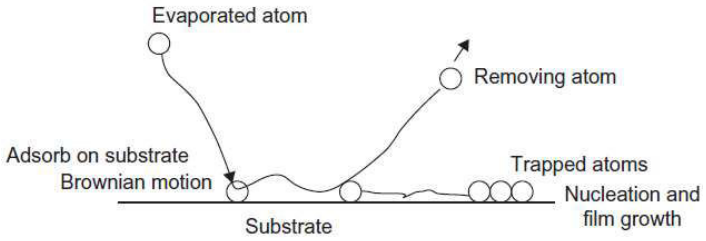

Figure 7.1 : The growth model of thin films.

Thin films show very different characteristic properties than bulk materials thus, to gain control over how to alter the properties of thin films is crucial. Deposition condition control, which can be achievable via vacuum chamber (Figure 7.2 [61]), can be considered as the most useful and easy tool to alter basic properties of thin films, such as film chemical composition, structural properties, film thickness, and different thin film properties than bulk materials can be observed;

I. Unique material properties depend on the atomic growth process on the growing substrate.

II. By including quantum size effects; size effects characterized by crystal orientation, thickness and multilayer aspects [60].

Generally, bulk materials are sintered from the powder of source material. Diameter of the powder is of the order of 1 μm. On the other hand, thin films are synthesized from ultrafine particles like atoms or a cluster of atoms.

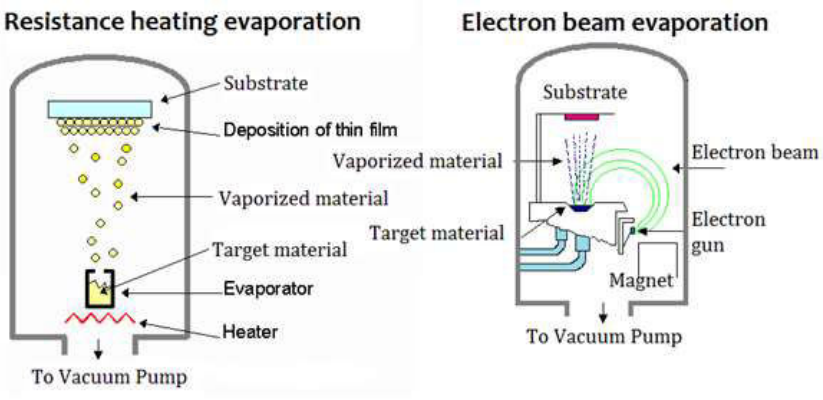

Figure 7.2 : Typical thin film deposition system in vacuum.

There are two main categories for deposition process, physical and chemical as can be seen in Figure 7.3 [62].

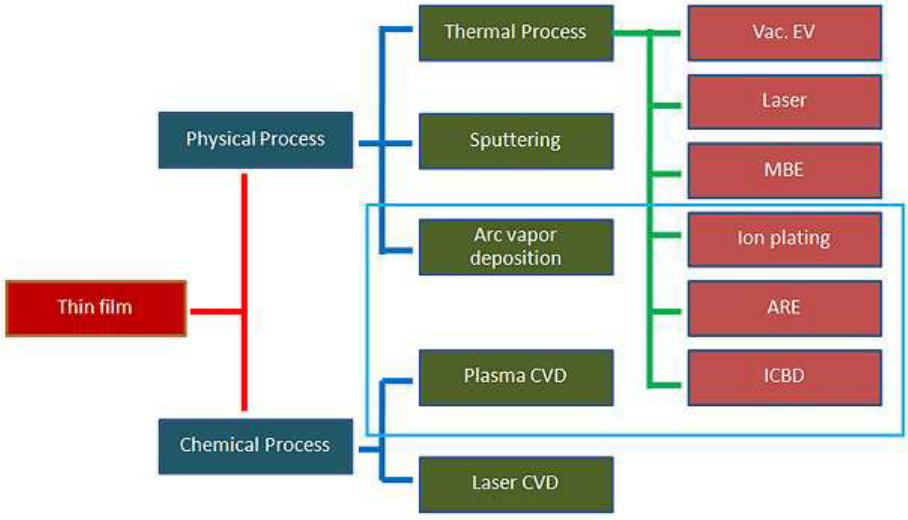

Figure 7.3 : Typical deposition methods of thin films.

Plating, chemical solution deposition, spin coating, dip coating, spray-up, chemical vapor deposition and atomic layer deposition are chemical deposition techniques. On the other hand, physical vapor deposition, sputtering, pulsed laser deposition, cathodic arc deposition and electro hydrodynamic deposition are physical techniques for thin film technology.

7.2.1 Dip coating

This relatively easy method, which the substrate vertically withdrawn from a desired coating solution, causes a complex process involving gravitational draining with

concurrent drying and continued condensation reactions. Environmental conditions (temperature, humidity, airflow) are very important parameters as much as withdrawn speed and must be monitored closely during experiments to gain total control over film parameters. The formation of thin films occurs through solvent evaporation, which concentrates nonvolatile species in the system, then leading to aggregation and gelation (Figure 7.4). The resulting film depends on these parameters:

I. Withdrawal speed
II. Capillary pressure
III. Size and structure of precursors
IV. Condensation and evaporation rates
V. Substrate surface [64]

It is the oldest and the most widely used deposition technique in industry because it is easy to use, high coating quality, flexibility and cost efficiency [65].

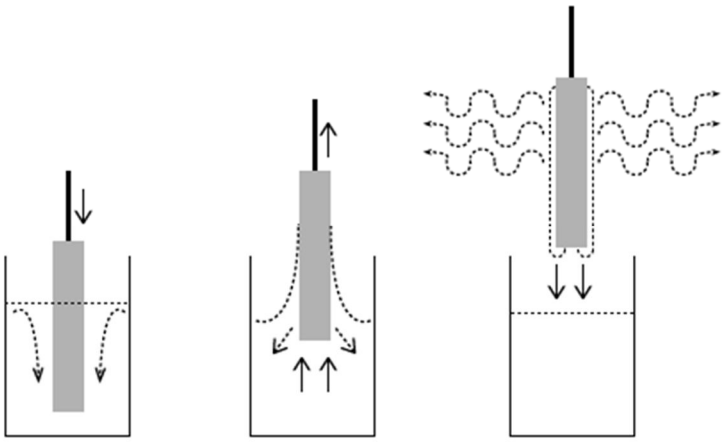

Figure 7.4 : Schematic view of dip coating process.

7.2.2 Spin coating

It is the simplest method for fabricating a uniform film on a substrate. Spin coating is a very practical way to deposit uniform thin films to flat substrate. The substrate is rotated at high speed in order to spread coating material by centrifugal force. Film thickness is managed by angular speed control: thinner films can be obtained with higher angular speeds of substrate (figure 7.5). The final thickness also depends on the concentration, surface tension and viscosity of the coating material. Even thicknesses below 15 nm films can be produced using this method [66].

Thin resist layers for photolithography are coated with this technique. Some of the solvent is removed during spinning process due to evaporation and some by baking at elevated temperatures. This technique is often used for planarization purposes because it results relatively planar surfaces [67]. The advantages of spin coating:

I. Fast process time,

II. Highly uniform surfaces even curved parts can be achieved,

III. Lenses with different curvatures can coated uniformly with minimal thickness edge effects or variation,

IV. Cost effective,

V. Sol is used once for each coating so avoiding contamination is easier then dip coating,

VI. Fewer amounts of sol is needed for experimental use which is better for expensive materials [68].

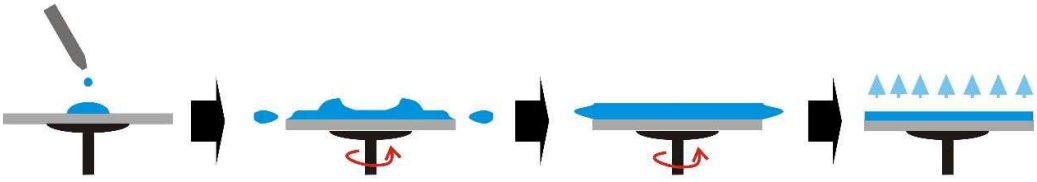

Figure 7.5 : Spin coating process; acceleration, dispensation, flow dominated and evaporation dominated.

7.3 Atomic Force Microscopy

Atomic force microscopy (AFM) is also known as scanning force microscopy (SFM), is a very high-resolution technique for scanning probe microscopy. Resolution can be approximately in the range of nanometers. Scanning tunneling microscopy is the precursor to the AFM. Interaction between mechanical probe and the surface gives information about surface. Piezoelectric element moves very tiny but accurate and precise for extremely precise scanning. It consists of a cantilever and a sharp tip

(probe) that scans sample surface. When the probe and sample surface approximate very closely, forces between them cause cantilever to deflect according to Hooke's Law. As can be seen from Figure 7.6 : reflection is measured by photodiodes that detect laser spot reflected from the top surface of cantilever. Contact, tapping and non-contact are the measurements types for AFM. It gives 3-dimensional surface profile.

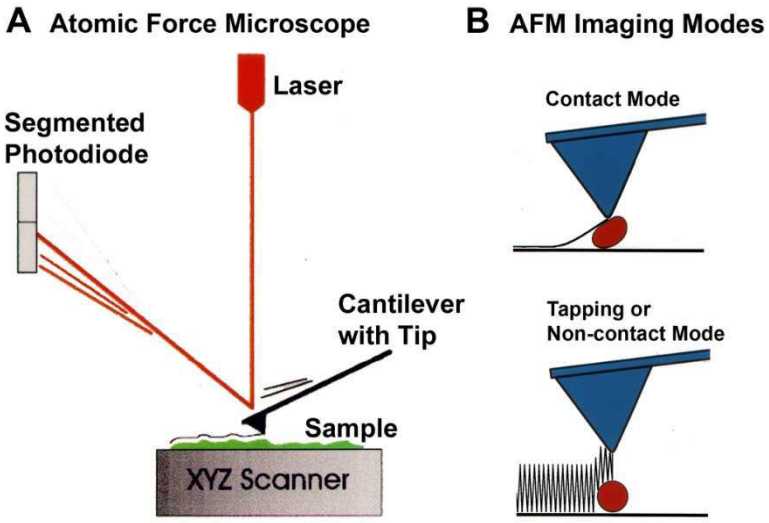

Figure 7.6 : Schematic view of AFM.

8. EXPERIMENTAL

8.1 Cleaning Glass Substrates

Glass slides were cleaned in chromic acid at room temperature, than rinsed with distilled water and dried at 100°C.

8.2 Coating Materials and Methods

All polymers were used directly as received. PP, HDPE and PPPE polymers were purchased from LyondellBasell, LDPE purchased from Honam Petrochemicals, PVOH was purchased from Merck, PA was purchased from DuPont.

Merck grade xylene, m-cresol, water, toluene and chloroform were used as solvents for the polymers.

Spin coatings were done by Cookson Electronics G3P-8 Spincoater. Samples were spin coated using 2µl of solution and 3000 rpm spin coating speed.

Dip coater was custom made with 10mm/min-1250mm/min withdraw capability and process performed at Piri Reis University.

A polyepoxide layer was deposited on glass slides as primer coating to compensate for the weak adherence of polymers onto glass substrates. Glass slides then dip coated at room temperature with 67 mm/min withdraw rate in order to obtain flat and uniform primer coating. Then coated samples were placed inside oven at 100°C for 1 hour to dry.

PVAc solutions were prepared using chloroform as solvent at room temperature and 40 mg/ml concentrations were used. Glass samples were coated using dip coating method with 150 mm/min withdraw rate at room temperature. Coated samples were left to dry at room temperature over night.

Polyolefins; PP, LDPE, HDPE and PPPE, were prepared inside silicone bath in order to achieve uniform solution temperature of 130°C using xylene. 10 mg/ml was the concentration of polymer solutions and also coating processes were done under 130°C temperature using dip coating method with 150 mm/min withdraw rate. Low withdraw rate and high temperature is important for for flat film formation. Coated samples were left to dry at room temperature over night.

PMMA and PS solutions were prepared at room temperature using toluen and 40 mg/ml concentrations were obtained. Glass samples were coated at room temperature using dip coating method with 150 mm/min withdraw rate. Coated samples were left to dry at room temperature over night.

PVOH solutions were prepared using water and 13.3 mg/ml concentration was obtained. 600 ml pure water stirred as fast as creating vortex inside and then PVOH was poured. Temperature set at 85°C after PVOH poured and water was added to stabilise solution volume. Solution was then left at room temperature to cool down after polymer completely dissolved. Glass samples were coated at room temperature using dip coating method with 150 mm/min withdraw rate. Coated samples were left to dry at room temperature over night.

PA solutions were prepared at room temperature using m-cresol and 10 mg/ml concentrations were utilized. Glass samples were coated at room temperature using dip coating method with 150 mm/min withdraw rate. Coated samples were left to dry at room temperature over night.

SiO_2 nanoparticle dispersed PS coatings were prepared by using spin coating method. HDK H18 hydrophobic pyrogenic silica, SiO_2, nanoparticles were purchased from WACKER Chemicals and dispersed in toluene as solvent by using Bandelin HD2200 ultrasonic homogenizer. SiO_2 dispersions in toluen were done using %90 amplitude with 2 cycles for 15 seconds. Dispersed SiO_2 poured inside the PS solution with same volume then another sonication performed with same configuration. Glass slides were coated by the resultant solutions using spin coating method with 3000 rpm spin and 2 µl solutions were poured on each glass slides for coating. Coated samples were left to dry under room temperature over night.

8.3 Characterization of Thin Films

8.3.1 Optical characterization

A NKD 7000 model (Figure 8.1) and UV–vis spectrophotometer (Figure 8.2, Aquila, UK) has been used to measure the optical transmittance and reflectance of polymer based thin films over the spectral range from 280 nm to 1000 nm at 30° angle of incidence. The optical constants such as refractive indices (n) and the extinction coefficients (k) of the films were calculated using the Pro-Optix software.

Figure 8.1 : NKD 7000 model UV-Vis spectrophotometer.

Agilent 8453 UV-Visible spectroscopy was used for optical characterization of samples. Ultraviolet-visible spectroscopy uses light from near-UV range to near infrared range (180nm-1200nm) and information about optical properties can be obtain for different wavelengths. This technique is applied on transition metal ions, highly conjugated organic compounds and biological macromolecules. Generally, solutions are investigated but solids and gases may be also studied thus, UV-vis is not exactly adequate method for characterization. Hydrogen or deuterium bulb is used for UV measurements; tungsten bulb is used for visible region.

Figure 8.2 : Agilent 8453 UV-Vis spectroscopy.

8.3.2 Thickness measurement

Thichness measurements were performed by Veeco Dektak 150 Surface Profiler (Figure 8.3). Thickness range of polymer coatings were between 90-250 nm.

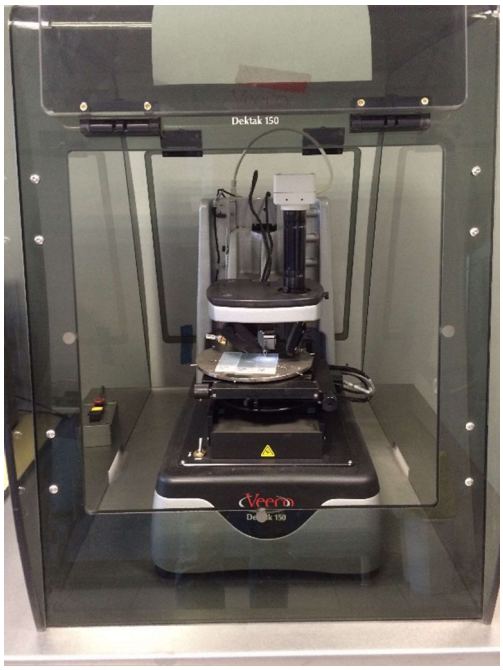

Figure 8.3 : Veeco Dektak 150 Surface Profiler

8.3.3 Surface characterization

8.3.3.1 Optical microscopy

Nikon LV150ND metal microscope was used to investigate the surface topographies of samples (Figure 8.4). Figure 9.1: displays microscope images of dip coated PVAc, PP, PPPE, HDPE, PVOH, LDPE, N66, N6, PS and PMMA polymer coatings with 200x and 500x magnification.

Figure 8.4 : Nikon LV 150 ND optical microscope.

8.3.3.2 Contact angle measurements

Water, ethylene glycol, formamide and diiodomethane (MERCK) liquids were used for CA measurments on polymer films. KSV Attension Theta Optical Tensiometer (Figure 3.2 :) was used to measure advancing (θ_a), receding (θ_r) and equilibrium (θ_e) contact angles under air. Figure 8.5 displays drop image during contact angle measurement. Computer controlled needle was used to adjust drop volume. 5µl drop volume was used for θ_e measurements and drop volume was increased from 3µl to 7µl during θ_a measurements, afterwards drop volume was decreased to 3µl to measure θ_r.

The needle was kept within the droplet during both advancing and receding measurements. Three different CA measurements were done on each polymer film surface and average CA values were reported with standard deviations of ±2. CA values of water, formamide and diiodomethane were also used in surface free energy calculations by using Fowkes and van Oss-Good-Chaudhury methods which were previously mentioned.

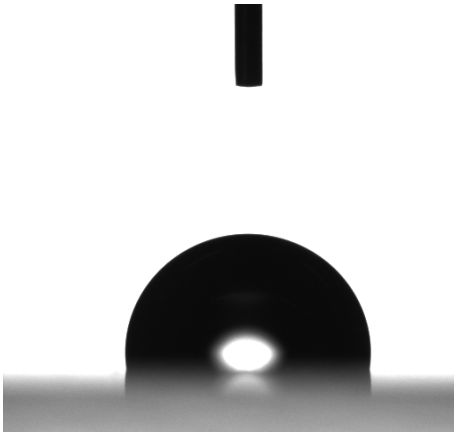

Figure 8.5 : Drop image obtained using Theta Optical Tensiometer.

8.3.3.3 AFM measurements

Nanosurf Easycan 2 AFM was used to investigate surface properties of SiO_2 dispersed PS coatings (Figure 8.6). Samples which are contain %10, %20, %40, %50, %60, %80 and %100 SiO_2 relative to the PS content were investigated. Measured areas were 30 μm for each sample. No preparation was needed before measurement.

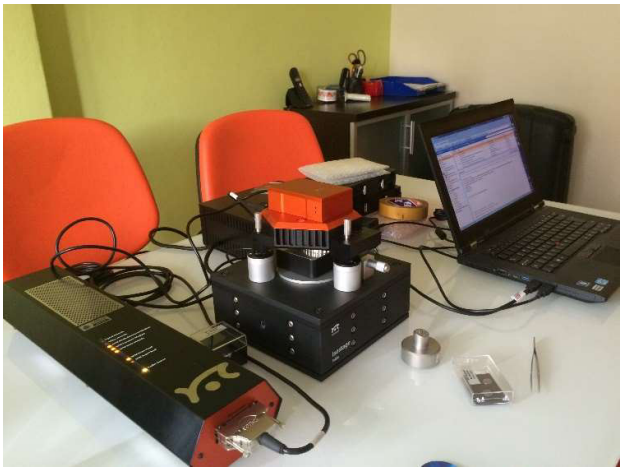

Figure 8.6 : Nanosurf Easycan 2 Atomic Force Microscopy.

9. RESULTS AND DISCUSSION

9.1 Flat Polymer Coatings

Surface free energy calculations were done by utilizing two methods; Fowkes and Van-Oss Good approaches [69]. Calculated surface energy values are given on Table 9.3. Test liquid (methylene iodide, ethylene iodide, formamide and water) contact angle values were needed, therefore all polymer surface water and test liquid contact angle values were measured by using KSV Attension Theta Optical Tensiometer and measurement values can be seen on Table 9.1 and 9.2.

Table 9.1 : Water contact angle values of coated polymer surfaces.

Polymer	θe	θa	θr	CAH
PVAc	62	81	32	49
PP	101	113	83	30
PPPE	95	104	65	39
HDPE	98	98	88	9
PVOH	48	64	37	31
LDPE	80	91	77	16
N6	61	64	26	38
N66	65	65	25	38
PS	96	95	81	14
PMMA	70	73	56	17

Table 9.2 : Methylene iodide (Mel_2), ethylene glycol (EG) and formamide (FA) contact angle values of polymer coatings.

Polymer	θ_{Mel2}	θ_{FA}	θ_{EG}
PVAc	39	68	77
PP	55	72	83
PPPE	51	73	80
HDPE	43	67	76
PVOH	37	16	26
LDPE	36	63	70
N6	32	39	44
N66	32	74	68
PS	30	74	68
PMMA	35	53	56

Table 9.3 : Surface free energy values of polymer coatings.

Polymer	(γtot) Van-Oss Good	(γtot) fowkes
PVAc	40.026	47.335
PP	31.919	32.094
PPPE	33.644	34.201
HDPE	38.070	39.194
PVOH	48.483	54.310
LDPE	41.564	41.943
N6	45.582	48.427
N66	43.373	47.233
PS	44.130	44.736
PMMA	41.940	44.226

Contact angle measurements were done by using KSV Attension Theta Optical Tensiometer and surface topography of flat polymer coatings examined by using Nikon LV150ND Metal microscope. Microscope and water droplet images for every polymer surface with 200x and 500x magnification were given in Figure 9.1:.

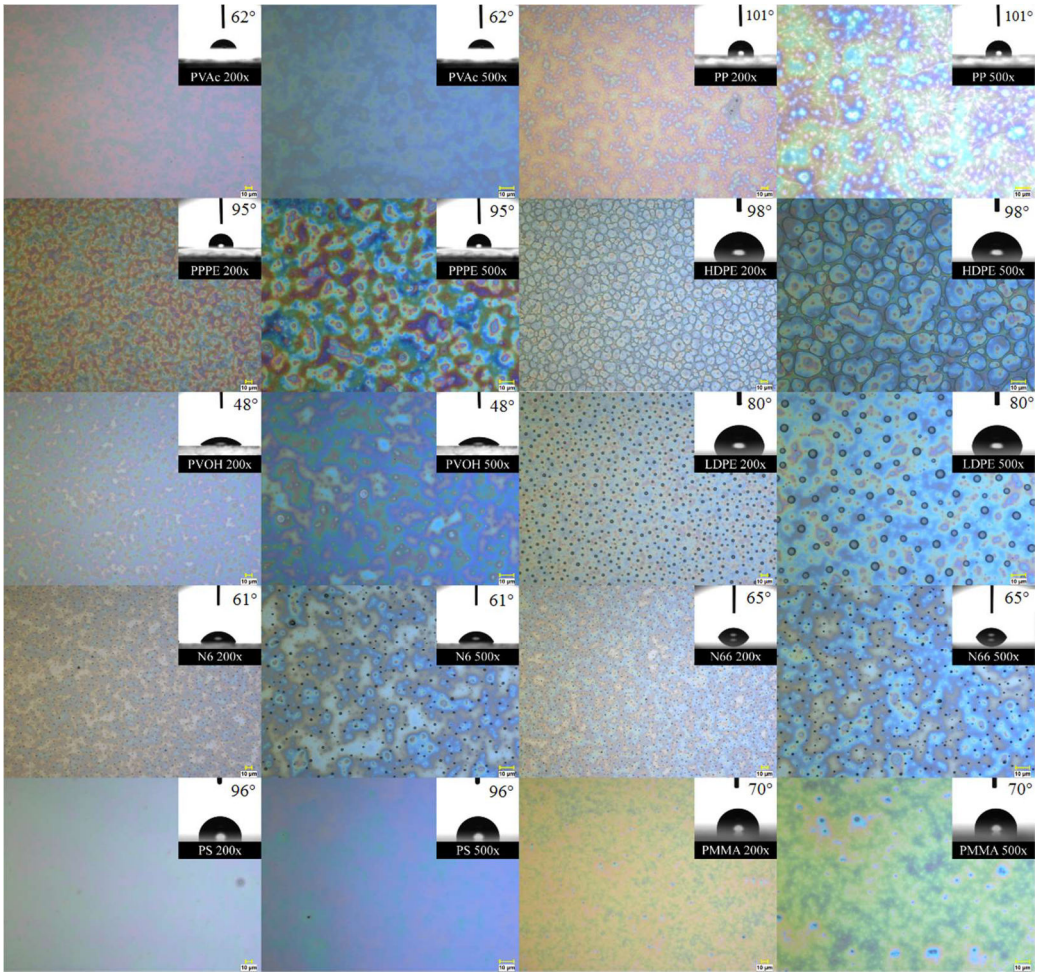

Figure 9.1: Microscope images of polymer coatings with 200x and 500x magnifications.

The transmittance (taken from both UV–Vis and NKD spectrophotometer) and reflectance values of the deposited films were measured by spectrophotometer analyses over the spectral range of 280-1000 nm. Figure 9.2: demonstrates transmittance values with respect to the energy of given wavelength of UV-Vis spectrophotometry results and Figure 9.3: and Figure 9.4: demonstrate transmittance and reflectance results with respect to the given spectral range of NKD spectrophotometer. It can be seen from these figures, transmittance and reflectance values changes dramatically with the polymer types for approximately same coating thicknesses, between 90nm and 210nm. Spectral transmittance values of HDPE and LDPE are the lowest ones. HDPE films decrease the transmission of the films in the visible range. These films are opaque and absorb light well. HDPE has ~2% reflectance, ~65% transmittance and ~30% absorbance at the visible range. Although

HDPE film has a very low transmittance value in the visible range, the transmittance value of this film shows a tendency to increase in the infrared region. The average transmittance values of PVOH, N66, N6, PS, PMMA, PP, PS and PVAc films ranged from ~70% to ~90% in the visible range. It can be concluded that polymer based films can be switched between opaque to transparent states through changing the polymer especially in the visible range, since absorption edges of the films are shifted to lower wavelength with HDPE polymer. In addition, a large difference of optical properties was observed, from over 90% to almost 15% for transmittance values of uniformly coated films. This indicates that; in choosen conditions, it is possible to synthesize reflective/antireflective and protective coatings for different applications.

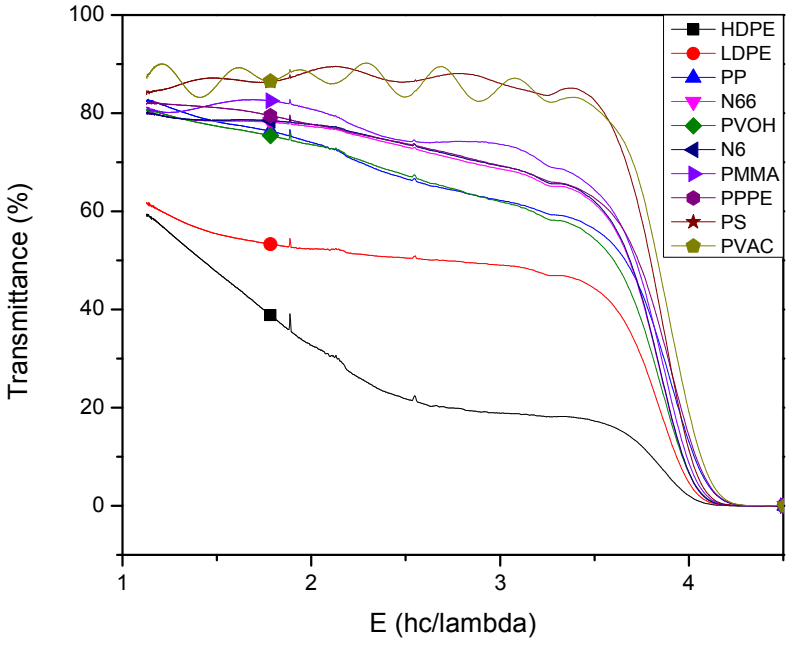

Figure 9.2: Transmittance values of polymer coatings with respect to the energy.

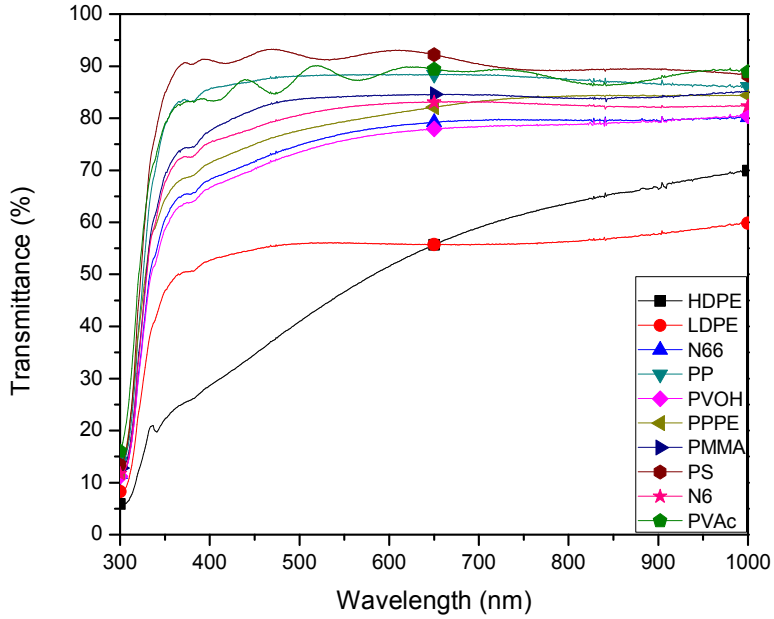

Figure 9.3: Transmittance values of polymer coatings.

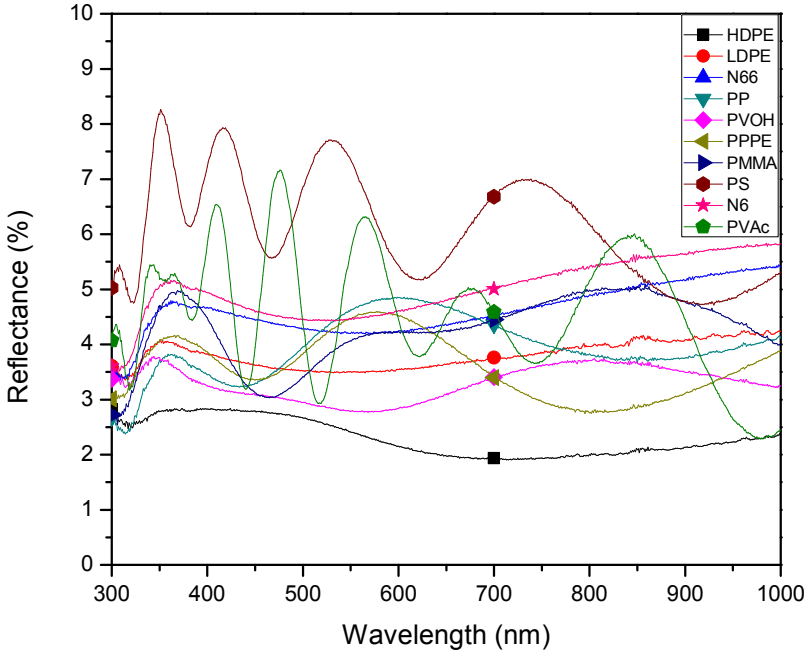

Figure 9.4: Reflectance values of polymer coatings.

Band gap of polymers were calculated using Tauc relation [70] which was presented in Equation 5.2. The needed data was calculated by the spectrometer software. For the extrapolation method [69] by placing the calculated absorption coefficient in the Tauc formula (αhν) and hν graphs were drawn (Figure 9.5-9.12). With the extrapolation of the linear parts of the graphs, band gaps of coatings are calculated and can be seen on Table 9.4 :. As can be seen on Table 9.4 :, LDPE films, which were deposited using xylene as solution, had lower band gap values due to higher roughness. Optical absorption studies indicated an increase in the band gap for the films deposited from about 2.3 eV to 3.5 eV. The maximum band gap achieved by PMMA and PPPE film. The band gap values are in good agreement with the literature. [71-78].

Table 9.4 : Bandgap values of polymer coatings.

Sample	**Bandgap (eV)**
PP	3.4
PPPE	4
HDPE	3.3
PVOH	3.5
LDPE	2.3
N66	3
PS	3.8
PMMA	3.9

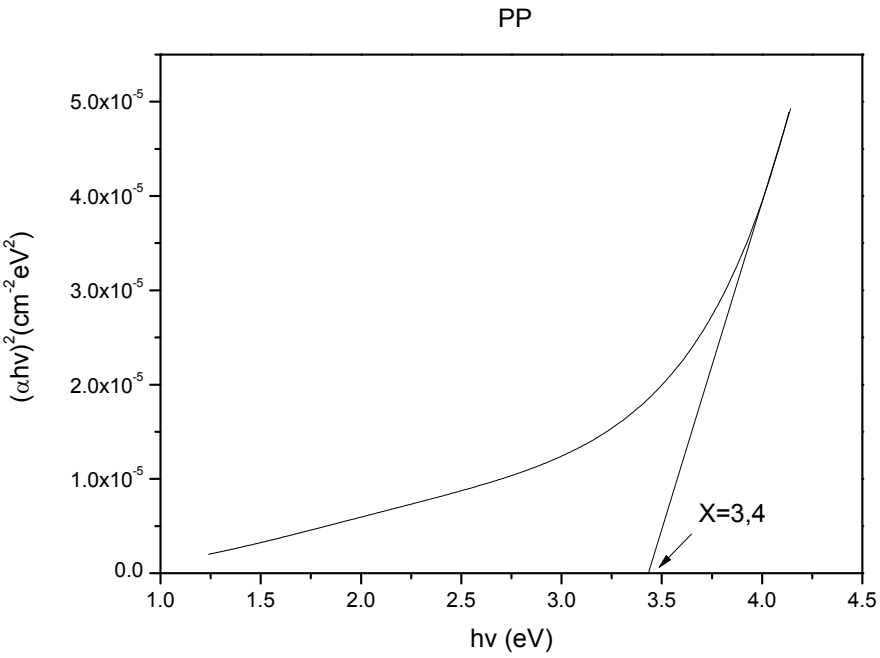

Figure 9.5: PP band gap, calculated using Tauc method.

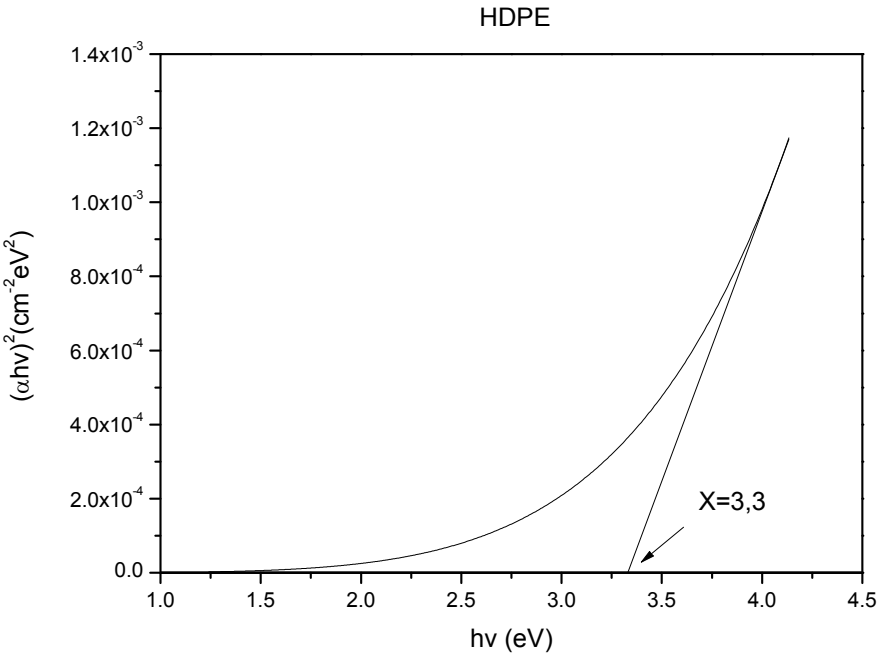

Figure 9.6: HDPE band gap, calculated using Tauc method.

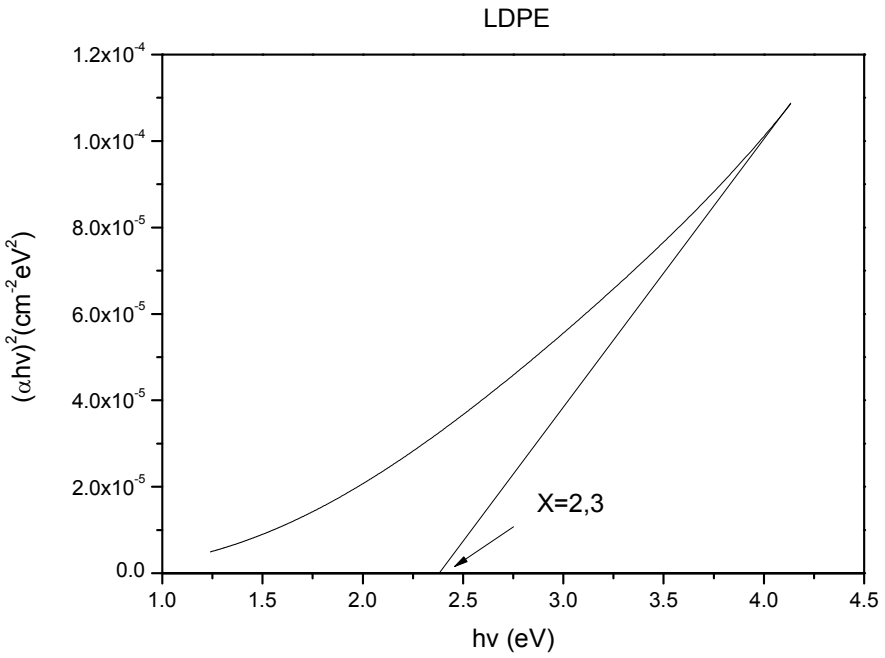

Figure 9.7: LDPE band gap, calculated using Tauc method.

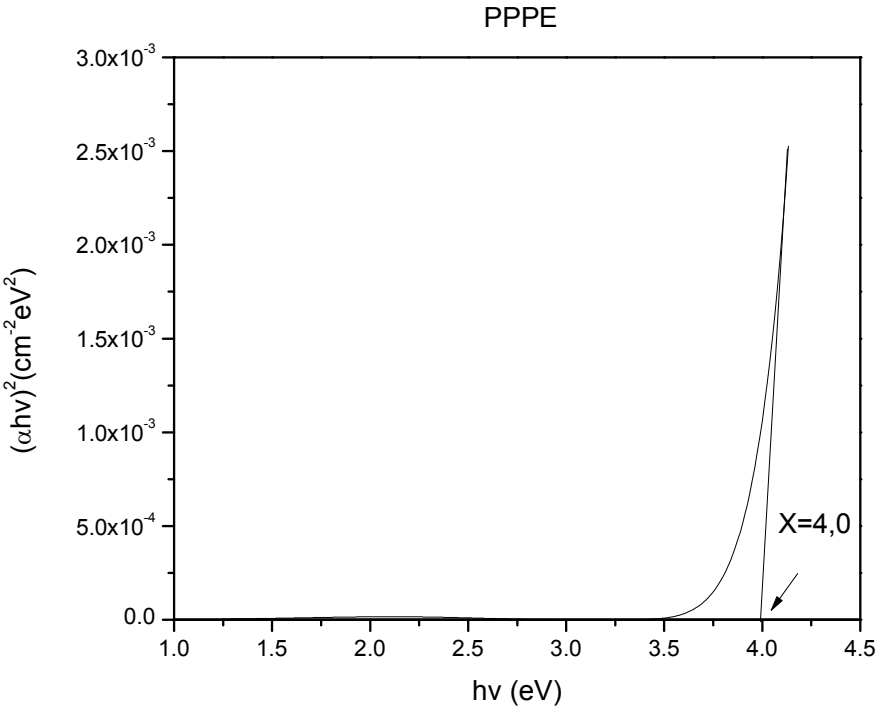

Figure 9.8: PPPE copolymer band gap, calculated using Tauc method.

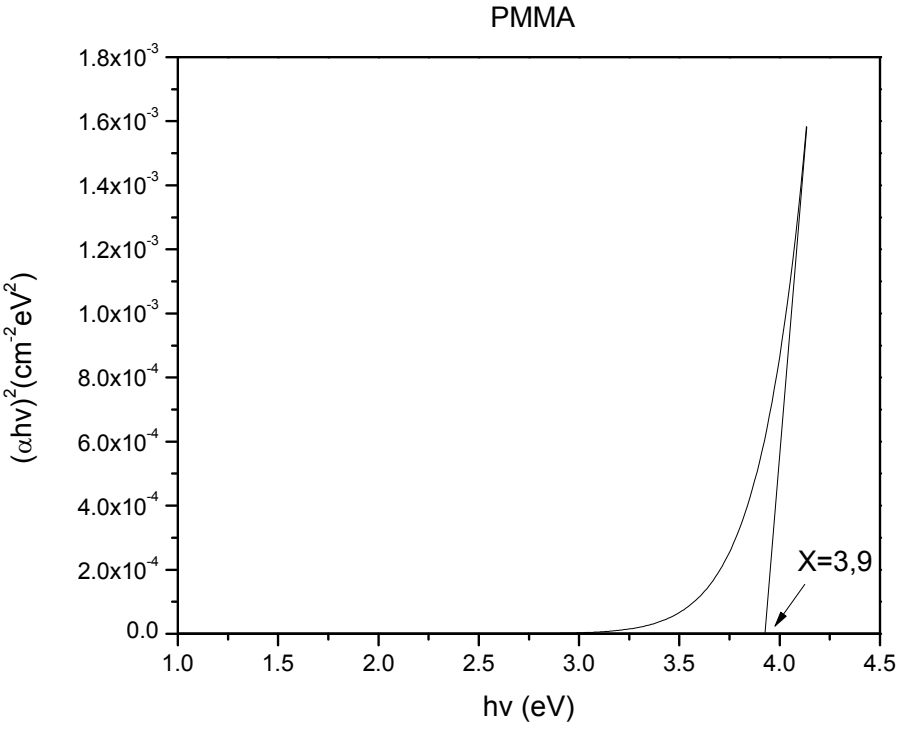

Figure 9.9: PMMA band gap, calculated using Tauc method.

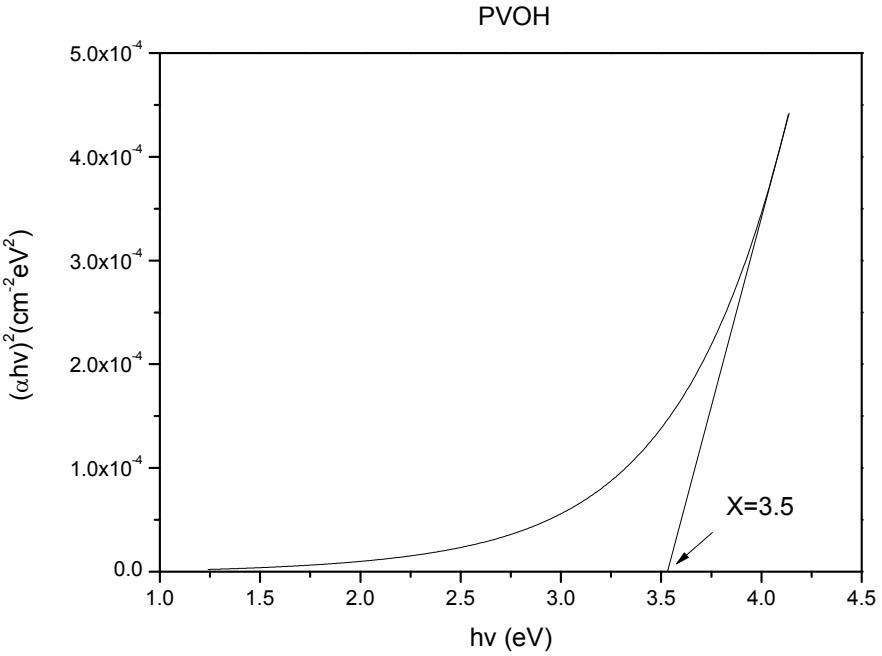

Figure 9.10: PVOH band gap, calculated using Tauc method.

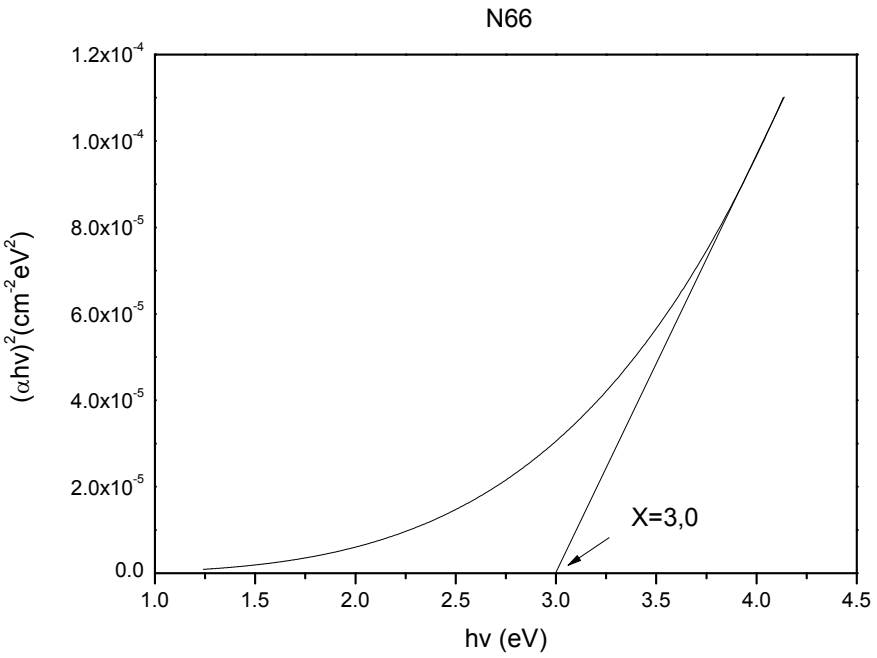

Figure 9.11: N66 band gap, calculated using Tauc method.

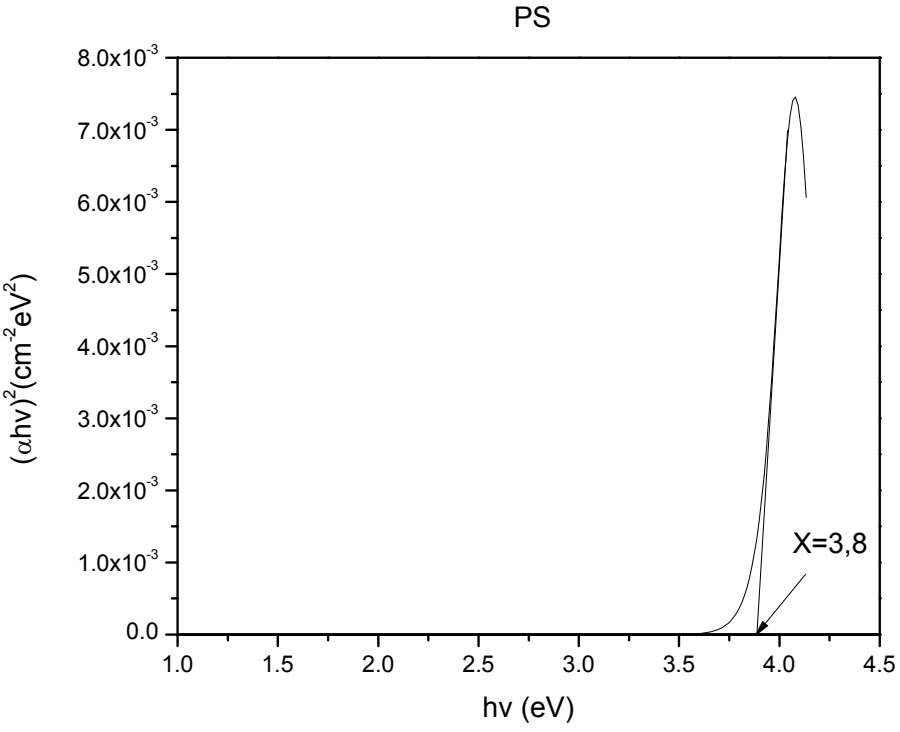

Figure 9.12: PS band gap, calculated using Tauc method.

Figure 9.13: and Figure 9.14: demonstrate correlations between equilibrium contact angle, CAH and calculated surface energies by using Fowkes approach. According to Fowkes dispersion component of surface free energy related with the London interactions resulted from the electron dipole fluctuations due to the attraction between the atoms and molecules of the matter [43]. Fowkes approach is valid for dispersive forces of nonpolar solid ($\gamma_S = \gamma_S^d$) and the liquid ($\gamma_L = \gamma_L^d$). According to Fowkes (later Owens and Wendt) geometric mean method beside the dispersive contribution of surface free energy, polar contribution should also be taken into account. Fowkes proposed that work of adhesion, W_a, and work of cohesion, W_c, can be separated into their dispersion, d, polar, p, induction, I, and hydrogen bonding, h components [71,69]. Eq. 4.6 was attained in order to calculate the polar and dispersive components of surface free energy, and the total surface free energy value of the solid surface. Combining Eq. 4.6 with Young Equation (Eq. 3.1) gives the Eq. 4.7 which express the relationship between the contact angle and surface free energy values of solid, liquid and also their polar ($\gamma_{SV}^p \gamma_{LV}^p$) and dispersive ($\gamma_{SV}^d \gamma_{LV}^d$) components. Eq. 4.7 exhibits two unknowns; γ_{SV}^p and γ_{SV}^d which are dispersive and polar components of free energy for solid-vapour interface. In order to obtain results at least two test liquids have to be chosen for the calculation. Owen and Wendt, used water and methylene iodide in order to calculate unknown parameters, using measured contact angle of polymers [30]. As a test liquid, water and methylene iodide are the most preferred ones for the aim of calculation the surface free energy with Fowkes method [79].

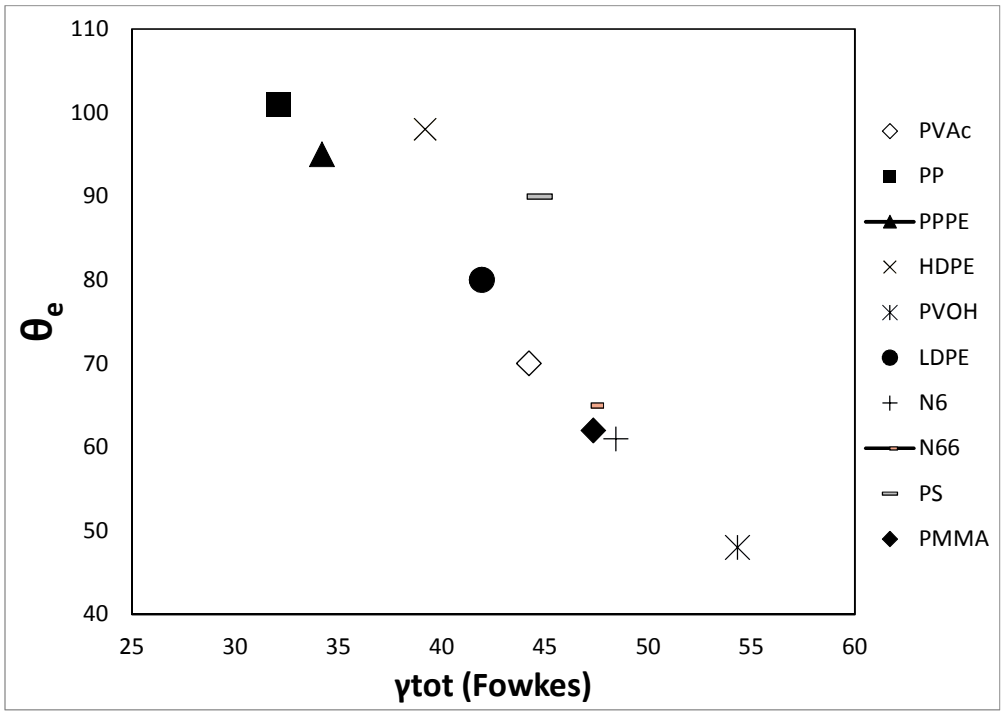

Figure 9.13: Relationship between equilibrium contact angles and surface free energies of polymers; calculated using Fowkes method

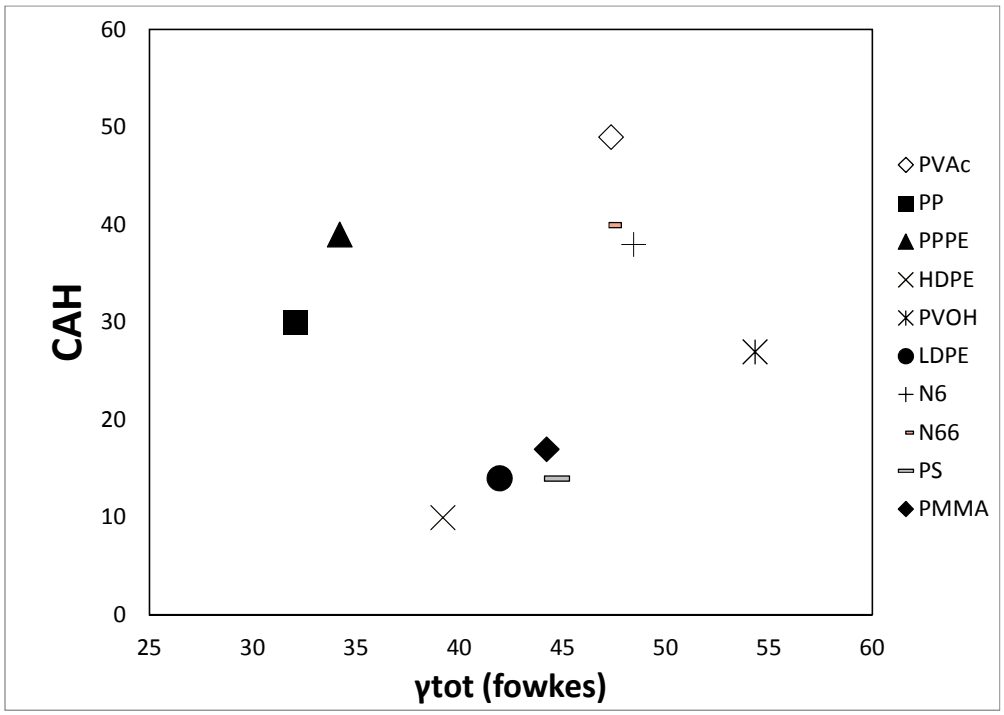

Figure 9.14: Relationship between CAH and surface energies of polymers; calculated using Fowkes method.

Contact angle measurement results of these test liquids were given in 0 and Table 9.1 : Lower polar component with respect to the dispersive component of PP, HDPE and PPPE indicates hydrophobicity behaviour and their CA values support that result as having contact angles above 90°. PVAc, N6, N66 and PVOH demonstrate higher polar characters and have higher surface free energy values but PVOH has approximately the same polar and dispersive component but demonstrates the highest total surface free energy value.. Therefore, PVOH has the lowest CA value with respect to the highest surface free energy value. PS and PMMA demonstrate the same surface free energy values but PMMA has higher polar component, thus, has higher water interaction and lower CA which can be seen Figure 9.13:. It can be seen from Figure 9.13: that increase in γ^{tot} caused a decrease in equilibirum water contact angle values of polymers and it should also be noted that a similar trend have been observed by the other studies [31,80]. Surface chemical heterogeneity and also roughness caused contact angle hysteresis (CAH) on polymer surface. All CAH values of polymer surfaces were calculated and high CAH values were found except HDPE, LDPE, PS and PMMA coated surfaces. HDPE, LDPE, PS and PMMA coated surfaces demonstrated low CAH values due to their low polar characteristics and flat morphologies. However, PP and PPPE coated surfaces demonstrate low polar components but presented larger CAH values which are the results of the roughness and impurities on polymer surfaces. Decrease in θr values of polymers, such as PVAc, PVOH, N6, and N66, which is the result of the pinning of the droplet on surface, caused to calculate larger CAH values. High polar characteristics of PVAc, PVOH, N6 and N66 also made contribution to the pinning of the droplet on surface, however, low polar characteristics of the HDPE, LDPE, PS, PMMA, PP and PPPE coated surfaces are the cause of relatively high θr values with respect to their θ_a values which results low CAH values except PP and PPPE coated surface. As mentioned before, PP and PPPE surfaces demonstrate low polar components however, large CAH values were calculated because of the impurities and roughness on their surfaces. CAH values of polymer coatings were demonstrated in Table 9.1 : and can be seen from Figure 9.14:. In general, hydrophobic surfaces demonstrate low CAH and hydrophilic surfaces low CAH.

Figure 9.15: and Figure 9.16: demonstrate correlations between equilibrium contact angle, CAH and calculated surface energies using Van-Oss Good approach. Van Oss,

Chaudhury and Good introduced the components of the surface free energy of solid (γ_S) such like γ_S^{LW} and γ_S^{AB}. Where γ_S^{LW} refers to Lifshits-Van der Waals component which is concerning long range interactions dominated by dispersion, dipolar and induction forces and γ_S^{AB} refers to acid-base component related with short range interactions such as hydrogen bonding. According to Van-Oss Good approach γ_S^{AB} component is divided into two subcomponent γ_S^+ which is Lewis acidic parameter and γ_S^- which is Lewis basic parameter. In order to calculate surface free energy data from Eq. 4.16 we need set of values for three unknowns of the material; γ_L^{LW} , γ_L^- and γ_S^-. At least three liquids should be used for reference liquids. The equation indicates that measureing reference values, polymer surface values can be calculated or γ_S^{LW} can be determined by using a nonpolar liquid first, then two other polar liquids are used to determine γ_S^+ and γ_S^-. Latter method sometimes produce negative square roots of Lewis acidic and basic parameter and this attracts objections [19].

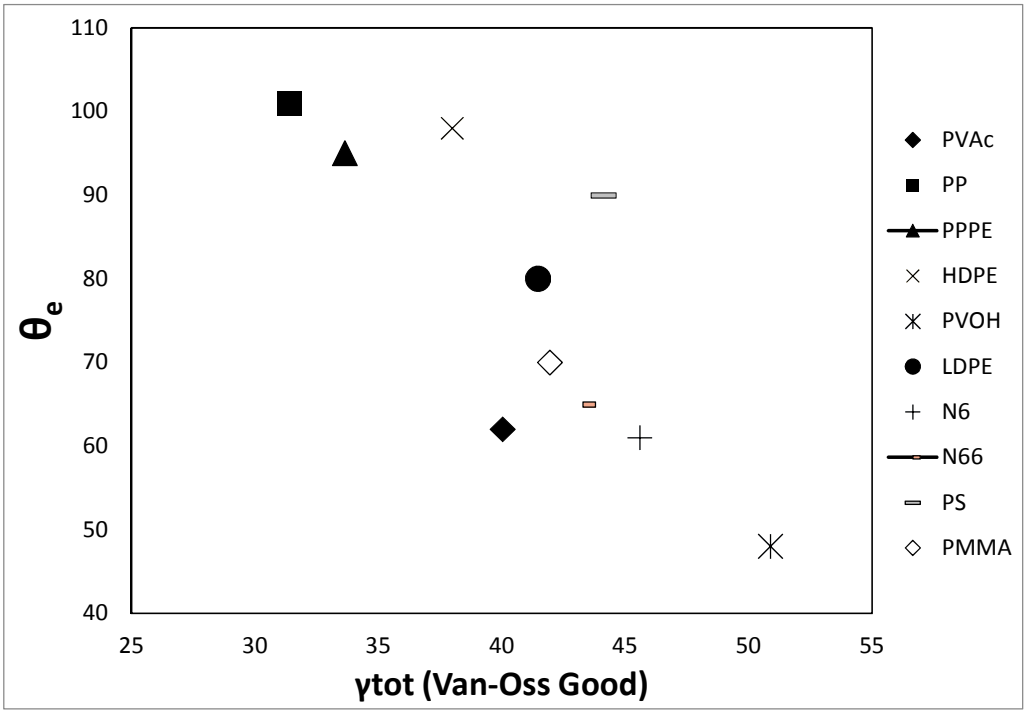

Figure 9.15: Relationship between equilibrium contact angle and surface energies of polymers; calculated using Van-Oss Good approach.

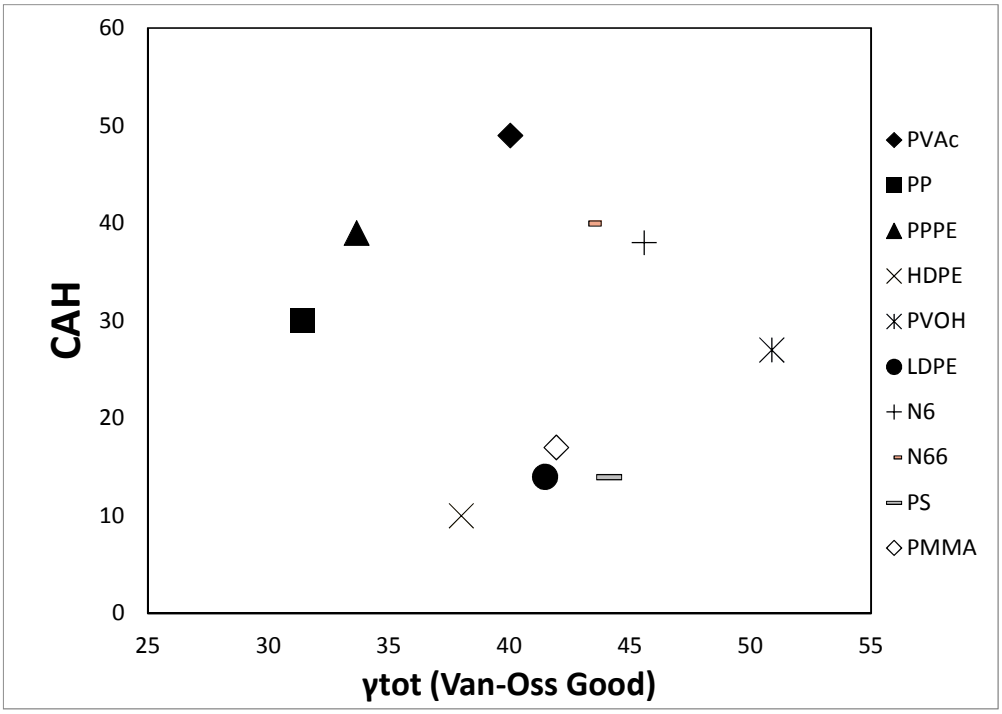

Figure 9.16: Relationship between CAH and surface energies of polymers; calculated using Van-Oss Good approach.

When surface free energy of a solid increases, the adhesion interactions between the solid surface and the waterdroplet also increase due to the high surface tension value of water. As a result of this, water CA values decrease which can also be seen from Figure 9.15: that increase in γ^{tot} caused a decrease in equilibirum water contact angle values of polymers and it can be stated that this trend have been also reported by the other studies [31,80]. Lower polar component values of PP, HDPE and PPPE with respect to their dispersive component and lower surface free energy values indicate hydrophobic behaviour and it can be seen from Figure 9.15: that polymer coatings demonstrate contact angle values higher than 90°. PVAc, LDPE, PMMA, N66, N6 and PVOH demonstrates lower CA values as having high surface free energy values which can seen in Figure 9.15:. Having higher surface free energy values caused lower CA angle values due to the higher surface-water interaction of LDPE, PMMA, N66, N6, PVAc and PVOH polymer surfaces. Also, PVOH coated surface demonstrated the lowest contact angle value due to the highest polar characteristic of PVOH coatings amongst polymer coatings used in this study. Surface chemical heterogeneity and roughness caused contact angle hysteresis (CAH) on polymer surfaces. All CAH values of polymer surfaces were calculated and high CAH values were found except

HDPE, LDPE, PS and PMMA coated surfaces. Calculated CAH values of HDPE, LDPE, PS and PMMA coated surfaces present low CAH values due to their low polar and thus hydrophobic characteristics and flat morphologies. However, PP and PPPE coated surfaces demonstrate larger CAH values despite having low polar components which is a result of the roughness and impurities on these polymer surfaces. Decrease in θr values of polymers, such as PVOH, PVAc and N6, which is the result of the pinning of the droplet on surface, caused to calculate larger CAH values and low polar characteristics of the HDPE, LDPE, PS, PMMA, PP and PPPE coated surfaces are the cause of relatively high θr values with respect to their θ_a and θ_e values which resulted in low CAH values except PP and PPPE coated surface. As mentioned before, PP and PPPE coated surfaces indicated low polar components, however, large CAH values were calculated because of the impurities and roughness on their surfaces. CAH values and correlation between surface free energy values which were calculated using Van-Oss Good approach are presented on Table 9.1 : and Figure 9.16:, respectively.

Surface free energy values of PVAc coated surfaces was found 40.026 mJ/m^2 using Van-Oss Good approach and 47,335 mJ/m^2 using fowkes method (Table 9.3 :). These results indicate close similarity with literature for both fowkes method [81] and Van-Oss Good approach [80]. In this thesis, high polar characteristics of PVAc coatings and low CA values according to polar characteristisc of PVAc surfaces were found which are also in accordance with the literature for both fowkes and Van-Oss Good approach [80,81].

PMMA coated surface characterization results show high surface free energy values, 41.940 mJ/m^2 using Van-Oss Good approach and 44.226 mJ/m^2 using fowkes method, also low CA values as having high surface free energy values which consistent with theory [19]. According to literature values, PMMA surfaces demonstrate high surface free energy values and low CA values [82] which supports findings of this study.

Surface free energy results of PVOH coated surfaces are 48.483 mJ/m^2 using Van-Oss Good approach and 54.310 mJ/m^2 using fowkes method, also surfaces demonstrate low CA values as having high surface free energy values with high polar component. In literature [82,83], low CA values associated with high surface free energy values were reported and high polar characteristic of PVOH coated surfaces was also noted which support our findings.

Surface free energy calculations of PS coated surfaces indicated 44.130 mJ/m^2 using Van-Oss Good approach and 44.736 mJ/m^2 using fowkes method. CA measurements show hydrophobic behaviour as having high contact angle values which is a result of very low surface free energy values with little to no polar component. Low polar component of PS coated surfaces and high CA values are in well accordance with the literature [84].

Surface free energy calculations of Nylon 6 and Nylon 6,6 coated surfaces demonstrate 45.582 mJ/m^2 and 43.373 mJ/m^2 using Van-Oss Good approach and 48.427 mJ/m^2 and 47.233 mJ/m^2 using fowkes method, respectively. One of the lowest CA values were measured along with PVAc and PVOH coated surfaces which is in a direct relation of high polar components of coated Nylon surfaces, especially the results of fowkes method. High polar characteristics and low CA values of Nylon surfaces were reported [85] which coherent with this study.

Polyolefins; PP, HDPE, LDPE and PPPE are hydrophobic by their nature [86] and demonstrate low surface energy values with very little interest in water. High temperature working conditions for preparing polyolefin coatings make the process difficult however, results are indicate good hydrophobic characteristics which is favourable for water repellent surface studies. CA values were in the order of PP>HDPE>PPPE>LDPE however, surface free energy values were in the order of LDPE>HDPE>PPPE>PP. HDPE demonstrate lower surface free energy value but higher CA than PPPE and even HDPE coated surfaces demonstrated higher polar component using fowkes method. It can be speculated that HDPE coated surfaces contain higher roughness which enhances surface behaviour towards liquid, further studies are needed.

PP coated surfaces show surface free energy values of 31.919 mJ/m^2 using Van-Oss Good approach and 32.094 mJ/m^2 using fowkes method which were the lowest calculated surface free energy values in this study. Also, PP surfaces demonstrated the highest contact angle values which is a result of the lowest surface free energy among studied coated surfaces. Literature also reported [87,83,84] low surface free energy values associated with high contact angle which is in accordance with this study.

Surface free energy studies of HDPE coated surfaces demonstrate 38.070 mJ/m^2 using Van-Oss Good approach and 39.194 mJ/m^2 using fowkes method which indicates CA values should be high. CA measurements demonstrated high values which in accordance with surface free energy calculations. In literature it was also reported that HDPE coated surfaces have low surface free energy values with high dispersive component and high CA values [81,86], as this study indicates.

PPPE coated surfaces indicated 33.644 mJ/m^2 using Van-Oss Good approach and 34.201 mJ/m^2 using fowkes method as surface free energy values with high dispersive component. High CA values were measured which is in accordance with the surface free energy values. In literature [86] low surface free energy values with high dispersive components and high CA values were reported as this study indicates.

LDPE coated surfaces show 41.564 mJ/m^2 using Van-Oss Good approach and 41.943 mJ/m^2 using fowkes method as surface free energy values which were the highest values amongst polyolefin coated surfaces. Having the highest surface free energy values amongst polyolefin coated surfaces should lead to the lowest CA measurement results because of the high surface-liquid molecular interaction where measurement results of this study demonstrated expected CA value drop amongst polyolefin surfaces. In literature [86], low CA values of LDPE surfaces with flat morphologies, relative to polyolefin surfaces, were reported which shows well concordance with findings of this study.

9.2 Superhydrophobic Coatings

Contact angle values of PS coated surfaces with the dispersed SiO_2 nanoparticle content increase can be seen in Table 9.5 :. CAH values are equal to the subtraction of θr from θa. Δcosθ values are also indicate contact angle hysteresis and calculated with using $\Delta\cos\theta = \cos\theta_r - \cos\theta_a$ formula.

Table 9.5 : CA values of PS coatings with varying SiO_2 nanoparticle content.

Sample %SiO_2	wt% SiO_2	θe	θa	θr	CAH (θa-θr)	Δcosθ
%5	0.277	95	100	81	19	0.330
%10	0.552	96	102	82	20	0.347
%15	0.826	96	103	79	24	0.415
%20	1.098	98	109	76	33	0.567
%25	1.369	98	110	77	33	0.566
%30	1.639	101	117	74	43	0.729
%35	1.907	108	121	70	51	0.857
%40	2.173	121	127	68	59	0.976
%45	2.439	123	128	62	66	1.085
%50	2.702	148	160	124	36	0.380
%55	2.964	168	171	152	19	0.104
%60	3.225	169	170	152	18	0.101
%65	3.485	169	171	153	18	0.096
%70	3.743	172	173	162	11	0.041
%75	4.000	171	171	169	2	0.006
%80	4.255	171	170	166	4	0.014
%85	4.509	171	172	167	5	0.015
%90	4.761	171	171	165	6	0.021
%95	5.013	170	170	164	6	0.023
%100	5.263	170	170	165	5	0.018

Figure 9.17: demonstrates 3D topographies of SiO_2 nanoparticle dispersed PS coatings with $30\mu m^2$ measurement area. From Figure 9.17: it can be stated that samples demonstrate homogeneous roughness for all coated surfaces.

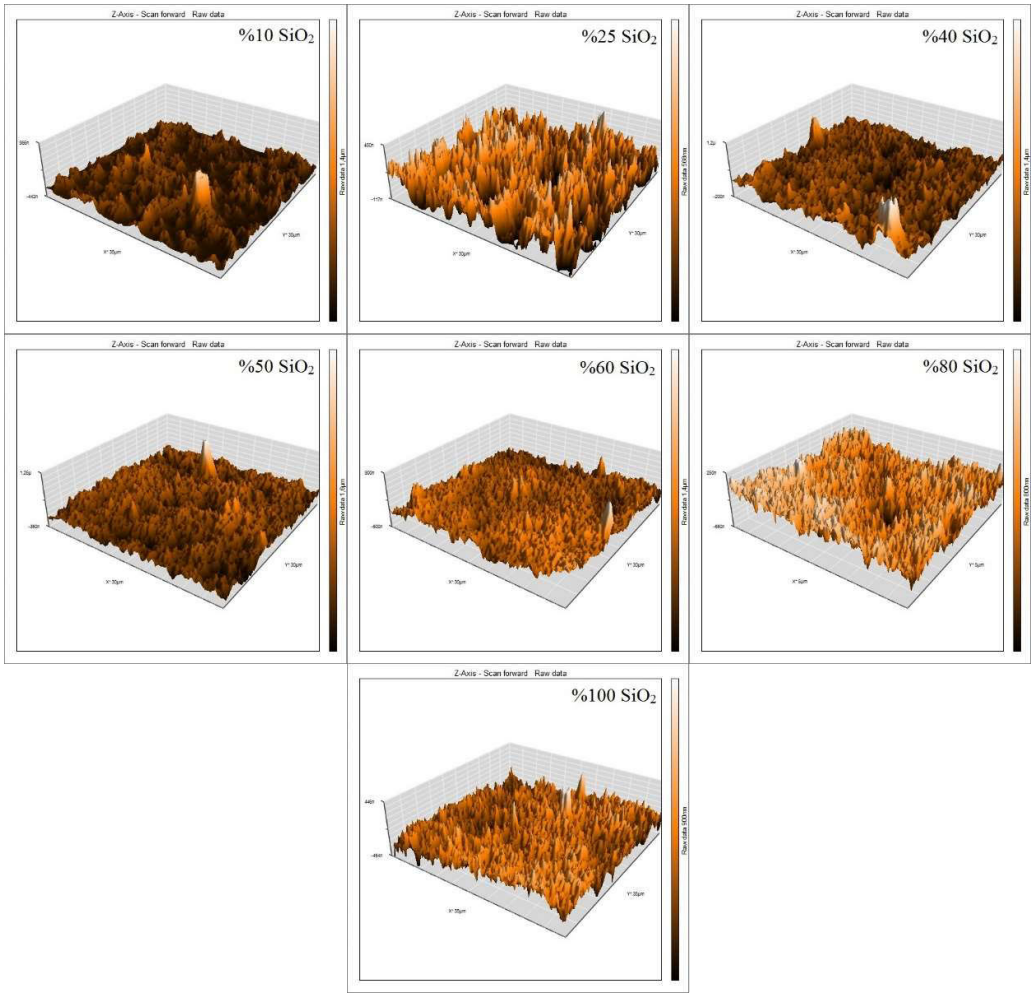

Figure 9.17: AFM images of PS coatings with varying SiO_2 nanoparticle content, with $30\mu m^2$ measured area.

Figure 9.18 demonstrates transmittance values with respect to the energy, measured by UV-Vis spectrophotometer. As can be seen transmittance values drop as nanoparticle content increases. This is also in concordance with NKD results.

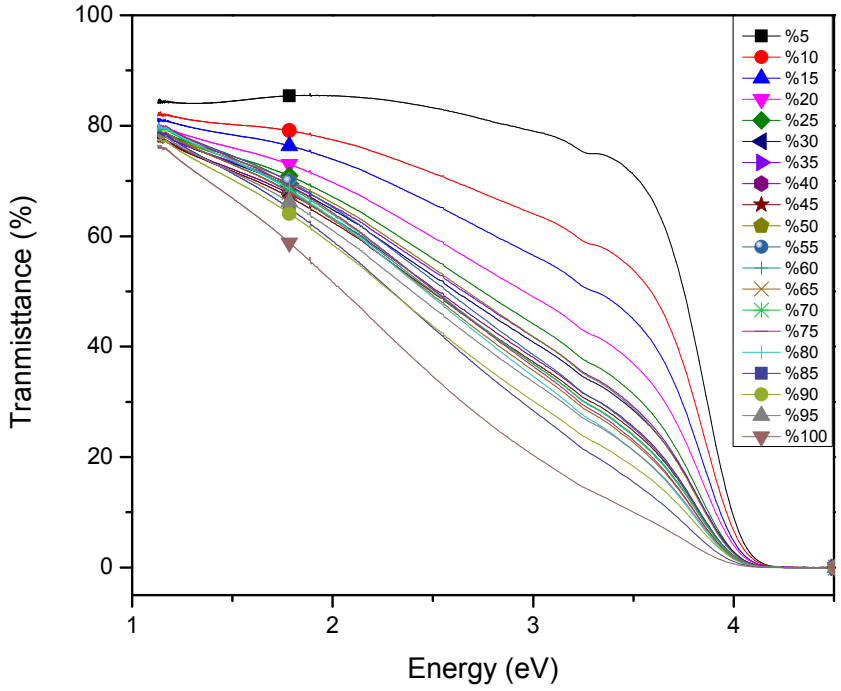

Figure 9.18: Transmittance values of PS coatings with varying SiO_2 nanoparticle content with respect to the energy (eV), measured by UV-vis spectrophotometer.

Figure 9.19: and Figure 9.20: demonstrates transmittance and reflectance values of SiO_2 nanoparticle dispersed PS coatings. As can be seen; reflectance and transmittance values decreases in respect to their SiO_2 content increase. After a certain point, relative difference of values between samples are decreases.

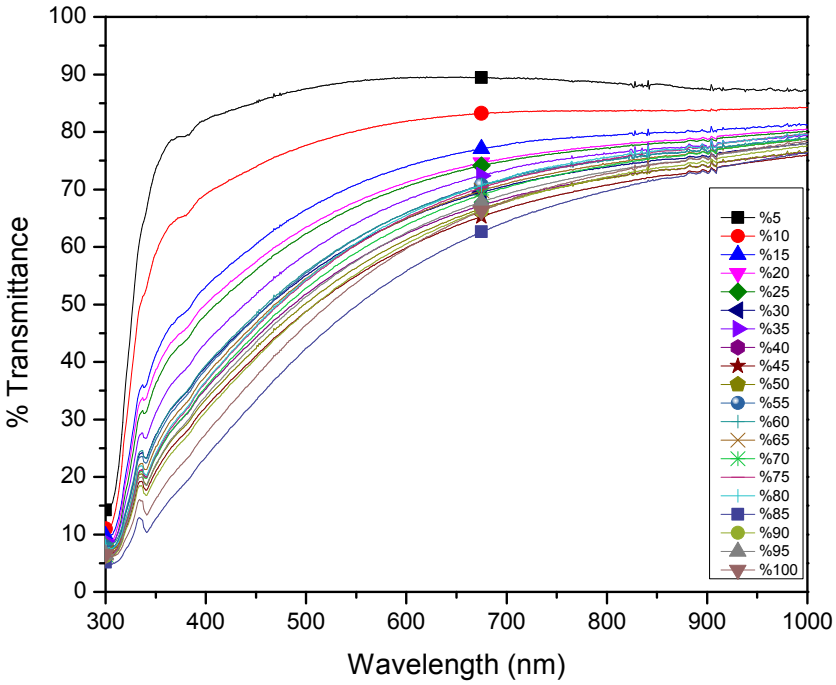

Figure 9.19: Transmittance values of PS coatings with varying SiO_2 nanoparticle content, using NKD spectrophotometer.

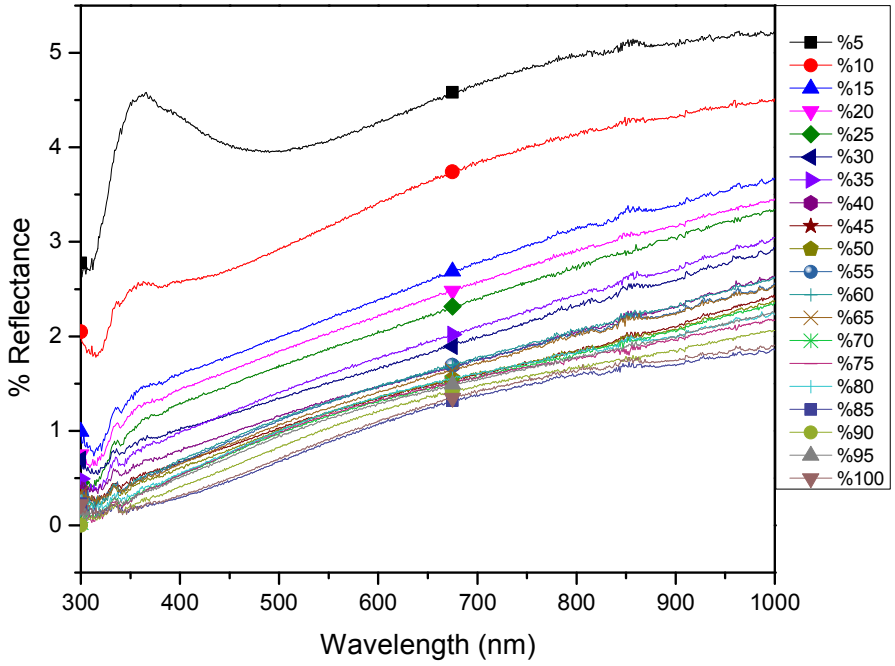

Figure 9.20: Reflectance values of PS coatings with varying SiO_2 nanoparticle content, using NKD spectrophotometer.

Band gap values of PS coatings with varying SiO_2 nanoparticle content were calculated using Tauc method and can be seen on Table 9.6. From Figure 9.21 and Figure 9.22, extrapolation method on sample with %70 SiO_2 content can be observed.

Table 9.6 : Direct and Indirect bandgap values of PS coatings with varying SiO_2 nanoparticle content.

Sample %SiO_2	Direct Bandgap (eV)	Indirect Bandgap (eV)
%5	3.883	3.668
%10	3.834	3.427
%15	3.779	3.338
%20	3.793	3.344
%25	3.806	3.344
%30	3.806	3.110
%35	3.806	3.165
%40	3.841	3.124
%45	3.800	3.041
%50	3.655	2.924
%55	3.724	3.144
%60	3.786	3.137
%65	3.786	3.158
%70	3.814	3.062
%75	3.745	3.055
%80	3.821	3.034
%85	3.668	2.744
%90	3.841	3.206
%95	3.806	3.089
%100	3.848	3.055

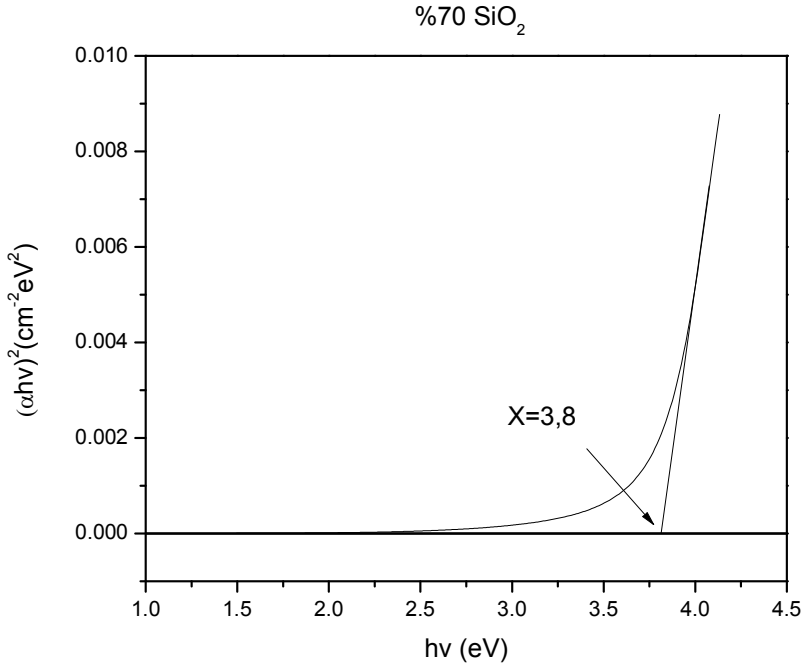

Figure 9.21: Direct band gap calculation of PS coatings with %70 SiO_2 content using Tauc method.

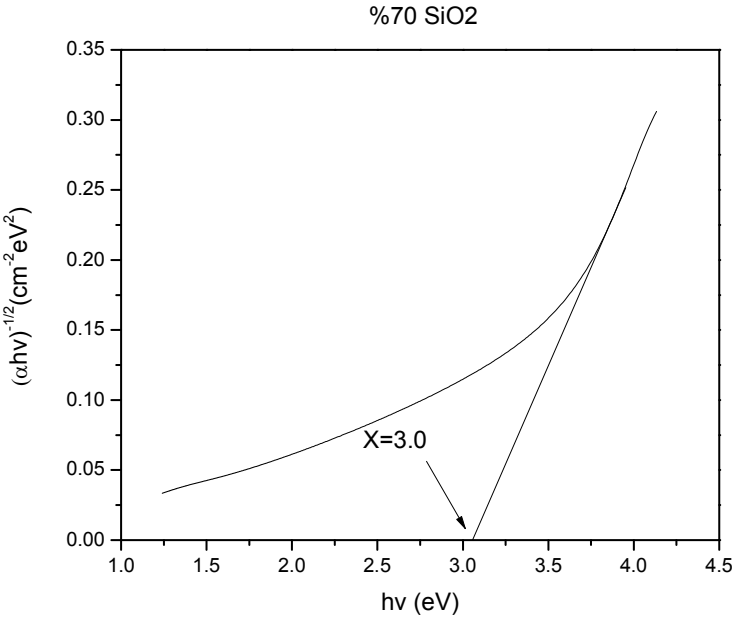

Figure 9.22: Indirect band gap calculation of PS coatings with %70 SiO_2 content using Tauc method.

Direct and Indirect Bandgap values of SiO_2 nanoparticle dispersed PS coatings, calculated using Tauc method are displayed in Figure 9.23:. Samples demonstrate wide bandgaps and our results in well accordance with literature [88].

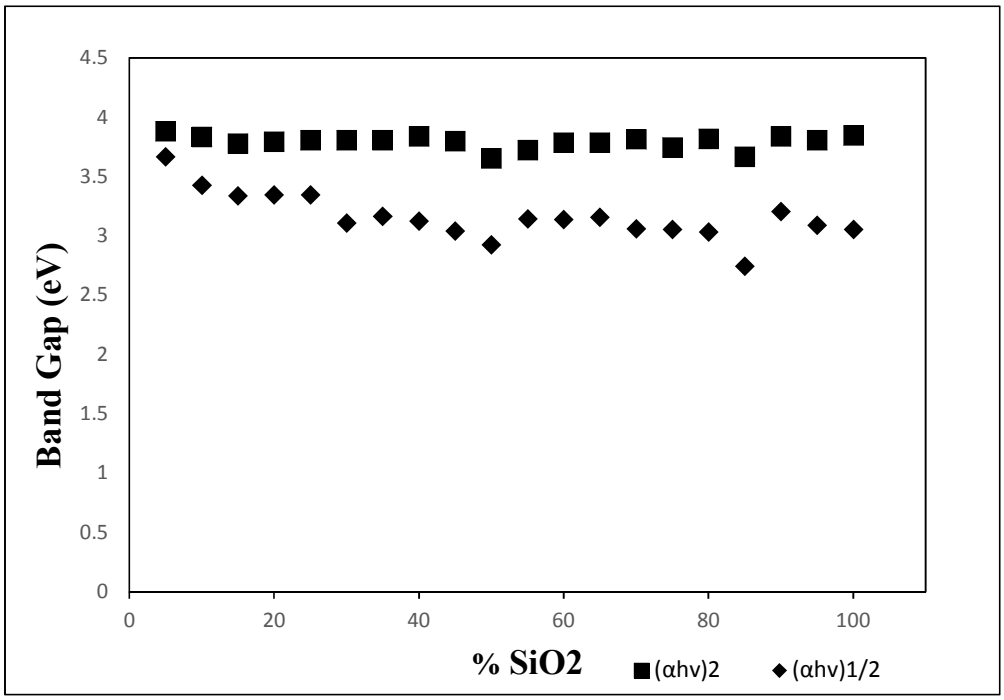

Figure 9.23: Direct and Indirect bandgap values of PS coatings with varying SiO_2 nanoparticle content, calculated using Tauc method.

Figure 9.24: presents the relationship between roughness values and SiO_2 content of PS coatings. Sample values demonstrate roughness increase with respect to the nanoparticle content increase, although, samples which have %25, %50, %60 and %100 SiO_2 nanoparticle content show roughness decrease regardless of the fact that their nanoparticle content were increased.

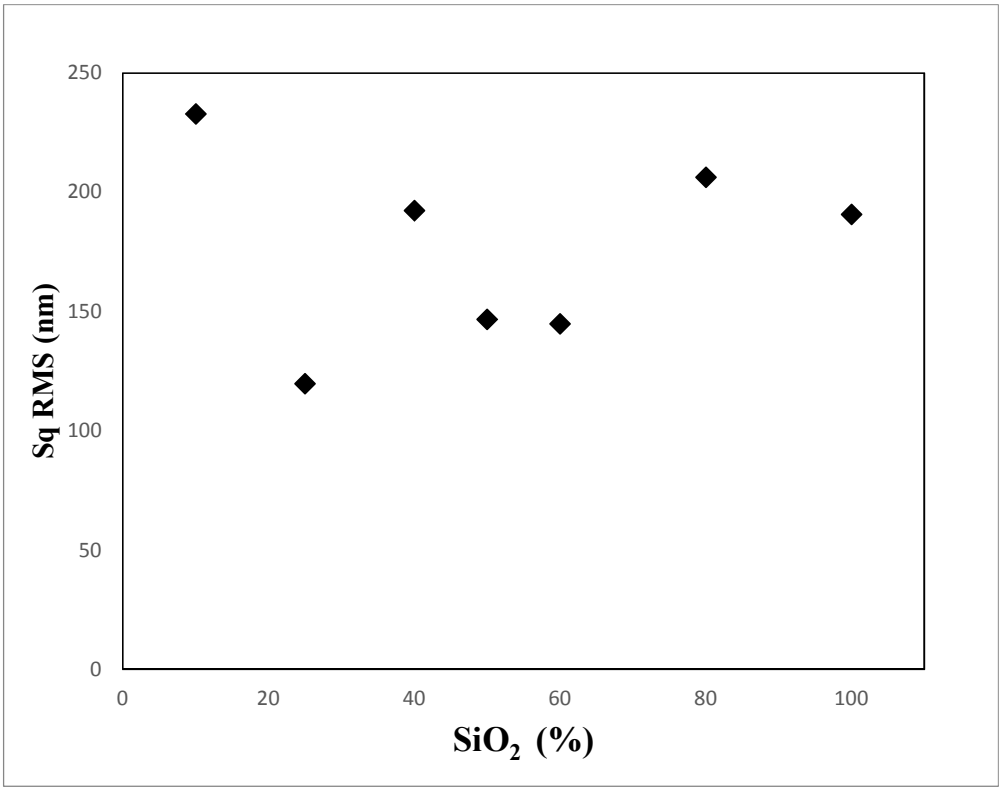

Figure 9.24: Roughness values of PS coatings with varying SiO_2 nanoparticle content.

Contrary to expectations, CA values of samples which have %25, %50, %60 and %100 SiO_2 nanoparticle content show no reduction. Table 9.5 : shows that; CA values indicate no reduction between samples with %10 and %25 content despite the roughness decrease. In spite of the fact that the samples with %40 and %100 content have similar roughness values however, %40 demonstrates hydrophobic behaviour and %100 demonstrates superhydrophobic behaviour with regard to their CA values. Without any roughness increase some factor must be favouring this contact angle increase. According to these results, it can be speculate that, networks of nanoparticle aggregates are more influential for the samples with %25, %50, %60 and %100 nanoparticle content which have also been reported in literature [16]. Homogeneus distribution of SiO_2 nanoparticles and aggregation can be observed in Figure 9.17: and the correlation between contact angle values and surface roughess can be observed from Figure 9.29:.

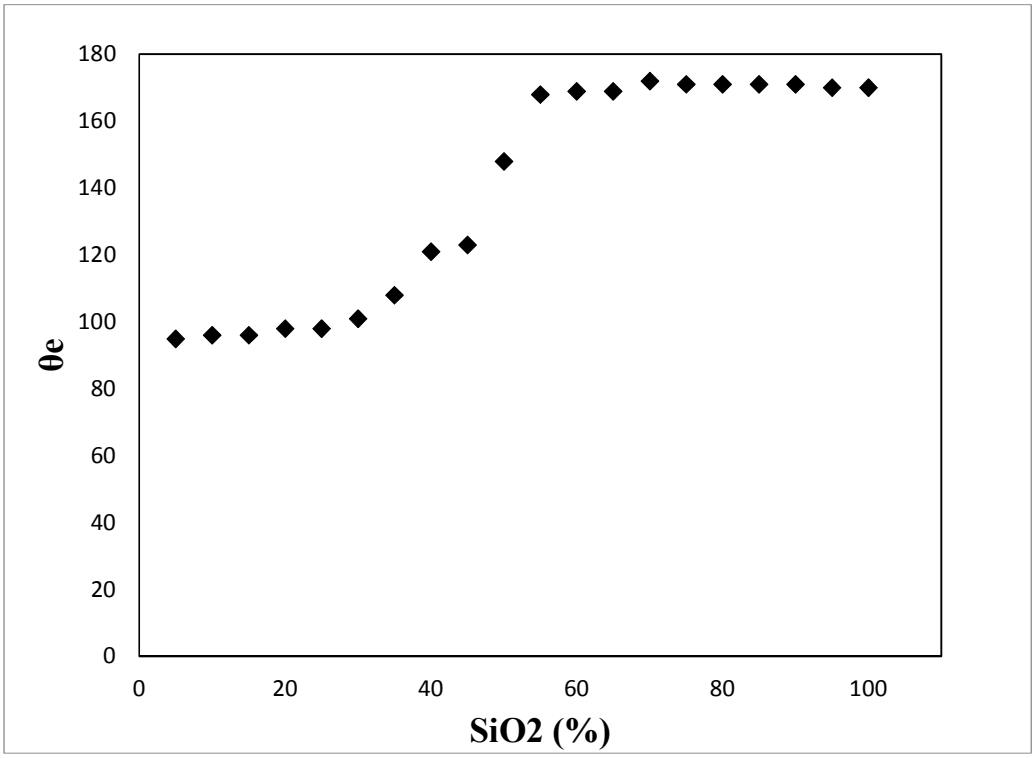

Figure 9.25: Equilibrium CA (θe) values of PS coatings with varying SiO_2 nanoparticle content.

Figure 9.25: demonstrates water equilibrium contact angle values of surfaces with varying SiO2 nanoparticle content. Graph indicates that every sample demonstrates hydrophobic behaviour as every CA value is above 90°; however, starting from %40 SiO_2 nanoparticle content contact angle values start to increase and reach saturation point at %55 as having the highest contact angle point and demonstrate superhydrophobic behaviour with contact angle exceed 150°. From that point nanoparticle content increase did not affect much to the contact angle increase.

Figure 9.26: and Figure 9.27: demonstrate dynamic contact angle values; θa and θ_r, respectively. Samples which have less nanoparticle content than %45 indicate θa increase in Figure 9.26: and θ_r decrease in Figure 9.27:. This indicates a CAH increase, as their difference increase, which demonstrated in Figure 9.28:.

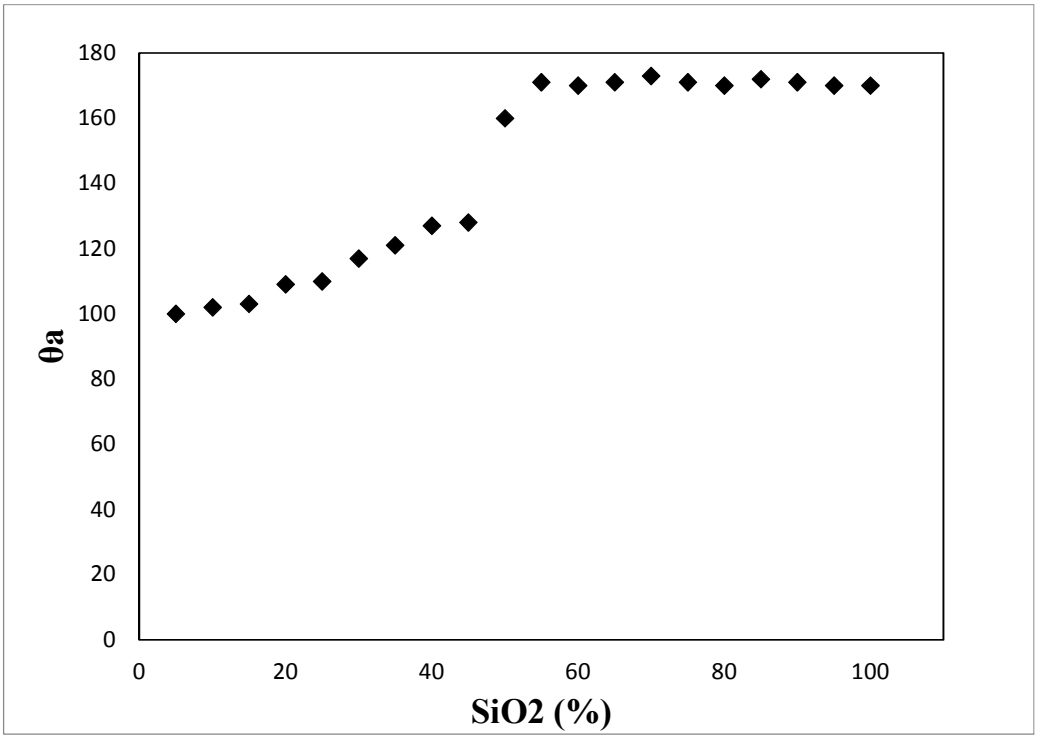

Figure 9.26: Advancing CA (θa) values of PS coatings with varying SiO_2 nanoparticle content.

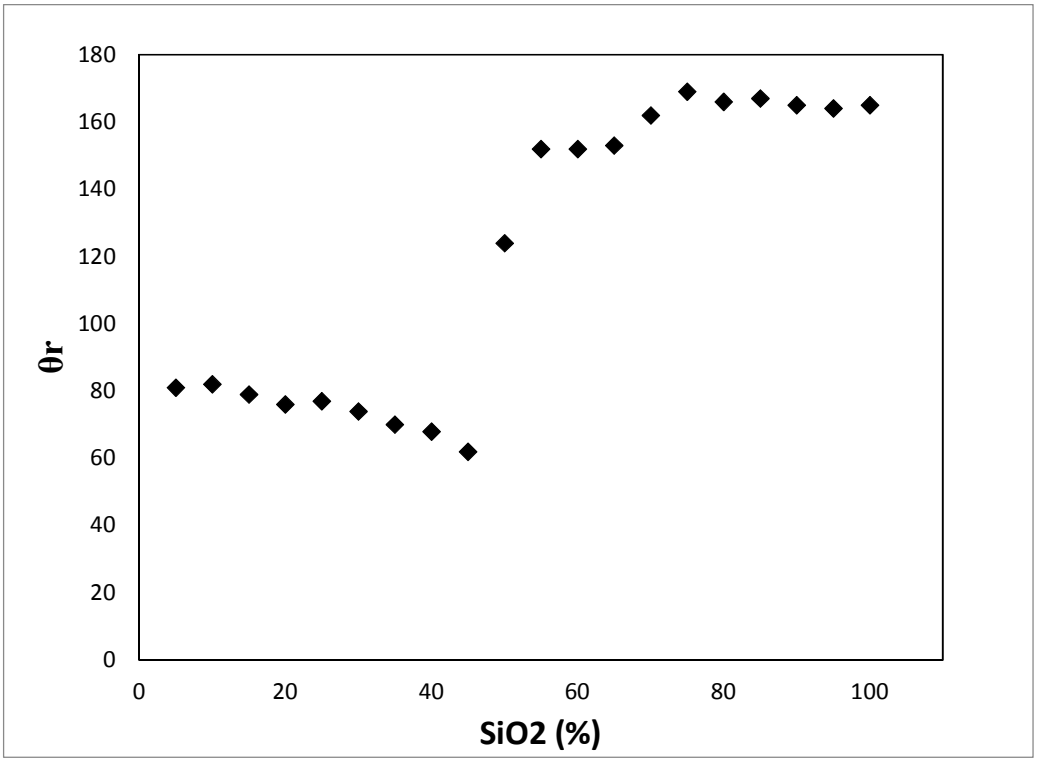

Figure 9.27: Receding CA (θa) values of PS coatings with varying SiO_2 nanoparticle content.

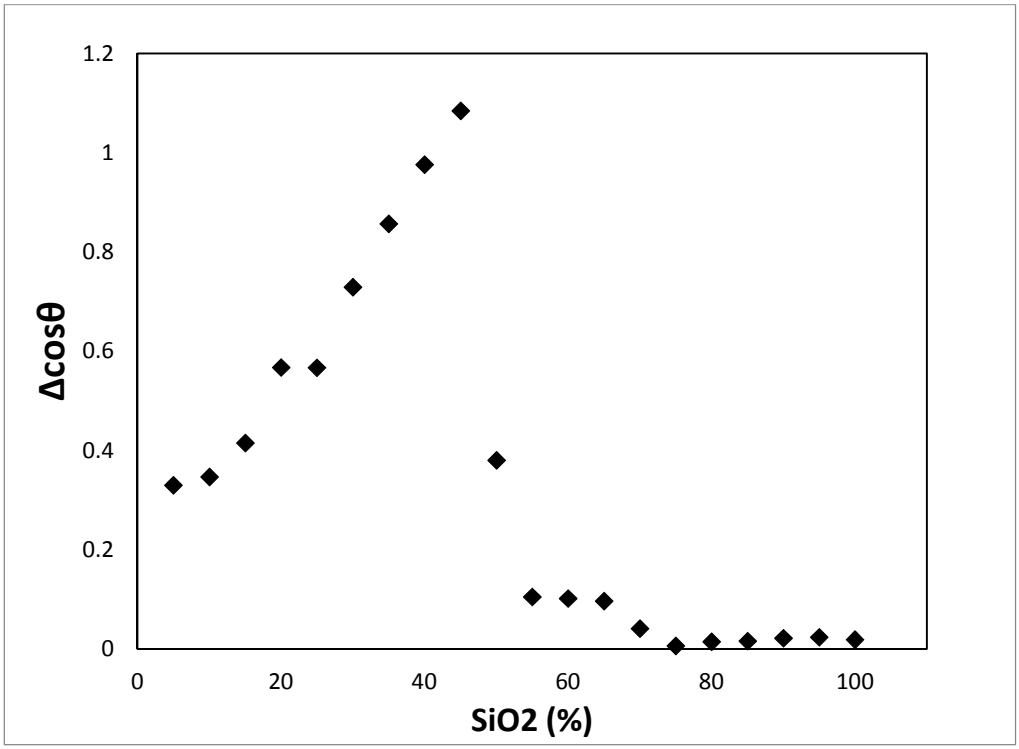

Figure 9.28: Contact angle hysteresis values (calculated with using $\cos\theta_a - \cos\theta_r$) of PS coatings with varying SiO_2 nanoparticle content.

Figure 9.28: shows contact angle hysteresis values, Δcosθ, which are calculated from subtraction of sample $\cos\theta_a$ values from $\cos\theta_r$ values. Figure 9.28: indicates a contact angle hysteresis increase associated with increasing SiO_2 nanoparticle content until the sample with %50 SiO_2 nanoparticle content. From that point CAH values drop and it can also be seen from Table 9.5 : that samples show superhydrophobic behaviour as their contact angle values started to exceed 150°. According to the theory, superhydrophobic surfaces should have low CAH and roll off angles [89] which supports results of this study.

In Figure 9.29:, θe values and surface roughess values were displayed. Roughness value increase as nanoparticle content increase is significant, especially at %60 and %80. They are also show the highest contact angle values beside samples which have %100 nanoparticle content.

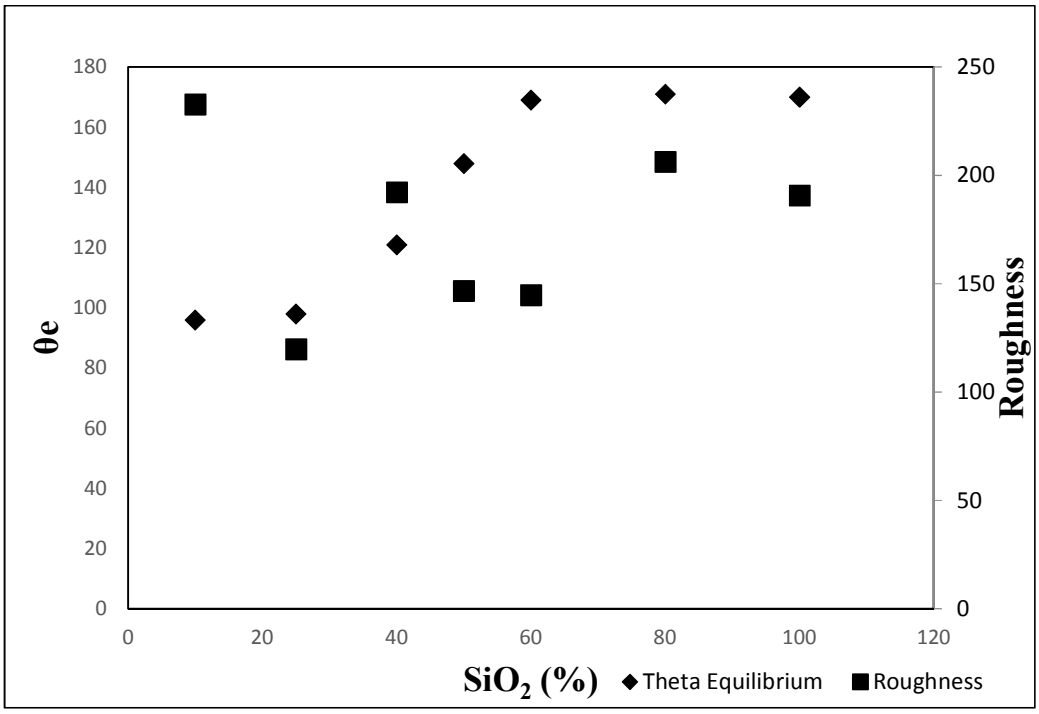

Figure 9.29: Relationship between equilibrium contact angle and surface roughness values of PS coatings with varying SiO_2 nanoparticle content.

%100 and %10 have the same roughness but %100 has the higher contact angle value. It was speculated before that formation of more perfect networks of nanoparticle aggregates is more important [16]. The sample which have %100 nanoparticle content have higher amount of SiO_2 content and it can be assumed that this sample, alongside with the sample which have %40 SiO_2 content, having more perfect networks of nanoparticle aggregates than the sample which have %10 SiO_2 nanoparticle content. Also this assumption can be extended for between the samples with %10 and %25 nanoparticle content which have similar contact angle values but the sample with %25 nanoparticle content demonstrates significantly higher roughness. According to the assumption, the sample with %25 nanoparticle content have higher roughness but demonstrate not as great networks of nanoparticle aggregate as the sample with %10 nanoparticle content. Also %55 has lower roughness than %25 but demonstrates higher contact angle, which indicates greater networks of nanoparticle aggregates.

Figure 9.30: and Figure 9.31: demonstrates θ_a, CAH and roughness correlation of coated films with respect to the %SiO_2 content increase. From Figure 9.30: it can easily be seen advancing contact angle value increase as SiO_2 content also increases. On the other hand Figure 9.31: demonstrates CAH value decrease as SiO_2 content increase,

starting from the sample with %50 SiO_2 content. It is in well accordance with the theory as superhydrophobic surfaces demonstrates high θ_a and θ_r values and low CAH [89].

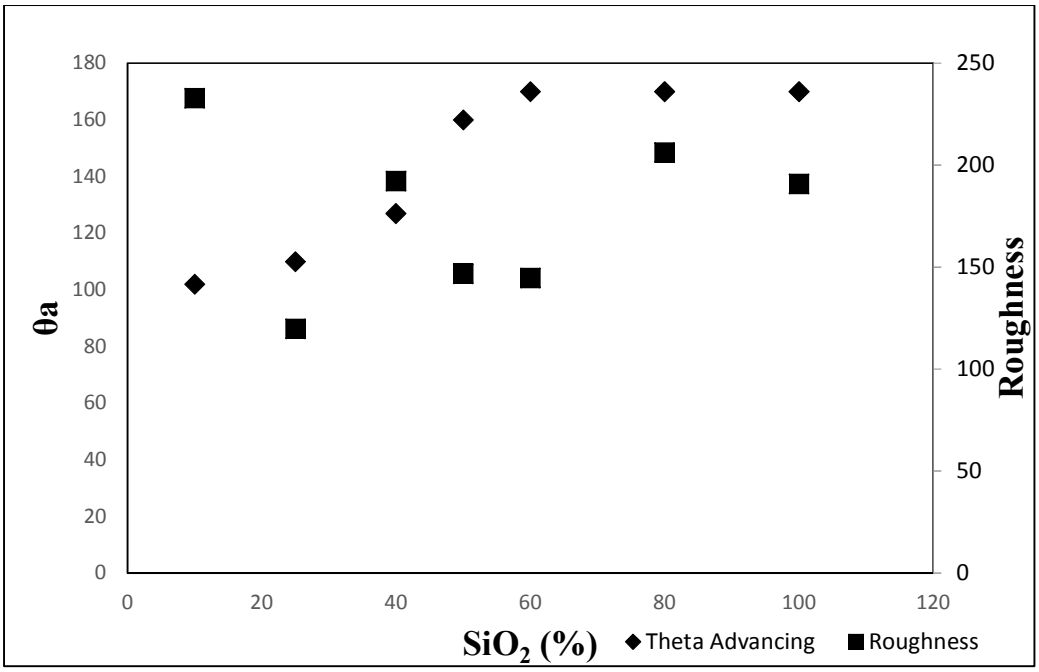

Figure 9.30: Relationship between θ_a and roughness values of PS coatings with varying SiO_2 nanoparticle content.

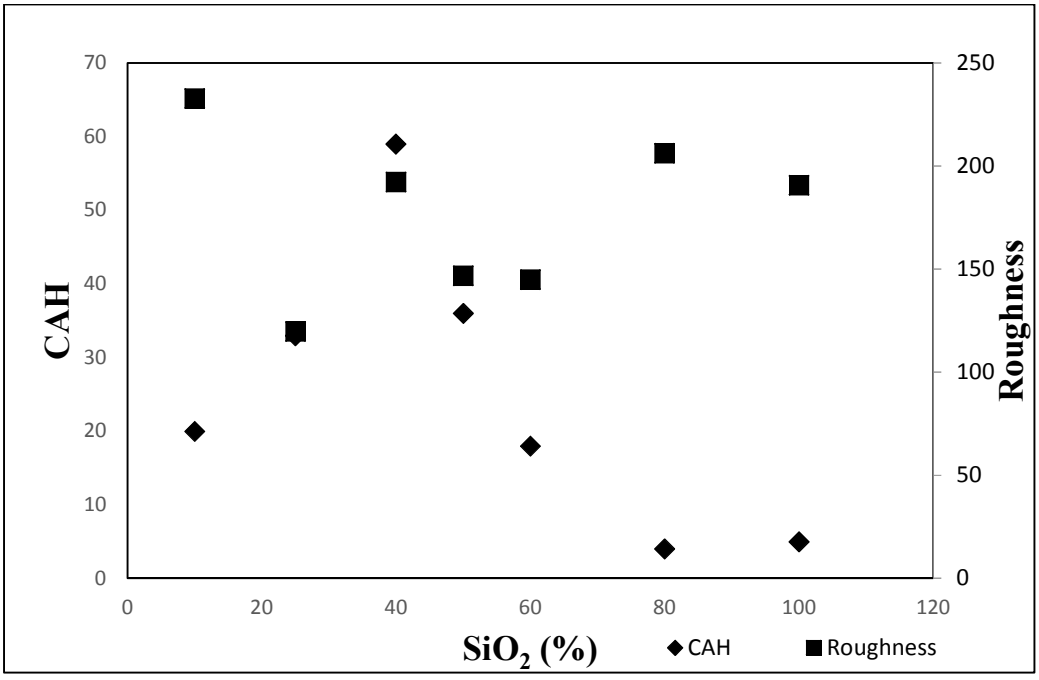

Figure 9.31: Relationship between CAH and roughness values of PS coatings with varying SiO_2 nanoparticle content, with respect to the %SiO2 content increase.

Nanoparticle content must have an equilibrium point which there would be no significant contact angle increase and/or would be more relative transmittance decrease after that point. Figure 9.32: and Figure 9.33: display transmittance and reflectance values of coated surfaces at 650nm which demonstrate superhydrophobic behaviour, respectively.

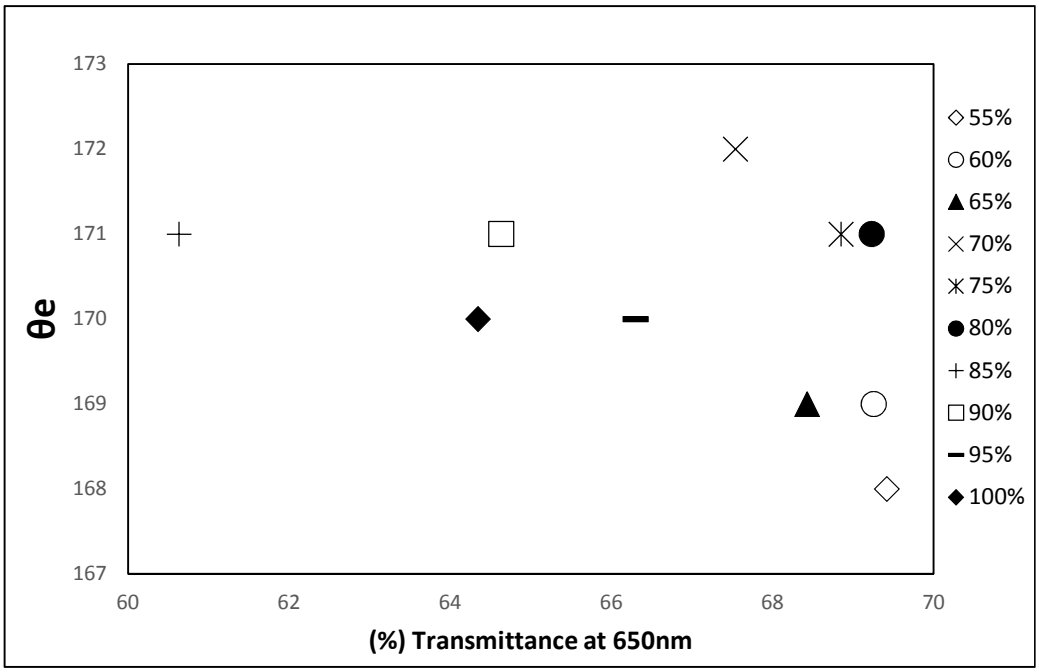

Figure 9.32: Relationship between θ_e and transmittance values of PS coatings with varying SiO_2 nanoparticle content, which demonstrate superhydrophobic behaviour.

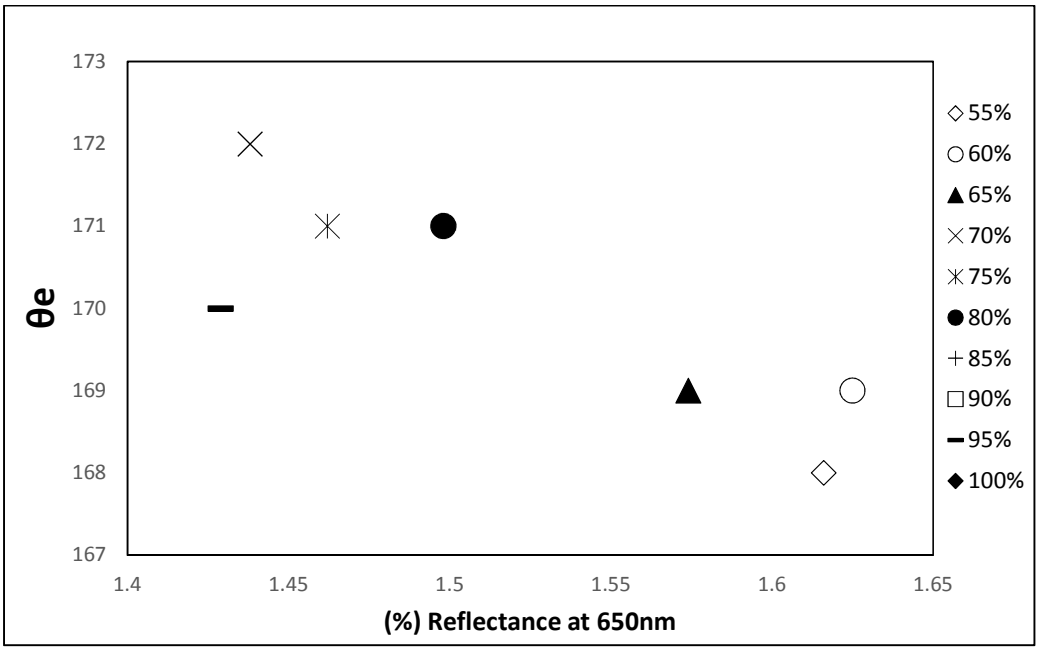

Figure 9.33: Relationship between θ_e and reflectance values of PS coatings with varying SiO_2 nanoparticle content, which demonstrates superhydrophobic behaviour.

According to these figures, the samples which demonstrate higher light propagation than %67 and higher CA value than 170° indicate this equilibrium point as these 3 samples have the highest CA values while having the highest transmittance values. Transmittance and CA values of these samples can also be seen from Table 9.5 : and Figure 9.19: where the sample with contain %70 nanoparticle has the highest CA but %80 has the highest transmittance while having a slightly less CA and %70 has same CA with %80 but demonstrates less light propagation. On the other hand, samples with higher nanoparticle content; %85, %90, %95 and %100 indicate less transmittance than any other superhydrophobic samples. Namely, %85 has the lowest and %95 has the highest transmittance inside this localised group of samples. However they present higher CA values than the samples with %65, %60 and %55 nanoparticle content which indicate the lowest CA values among superhydrophobic samples but somewhat higher transmittance values due to the lesser nanoparticle content. These results indicate that using %80 nanoparticle content to achieve superhydrophobicity with polystyrene coatings is meaningless because of the increase SiO_2 nanoparticle content decrease the light propagation and CA values. If the transmittance is more vital for the product or study, SiO_2 content can even be decreased in order to obtain more water repellency, as can be seen from Figure 9.32: %70 has higher CA than %80.

10. CONCLUSION

In this thesis, flat coatings of polypropylene, high density polyethylene, low density polyethylene, polypropylene-polyethylene copolymer, poly(methyl methacrylate), polystyrene, Nylon 6, Nylon 6.6, polyvinyl acetate and polyvinyl alcohol flat polymers and PS polymers with varying SiO2 nanoparticle contents were prepared. Surface and optic characterizations were conducted and correlations were derived. It was found and demonstrated that contact angle is highly dependent on both surface morphology and chemical properties of surfaces.

We found from study of flat polymer coatings that transmittance and reflectance values changes dramatically with the polymer types for approximately same coating thicknesses. Transmittance and reflectance measurements were conducted and concluded that polymer based films can be switched between opaque to transparent states through changing the polymer especially in the visible range. It was also found that, it is possible to synthesize reflective/antireflective and protective coatings for different applications as polymer coatings demonstrated a great range of transmittance values from %15 to %90 of uniformly coated films.

Surface fre energy calculations were done using Fowkes and Van-Oss Good approach. Test liquids were used to calculate the unknown components; water, methylene iodide, ethylene glycol and formamide. It was found that PP, HDPE, PS and PPPE coated polymer surfaces indicate low polar components and demonstrate hydrophobic behaviour as having higher contact angle values than 90°. As having low polar characteristics, PP, HDPE, PS and PPPE coated surfaces demonstrate low liquid-solid molecular interaction which resulted in hydrophobic behaviour. On the other hand polymer surfaces which have low polar components but high total surface energies, such as LDPE, did not demonstrate hydrophobicity as a result of high adhesion interaction between surface-water molecules. It was found that contact angle value decreases as a result of the surface energy increase and dominance between polar-dispersive components have a direct effect on hydrophobic behaviour of polymer

surfaces. Van-Oss Good approach and Fowkes method results demonstrated well accordance between two methods.

PS surfaces with varying SiO2 contents were also prepared. AFM measurements of samples indicated even distribution of nanoparticles through the polymer coatings. AFM measurements also indicated that surface roughness values show increase with respect to the nanoparticle content increase, as expected.

CA measurements were conducted and it was found that CA values increase with nanoparticle content as well as roughness increase. CAH calculations were indicated that superhydrophobic samples which have more than %50 SiO_2 nanoparticle content, demonstrate low CAH values as a result of their high advancing and receding contact angle values.

It was also found that samples of %10 and %25 as well as %40 and %100 which demonstrate roughness decrease despite their nanoparticle content increase, demonstrate no CA reduction. However CA results were either same or higher. From these results, it was speculated that, formation of more perfect networks of nanoparticles aggregates is more important for these samples therefore, higher CA values had obtained.

Transmittance values of PS-SiO_2 show decrase as nanoparticle contact increase but relative difference between samples were getting smaller therefore, from optical characterizations of samples it was assumed that there has to be some equilibrium point where there would be no significant CA increase and/or would be more relative transmittance decrease after that point. It was found that after %80 SiO_2 additive is meaningles as beyond that point transmittance and CA values begin to drop indicating %80 is the saturation point for PS-SiO_2 coatings. Even decresing nanoparticle content can lead to CA increase with a cost of transmittance loss.

11. REFERENCES

[1] Kulinich, S.A, Farzaneh, S., Farhadi, S. (2009) Ice Adhesion on Superhydrophobic and Hydrophobic Surfaces: Effect of Wetting Hysteresis. *Proceedings of the 13th International Workshop on Atmospheric Icing of Structures,* IWAIS 2009, Andermatt, Suisse, Poster Session, September.

[2] Ryerson, C. (2011) Ice protection of offshore platforms, *Cold Regions Science and Technology*, 65, 97-110.

[3] Weng, C.J., Chang, C.H., Lin, I.L., Yeh, J.M., Wei, Y., Hsu, C.L., and Chen, P.H. (2012) Advanced anticorrosion coating materials prepared from fluoro-polyaniline-silica composites with synergistic effect of superhydrophobicity and redox catalytic capability, *Surface and Coatings Technology*, 207, 42-49.

[4] Parkin, I., and Palgrave, R. (2004) Self-cleaning coatings, *Journal of Materials Chemistry*, 15, 1689–1695.

[5] Xue, C., Chen, J., Yin, W., Jia, S., and Ma, J. (2012) Superhydrophobic conductive textiles with antibacterial property by coating fibers with silver nanoparticles. *Surface Science*. 258, 2468–2472.

[6] Tropmann, A., Tanguy, L., Koltay. P., Zengerle, R., Riegger, L., and Zengerle, R. (2012) Completely Superhydrophobic PDMS Surfaces for Microfluidics, *Langmuir,* 28, 8292–8295.

[7] Bhushan, B. (2012) Bio inspired Surfaces. *Langmuir,* 28, 1698–1714.

[8] Bixler, G.D., and Bhushan. B. (2013) Fluid drag reduction and efficient self cleaning with rice leaf and butterfly wing bioinspired surfaces. *Nanoscale*, 5, 7685-7710.

[9] Daniello, R., Waterhouse, N., and Rothstein, J. (2009) Drag reduction in turbulent flows over superhydrophobic surfaces. *Physics of Fluids*, 21, 085-103.

[10] Feng, L, Zhang, Z., Mai, Z., Ma, Y., Liu, B., Jiang, L., and Zhu, D. (2004) A Super-Hydrophobic And Super-Oleophilic Coating Mesh Film For The Separation Of Oil And Water. *Angewandte Chemie International Edition*, Vol. 116, 15, 2046-2048.

[11] Zenkiewicz, M. (2007) Comparative study on the surface free energy of a solid calculated by different methods. *Polymer Testing,*26, 14–19.

[12] Zenkiewicz, M. (2007) Methods for the calculation of surface free energy of solids. *Journal of Achievements in Materials and Manufacturing Engineering*, 24, 137–145.

[13] Gala, D., Hodesa, G., Lincotb, D., Schock, H. W. (2000) Electrochemical deposition of zinc oxide films from non-aqueous solution: a new buffer/window process for thin film solar cells. *Thin Solid Films*, Vol.361-362, 79-83.

[14] Sparvolia, M., Mansanoa, R. D., Chubaci J. F. D. (2013) Study of Indium Nitride and Indium Oxynitride Band Gaps. Materials Research, Vol.16, 4, 850-852.

[15] Baba, E.M., Cansoy, C.E., Zayim, E.O. (2015) Optical and wettability properties of polymers with varying surface energies. Applied Surface Science, doi:10.1016/j.apsusc.2015.02.150.

[16] He, Z., Ma, M., Xu, X., Wang, J., Chen, F., Deng, H., Wang, K., Zhang, Q., Fu, Q. (2012) Fabrication of superhydrophobic coating via a facile and versatile method based on nanoparticle aggregates. Applied Surface Science, 258, 2544–2550.

[17] Blinker, J., and Scherer, G. (1989) Sol-Gel Science. Academic Press, New York.

[18] Blinker, C. J., and Scherer, G. W. (1984) Ultrastructure Processing of Ceramics, Glasses, and Composites. L. L. Hench and D. R. Ulrich, Edition, pp. 43-49, Wiley, New York, 1984.

[19] Erbil, H. Y. (2006) Surface Chemistry of Solid and liquid interface. Blackwell Publishing, Oxford.

[20] Adam, N.K. (1968) The Physics and Chemistry of Surfaces. Dover, New York.

[21] Hirschfelder, J.O., Curtiss, C.F. and Bird, R.B. (1954) Molecular Theory of Gases and Liquids. Wiley, New York.

[22] Butt, H.J., Graf, K., Kappl, M. (2003) Physics and Chemistry of Interfaces.Wiley-VCH, Weinheim.

[23] Liu, Y., Lin, Z., Lin, W., Moon, K., and Wong, C. (2012) Reversible superhydrophobic-superhydrophilic transition of ZnO nanorod/epoxy composite films. ACS Applied Material Interfaces, 4, 3959–3964.

[24] Hou, W., and Wang, Q. (2009) UV-driven reversible switching of a polystyrene/titania nanocomposite coating between superhydrophobicity and superhydrophilicity. Langmuir, 25, 6875–6879.

[25] Liu, H., Feng, L., Zhai, J., Jiang, L., and Zhu, D. (2004) Reversible Wettability of a Chemical Vapor Deposition Prepared ZnO Film between Superhydrophobicity and Superhydrophilicity. Langmuir, 20, 5659-5661.

[26] Aveyard, R, and Haydon, DA. (1973) An introduction to the principles of surface chemistry. Cambridge, Great Britain.

[27]Url-1 <http://www.sita-process.com/uploads/RTEmagicC_Groesse_Oberflaechenspannung1-E _10>

[28] Zisman, W. A. (1964) W.A. Contact angle, wettability and adhesion, in: Advances in Chemistry Series, vol. 43, 1, 1-51, American Chemical Society, Washington, DC.

[29] Fowkes, F.M. (1964) Attractive Forces at Interfaces. Industrial and Engineering Chemistry Research. Vol. 56, 12, 40–52.

[30] Owens, D. K., and Wendt, R. C. (1969) Estimation of the surface free energy of polymers, Journal of Applied Polymer Science, Vol. 13, 8, 1741-1747.

[31] Doganci, M.D., Cansoy, C.E., Ucar, I.O., Erbil, H.Y., Mielczarski, E., Mielczarski, J.A., (2012) Combined XPS and Contact Angle Studies of Flat and Rough Ethylene-Vinyl Acetate Copolymer Films Journal of Applied Polymer Science, 124, 2100–2109.

[32] Erbil, HY. (1998) Determination of the peripheral contact angle of sessile drops on solids from the rate of drop evaporation, Journal of Physical Chemistry B, Vol. 102, 46, 9234–9238.

[33] Url-2 <http://www.biolinscientific.com/attension/applications/?card=AA7>

[34] Young, T. (1805) An Essay on the Cohesion of Fluids. Philosophical Transactions of the Royal Society of London, 95, 65–87. doi:10.1098/rstl.1805.0005

[35] McHale, G., Erbil, H. Y., Newton, M. I., and Natterer, S. (2001) Analysis of shape distortions in sessile drops. Langmuir, Vol. 17, 22, 6995–6998.

[36]Url-3<http://upload.wikimedia.org/wikipedia/commons/3/38/Dynamic_contact _angle_measurement.svg>

[37] Wenzel, R. N. (1936) Resistance of solid surfaces to wetting by water. Industrial and Engineering Chemistry Research, Vol. 28, 8,988–994.

[38] Ucar, I. O., Cansoy, C. E., Erbil, H., Pettitt, M., Callow, M., and Callow, J. (2010) Effect of contact angle hysteresis on the removal of the sporelings of the green alga Ulva from the fouling-release coatings synthesized from polyolefin polymers. Biointerphases Vol. 5, 3, 75–84.

[39] Cassie, A. B. D., and Baxter, S. (1944) Wettability of porous surfaces. Transactions of the Faraday Society, 40, 546-551.

[40] Fowkes, F. (1987) Role of acid-base interfacial bonding in adhesion, Journal of Adhesion Science and Technology, Vol. 1, 1, 7-27.

[41] Chaudhury, M.K. (1984) Short range and long range forces in colloidal and macroscopic systems. Ph.D. Thesis, SUNNY Buffalo, NY.

[42] Oss, C., Chaudhury, M., and Good, R. (1988) Interfacial Lifshitz-van der Waals and polar interactions in macroscopic systems. Chemical Reviews, 88, 927-941.

[43] Fowkes, F.M. (1963) Additivity of intermolecular forces at interfaces. i. determination of the contribution to surface and interfacial tensions of dispersion forces in various liquids. Journal of Physical Chemistry Vol. 67, 12, 2538–2541.

[44] Good, R. J., and Girifalco, L. A. (1960) A theory for estimation of surface and interfacial energies. III. Estimation of surface energies of solids from

contact angle data. The Journal of Physical Chemistry, Vol. 64, 5, 561-565.

[45] Girifalco, L. A., and Good, R. J. (1957) A theory for the estimation of surface and interfacial energies. I. Derivation and application to interfacial tension. Journal of Physical Chemistry, Vol. 61, 7, 904–909.

[46] Oss, C. J., and Giese. R. F. (2002) Colloid and surface properties of clay and relatd minerals. New York, Marcel Dekker.

[47] Good, R. J. (1992) Contact angle, wetting, and adhesion: a critical review. Journal of Adhesion Science and Technology, Vol. 6, 12, 1269-1302.

[48] Mittal K. L. (2002) Contact angle, wettability and adhesion. CRC Press Taylor & Francis Group, New York.

[49] Whiteley, K. S., Heggs, T. G., and Koch, H. (2000) Polyolefins. Ullmann's Encyclopedia of Industrial Chemistry doi: 10.1002/14356007.a21_487

[50] Url-4 <wikimedia.org/wikipedia/commons/f/f7/Polyethylene-repeat2Dflat.png>

[51] Maier, C., Calafut, T. (1998) Polypropylene. The Definitive User Guide and Databook, William Andrew Publishing, Plastics Design Library.

[52] Url-5 <http://upload.wikimedia.org/wikipedia/commons/>

[53] Monrabal, B., Hierro, P. (2011) Characterization of polypropylene–polyethylene blends by temperature rising elution and crystallization analysis fractionation. Analitical and Bioanalitical Chemistry Vol. 399, 4, 1557-1561.

[54] Url-6 <wikimedia.org/wikipedia/commons/thumb/6/60/Polystyrene.svg>

[55] Zeng, Z., Yu, J., and Guo, Z. (2004) Preparation of Carboxyl-Functionalized Polystyrene/Silica Composite Nanoparticles. Macromolecular Chemistry and Physics, 205, 2197–2204.

[56] Url-7 <sigmaaldrich.com/content/dam/sigma-aldrich/structure4/>

[57] Palmer, R. J. (2006) Polyamides, plastics, Kirk-Othmer Encyclopedia of ChemicalTechnology. doi:10.1002/0471238961.1612011916011213.a01.pub2

[58] Url-8 <chemtube3d.com/polymer/_Nylon66F.html >

[59] Url-9 <mpbio.com/images/product-images/molecular-structure/02151938.png>

[60] Maissel LI, Reinhard G. (1983) Handbook of thin film technology. New York: McGraw-Hill;

[61] Url-10 <http://hivatec.ca/consulting-design/thin-film-deposition/>

[62] Url-11 <http://www.vt-sun.com/picture/knowledge/thinfilm.png>

[63] Avnir, D., Braun, S., Lev, O., and Ottolenghi, M. (1994) Enzymes and Other Proteins Entrapped in Sol-Gel Materials. Chemistry of Materials, 6, 1605.

[64] Macagnano, A. New Applications of Nanoheterogeneous Systems Institute of Atmospheric Pollution Research, National Research Council (IIA-CNR), Rome, Italy.

[65] Aegerter, M. A. (2004) Menning M. Sol-Gel technologies for glass producers and users. Boston/Dordrecht/New York/London: Kluwer Academic Publishers.

[66] Schubert, D.W., Dunkel, T. (2003) Spin coating from a molecular point of view: its concentration regimes, influence of molar mass and distribution. Materials Research Innovations, Vol. 7, 314.

[67] Madou, M. J. (2002) Fundamentals of Microfabrication: The Science of Miniaturization. 2nd ed., CRC Press, Boca Raton, FL.

[**68] MacCraith, B. D., McDonagh, C., Mcevoy, A. K., Butler, T., Keeffe, G. O., and Murphy, V.** (1997) Sol-Gel Science and Technology, 8, 1063.

[69] Deshmukh, R. R., Shetty, A. R. (2008) Comparison of surface energies using various approaches and their suitability. Journal of Applied Polymer Science, 107, 3708-3717.

[70] Kodolbas, A.O. (2003) Empirical calibration of the optical gap in a-Si1–xCx:H (x<0.20) alloys, Material Science and Engineering, 98, 161–166.

[71] Abdul-Kader, A.M. (2013) The optical band gap and surface free energy of polyethylenemodified by electron beam irradiations. Journal of Nuclear Materials, 435, 231–235.

[72] Rizk, R. A. M., Abdul-Kader, A. M., Ali, Z. I., Ali, M. (2009) Effect of ion bombardmenton the optical properties of LDPE/EPDM polymer blends. Vacuum, 83, 805–808.

[73] Khalifa, N., Souissi, A., Attar, I., Daoudi, M., Yakoubi, B., Chtourou, R. (2013) Uncommonphotoluminescence behavior of Fe+3 doped polyvinyl alcohol films. Optics and Lasers Technology, 54, 335–338.

[74] Gupta, S.K., Singh, P., Kumar, R. (2014) Modifications induced by gamma irradiationupon structural, optical and chemical properties of polyamide nylon-6,6 polymer. Radiation Effects and Defects in Solids, 169, 679–685.

[75] Colmenares, J.C., Kuna, E., Jakubiak, S., Michalski, J., Kurzydlowksi, J. (2015) Polypropylene nonwoven filter with nanosized ZnO rods: Promising hybrid photocatalyst for water purification. Applied Catalysis B: Environmental, 170-171, pp. 273–282.

[76] Singh, L., Samra, K.S. (2008) Opto-structural characterization of proton (3MeV) irradiated polycarbonate and polystyrene. Radiation Physics and Chemistry, 77, 252–258.

[77] Yadav, J.B., Puri, R.K., Puri, V. (2007) Improvement in mechanical and optical properties of vapour chopped vacuum evaporated PANI/PMMA composite thin film. Applied Surface Science, Vol. 254, 5, 1382-1388.

[78] Zidan, H.M., Abu-Elnader, M. (2005) Structural and optical properties of pure PMMA and metal chloride-doped PMMA films. Physica B, 355, 308–317.

[79] Mangipudi, V., Tirrell, M., (1995). Direct measurements of the surface energy of coronatreated Polyethylene using the surface forces apparatus. Langmuir, 11, 19-23.

[80] Ucar, I.O., Doganci, M.D., Cansoy, C.E. Erbil, H., Avramova, I., and Suzer. S. (2011) Combined XPS and contact angle studies of ethylene vinyl acetate and polyvinyl acetate blends. Applied Surface Science, Vol. 257, 22 9587-9594.

[81] Kaczmarek, H., Drag, R., Swiatek, M., Oldak, D. (2002) The influence of UV irradiation on poly(vinyl chloride) modified by poly(vinyl acetate). Surface Science, vol. 507–510, pp. 877–882.

[82] Doganci, M. D., Cavusoglu, S., Oksuz, M., Erbil, H. Y. (2014) Effect of surface free energy to control the deposit morphology during evaporation of graphite/SDS dispersion drops. Colloids and Surfaces A: Physcochemical and Engineering Aspects, 461, 310-322

[83] Aoi, K., Aoi, H., Okada, M. (2002) Synthesis of a Poly(vinyl alcohol)-Based Graft Copolymer Having Poly(e-caprolactone) Side Chains by Solution Polymerization. Macromolecular Chemistry and Physics, 203, 1018–1028.

[84] Shimizu, R. N., Demarquette, N. R. (2000) Evaluation of Surface Energy of Solid Polymers Using Different Models. Journal of Applied Polymer Science, 76, 1831–1845.

[85] Roh, S. C., Choi, E. Y., Choi, Y. S., Kim, C. K., (2014) Characterization of the surface energies of functionalized multi-walled carbon nanotubes and their interfacial adhesion energies with various polymers. Polymer, Vol. 55, 6, 1527–1536.

[86] Ucar, I. O., Erbil, H. Y., (2012) Dropwise condensation rate of water breath figures on polymer having similar surface free energies surfaces. Applied Surface Science, 259, 515–523.

[87] Pandiyaraj, K. N., Selvarajan, V., Deshmukh, R. R., Gao, C., (2008) Adhesive properties of polypropylene (PP) and polyethylene terephthalate (PET) film surfaces treated by DC glow discharge plasma. Vacuum, Vol. 83, 2, 332–339.

[88] Glinka, Y. D., Lin, S. H., Hwang, L. P., Chen, Y. T., Tolk, N. H. (2001) Size effect in self-trapped exciton photoluminescence fromSiO2-based nanoscale materials. Physics Review B, 64, 8, 5421.

[89] McHale, G., Shirtcliffe, N. J., Newton, M. I. (2004) Intrinsically super hydrophobic organo-silica sol-gel foams. Langmuir, 20, 10146-10149.

CURRICULUM VITAE

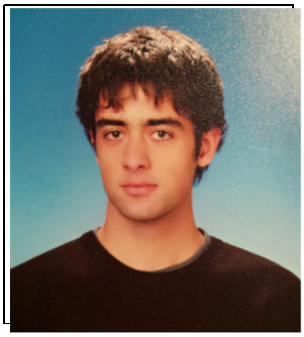

Name Surname: Elbruz Murat Baba

Place and Date of Birth: Edremit 18.04.1989

E-Mail: elbruzmurat@gmail.com

EDUCATION: Nano Science and Nano Enginering

B.Sc.: Naval Architecture and Marine Engineering

PUBLICATIONS ON THE THESIS

- **Baba E.M., Cansoy C.E., Zayim E.O., (2015)** Optical and wettability properties of polymers with varying surface energies App. Surf. Sci. doi:10.1016/j.apsusc.2015.02.150
- **Baba E.M., Cansoy C.E., Zayim E.O., (in progress)** Investigation of Optical and Wettability Properties of Polystyrene-SiO_2 Nanoparticle Composite Films.

PRESENTATIONS ON THE THESIS

- **ICCE 21st International Conference on Composites or Nano Engineering 2013** "The Relationship Between Hydrophobicity And Transmittance Properties Of Polyolefin/Inorganic Oxide Surfaces" **Oral Presentation**
- **SATF Science & Application Of Thin Films, Conference & Exhibition 2014** "Dependence Of Optical And Mechanical Properties On Wettabilities And Surface Free Energies Of The Polymers" **Poster Presentation**
- **ECASIA 16th European Conference On Applications Of Surface And Interface Analysis 2015** "Investigation Of Optical And Wettability Properties Of Polystyrene-SiO_2 Nanoparticle Composite Films" **September28-October 01**